View metadata, citation and similar papers at core.ac.uk

brought to you by CORE

provided by Texas A&M Repository

X-RAY PHOTOELECTRON SPECTROSCOPY AND KINETIC STUDY:

Pt-GROUP METALS AND BIMETALLIC SURFACES

A Dissertation

by

KERRIE K. GATH

Submitted to the Office of Graduate Studies of
Texas A&M University
in partial fulfillment of the requirements for the degree of

DOCTOR OF PHILOSOPHY

December 2008

Major Subject: Chemistry

X-RAY PHOTOELECTRON SPECTROSCOPY AND KINETIC STUDY:

Pt-GROUP METALS AND BIMETALLIC SURFACES

A Dissertation

by

KERRIE K. GATH

Submitted to the Office of Graduate Studies of
Texas A&M University
in partial fulfillment of the requirements for the degree of

DOCTOR OF PHILOSOPHY

Approved by:

Chair of Committee,	D. Wayne Goodman
Committee Members,	Marcetta Y. Darensbourg
	Michael P. Rosynek
	Mahmoud El-Halwagi
Head of Department	David H. Russell

December 2008

Major Subject: Chemistry

ABSTRACT

X-ray Photoelectron Spectroscopy and Kinetic Study:

Pt-Group Metals and Bimetallic Surfaces. (December 2008)

Kerrie K. Gath,

B.S., Texas A&M University

Chair of Advisory Committee: Dr. D. Wayne Goodman

Pt-group metals were some of the first metals to be studied as catalysts for industrial use. The goal of these studies was to ascertain a fundamental understanding of CO oxidation and acetylene cyclotrimerization reactions on Pt-group metals. A further goal was to determine the optimal conditions for each reaction.

CO oxidation on Rh(111),Pt(100), and Pd(100) was scrutinized on various oxide surfaces from chemisorbed to bulk metal oxides. Low pressure reactions on Rh(111) reveal the highest activity was a CO uninhibited surface with <1ML of chemisorbed oxygen. Pt(100) high pressure oxidation revealed that only <1ML oxygen is formed during high pressures reactions. High pressure CO oxidation reactions on Pd(100) show oxygen penetration after CO has been consumed; however, during the highest activity XPS found only chemisorbed species.

The cyclotrimerization of acetylene to benzene is another reaction found in industry typically carried out on Pd. The active site is considered to be a 7

atom configuration with 6 atoms surrounding a central atom. By adding relatively catalytically inert Au atoms to the active Pd(111) surface the acetylene coupling activity is enhanced. Cyclization activity is a function of the surface composition and the surface structure. A single Pd atom surrounded by six Au atoms is found to have the highest activity at 300K for acetylene cyclotrimerization.

This is dedicated to my mom, dad, brother, and friends

for all of their love and support through the years.

When all others said it could not be done,

you believed in me.

ACKNOWLEDGEMENTS

First, I would like to thank my family and close friends who have been an inspiration to me all my life. My parents, Jane and Henry Gath, throughout my life, have always given me support no matter what goal I set for myself. I know that without such great parents, who were willing to sacrifice so much for me and my brother, I would not be where I am today. My brother, Mike Gath, has shaped my life and ever since I can remember, I have always wanted to be just like him. I know I would not have made it this far without his help and support. I am also lucky to have such a nice sister-in-law Lindsay (Popp) Gath and my wonderful nephew Bryson and niece Finley. I am very grateful to have many strong women in my family, including my mom and both of my grandmothers. Grandma Thelma Gath graduated with a college degree in the 1930's when most women did not consider going to college and Grandma Florence McGee raised eight prosperous children on a very modest budget in a small house. At this time, I would also like to thank Mary Gath for her support and all of my aunts, uncles, and many cousins. I would also like to thank my longest friend, Layla (Aflatooni) Mansuri, and her family. We have been friends since my first memories and have both supported each other on various paths in life. I could not have made it through without the support of all these people.

Next, I would like to thank my co workers and Dr. D. Wayne Goodman, for all the support and help they have given me during my years in graduate

school at Texas A&M University. After Dr. Goodman accepted me into the group, I started on the STM. During this time I worked in the basement room, nicknamed the “hole”, where I met Fan Yang and Dr. Billy Wallace. It was not easy working in such a small room with two large chambers, yet we managed to pull it off with class and I really miss those days with the guys. Next, I moved (after a small detour) to the XPS chamber upstairs and began working with Dheeraj Kumar and MingShu Chen. I would like to thank both of them for helping me understand XPS and, more importantly, how to develop and execute a well prepared experiment. Other members of the group during my term here include Emrah Ozensoy (my first contact with this group and to this day I look up to him as an excellent researcher and mentor), Sivadinarayana Chinta, Stefan Wendt , Bo Wang, Cheol-Woo Yi, Sungsik Lee, Zhen Yan (who was a great help fixing my chamber), Sean McClure, and Matt Lundwall (who also became a close friend). Toward the end of my term, I had a chance to work with Feng Gao and Qinlin Guo, both gave me excellent guidance and helped me with my final project. I would like especially to thank Yun Cai for sticking it out with me, I knew if we both remained in the group, we could both make it through. Additionally, I would like to thank Amy Liu, Dr. Goodman’s assistant, for running the group and making a grad student’s life as easy as possible. Last and certainly not least is Sandy Manning who, during my whole time here, has been there for each and every graduate student. She goes beyond her job description and has truly made a difference in this department and in the lives of each

graduate student. Without Sandy, I know fewer graduate student would have made it through.

I would like to thank my great friends, teachers, and mentors who have helped me through this journey. Before making it to grad school, I had to make it through chemical engineering at Texas A&M, and I could not have done this without the help of Lale Yurttas who mentored me through all the trials and tribulations. During my undergraduate career, I had a great chance to do research in the Geochemistry Laboratory in Geology with Bruce Herbert. He taught me that research needs a direction and it is hard work, but, also, if you do not enjoy what you do, there is no reason to continue doing it. Kayleen Helms and I became friends my last year in undergraduate. She has been an inspiration to me and I have cherished our friendship through the years. Billy Wallace had not only been a post doc to me, but a good friend who made this dissertation and my sanity possible through this process. He is joined by Eric Reinheimer, who became my best friend and, for a time, my roommate. Along with Billy and Eric, I must include Adriana Gonzalaz with whom I spent many hours helping each other maintain our sanity. Some more College Station friends include Vickie (Skach) and Ryan Podsim; Anthony Skach, Scott Lutter Brenda and Brian Richardson; all of them mean the world to me and have helped me in their own ways during this expedition of graduate school. Toward the end of my school career, I had the chance to meet some one who would change my outlook on research and gave me a renewed interest in learning.

Chad Baker and I met through similar research interests after we had known each other for a while off and on through the years. Although Blaine is not a conventional mention for an acknowledgement, he should be noted as being a constant, albeit not always easy, companion and friend. I rescued him from a shelter midway through my graduate school career, and he has not left my side since. Through everything, he is always there with a happy grin and a wagging tail, especially after a long day of research.

TABLE OF CONTENTS

CHAPTER Page

Page

LIST OF FIGURES

Page

Page

Page

Page

CHAPTER I

INTRODUCTION

Surface Science

The study of surfaces is a relatively new exploration in science and engineering. Heterogonous catalysts were first documented in the early 1800's and by the 1840's catalysts began to be heavily studied. During this time the process for photography was introduced and soon after surface catalyzed technologies first appeared beginning with simple reactions such as reacting methane with steam to produce methane and hydrogen gas (Mond 1888). Surface science began to gain distinction early in the 20th century with Langmuir (1915) as the leading proponent exploring the properties of chemisorbed and physisorbed adsorbents, energy exchange, and sticking coefficients. By the 1950's techniques based on solid state devices enabled surface scientists to get a more detailed view of surface reactions. Clean single crystal surfaces could now be studied; however, they required very low pressures. The availability of surface characterization techniques resulted in an explosion of research culminating in a deeper understanding of surface phenomena impacting a plethora of fields in chemistry, physics, and engineering. [1]

This dissertation follows the style used in Surface Science.

Two complications associated with the aforementioned surface science techniques are the pressure gap created by working in pressures below 10^{-6} torr and the materials gap from working with smaller pure single crystals, wire, and foil. However, with proper vacuum chamber design a reaction cell can alleviate the pressure gap issue. Recent advances now allow the use techniques at high pressures reducing the pressure gap and helping prove that it is not as significant an effect as previously thought.[1,2] The materials gap can be partially solved by performing reactions at various scales increasing the complexity each time.

CO Oxidation over Pt-group Metals

The oxidation of CO on late transition metals is an important catalytic reaction both in basic research and industry. An understanding of the fundamental characteristics of catalytic oxidation of CO by O_2 on Pt-group metals is of great importance in fuel processing, chemical production, and pollution from automotive and industrial emissions.[1-9] The introduction of the three way catalytic converter in the United States for model year 1975 greatly reduced dangerous toxins including CO, unburned, and partially burned hydrocarbons from automotive exhaust.[1-5,8-12] New restrictions from the Environmental Protection Agency (EPA) demand more from these catalysts.[13] In addition to catalytic converters for clean burning cars, trace CO removal from hydrogen depends heavily on transition metal catalysts, essential for fuel cell

technology.[2,14,15] A key question is whether the surface, under catalytic reaction conditions, is metallic or a metal oxide. If an oxide is the primary constituent then the question becomes: which type of oxide is most conducive to CO oxidation. An ideal model for surface reactions, the simplicity of the CO oxidation mechanism allows firm conclusions to be drawn from single crystal studies and aids in bridging the well-known pressure and materials gaps in heterogeneous catalysis.[1-5] Multiple studies performed regarding the oxidation of CO over Pd, Pt, and Rh under reducing or mildly-oxidizing conditions aided in the understanding of the mechanism, concluding that the catalytic process is governed by a Langmuir-Hinshelwood mechanism.[6,7] In these conditions both CO and atomic O are chemisorbed to the surface with CO as the dominant surface species. Thus the overall reaction rate is controlled by the rate at which CO desorbs allowing open adsorption sites for O_2 to adsorbed and dissociate. For reducing or mildly-oxidizing conditions Pd, Pt, and Rh reveal a first order dependence for O_2 and negative first order in CO, with the CO desorption energy approximately equivalent to the apparent activation energy for CO2 formation. [16]

CO oxidation over Ru has an anomalous phenomena unlike that of Pd, Pt, and Rh. Under stoichiometric conditions (O_2/CO=0.5) and at high pressures Ru is more active for CO oxidation compared to Pd, Pt, and Rh; however, at low pressures (including the studies done in UHV) Ru is the least active. [16] Why does Ru react so differently from these other metals? [7] For the past 30 years a

plethora of papers have covered CO oxidation on Ru and these studies conclude CO oxidation is more active on an oxygen chemisorbed surface than on a bare metal surface. [7,11,16-18] The surface of Ru, under stoichiometric conditions is covered in chemisorbed oxygen where as Pd, Pt, and Rh are saturated in CO.[17,24] During CO oxidation, studies done in the 1980's established Ru maintains a surface oxide ~1ML.[18] This research was recently corroborated by Chen et al. with a kinetic study on the catalytic behavior of Ru. [11] Next, CO oxidation on Pd, Pt, and Rh was studied by our group in oxygen rich conditions where the O_2/CO ratio was greater than that at stoichiometric conditions. These reaction rates, in conditions conducive to chemisorbed atomic oxygen forming on the surface of the metal, were 1-3 orders of magnitude higher than those on oxygen deficient surfaces.[11]

Acetylene Cyclotrimerization on Bimetallic Au-Pd Surfaces

Benzene, essential to our chemical industry, is currently used in the manufacturing of dyes, detergents, pharmaceuticals, and used extensively for nylon and Styrofoam. Bimetallic catalysts are attracting considerable attention due to properties that often deviate from either of the original components, with mixtures often exhibiting enhanced catalytic selectivity, activity, and stability. Pd-Au alloys are frequently utilized as catalysts for a plethora of reactions including hydrogenation of hydrocarbons, synthesis of vinyl acetate monomer,

CO oxidation, and other industrially important reactions. Bulk Au acting alone is a poor catalyst; in contrast to Pd, an excellent catalyst for many reactions including cyclotrimerization of acetylene to benzene.

Cyclotrimerization of acetylene to form benzene on Pd-based catalysts is a well-studied alternative process. Kinetic investigations of acetylene cyclotrimerization on Pd/Mo(110) and Au-Pd/Mo(110) have been carried out using temperature programmed desorption (TPD) and elevated pressure/temperature reaction conditions. The surface composition was measured by Auger electron spectroscopy, ion scattering spectroscopy, and X-ray photoelectron spectroscopy. Infrared reflection absorption spectroscopy using CO as a probe shows the formation of Pd monomers isolated in an Au matrix. These sites are proposed to be the active site for the cyclotrimerization reaction on Au-Pd surfaces since the turnover frequency for the formation of benzene correlates directly with their population.

CHAPTER II

EXPERIMENTAL

Ultrahigh Vacuum (UHV) Chamber and High Pressure Reactor

A vacuum chamber is necessary to study surfaces ensuring the surface under study is free from unwanted contamination. The optimum conditions are ultra high vacuum (UHV) with operation pressures in the 10^{-10} torr range, where a surface remains free of contamination for at least three hours and thus allowing sufficient time to complete reproducible experiments. In an UHV environment the mean free path of subatomic particles is greatly reduced as is the interference of the background gases. Thus electrons, photons, and free atoms can be utilized in surface spectroscopic studies such as low-energy electrons without problems arising from scattering off other particles. [1]

The experimental set-up or chamber used for these experiments is a commercial PHI 5500 system with a bell-jar analysis chamber and an added preparation chamber with retraction bellows for sample movement as shown in Figure 1. The analysis section houses a hemispherical analyzer, X-ray source with Mg and Al anodes, Auger gun, differentially pumped ion gun, monochromator, external light source, ion pump, and titanium sublimation pump. The preparation section is connected to the analysis chamber through a gate valve that can be closed when needed. This part of the chamber is smaller

in volume than the analysis section and is pumped by a turbo-mechanical pump and a titanium sublimation pump with a liquid nitrogen trap; additionally there are five metal dosers, an E-beam filament, leak valve connected to the manifold, and a quadrapole mass spectrometer. Connected to the preparation section is a smaller high pressure (~1 atmosphere) reactor that allows the sample to be transferred contiguously, via a gate valve, to the UHV sections of the chamber without exposure to air (figure 2). The reactor is separated from the retraction bellows through a Teflon sleeve, mechanically pumped to prevent leaking of the reactor gases into the bellows. The bellows and the reactor are connected to a double manifold through separate Swagelock valves and all can be pumped by mechanical pump or turbo-mechanical pump thus allowing high pressure reactions.

Prior to performing an experiment the single crystal sample will be checked for chemical composition and contamination by either X-ray photoelectron spectroscopy (XPS) or Auger electron spectroscopy (AES). The sample can be cleaned by either sputtering with the differentially pumped ion gun, heating it to high temperatures in the preparation chamber with the E-beam filament, resistive heating, or a combination of procedures depending on the sample type. For experiments with more than one metal the dosers can be

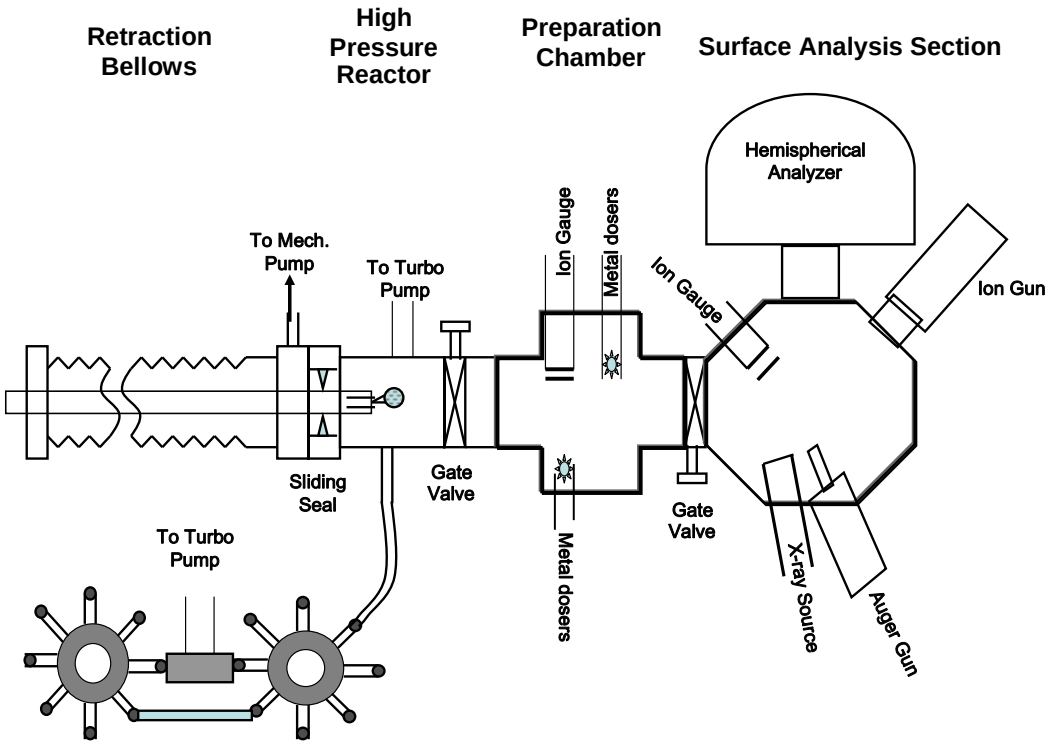

Figure 1: Schematic of vacuum chamber including the bellows, high pressure reactor, preparation chamber, and analysis chamber with the XPS.

High Pressure Reactor

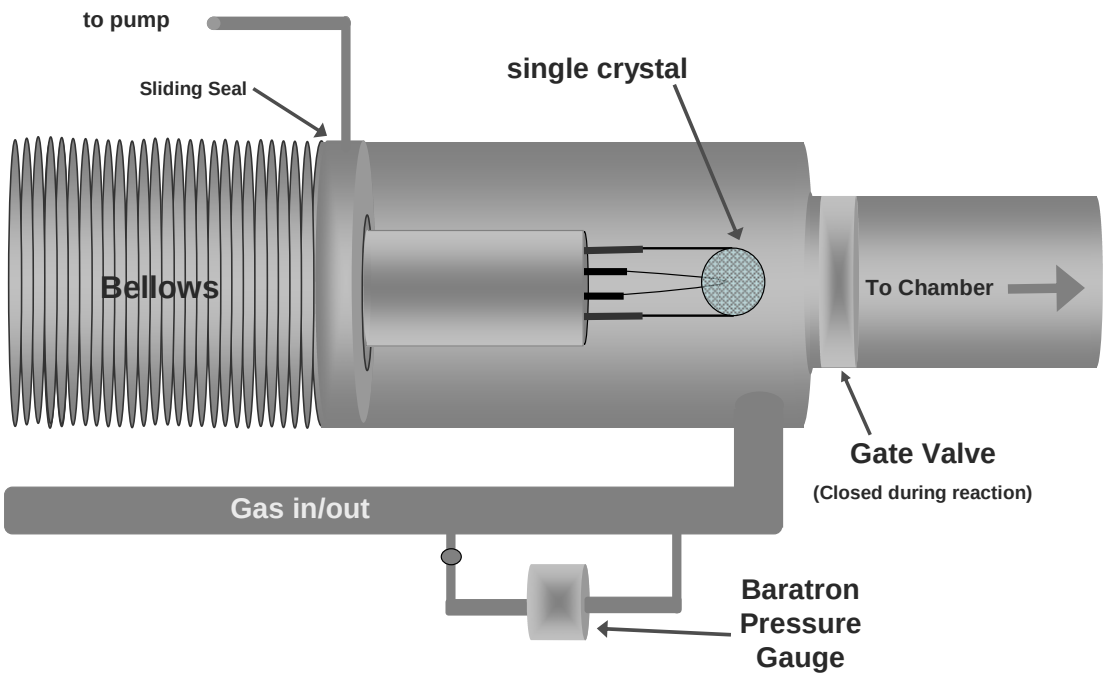

Figure 2: Detailed schematic of the high pressure reactor including the delivery system to the GC and manifold.

employed, where a metal wire (i.e. Pd, Si, Ni, Au) is wrapped around a tantalum wire similar in appearance to a light bulb filament. When an adequate current is flowing through the Ta wire the metal wire vaporizes onto the single crystal sample. During a typical reaction the sample is moved into the reactor, the gate valve between the preparation section and the reactor is closed and the reactor is filled with the desired gases. The pressure is measured using a baratron pressure gauge. The sample is then resistively heated and the temperature measured with a C type thermocouple spot welded to the back of the sample. After the reaction is complete the product gases are removed first by a mechanical pump and then by a turbo-mechanical pump. Once the reactor is sufficiently evacuated (~1x10^{-7}torr) the gatevalve leading to the preparation chamber is fully opened and the sample is introduced into the UHV chamber.

X-ray Photoelectron Spectroscopy (XPS)

History

X-ray photoelectron spectroscopy is based on the photoelectric effect, when a surface is exposed to electromagnetic waves there is an emission of electrons from the surface of a solid. Heinrich Hertz discovered the photoelectric effect in 1887 when he saw charged metals lose charge more rapidly when exposed to UV radiation. Physicist Albert Einstein, 18 years later, provided a theoretical explanation for the photoelectric effect as the adsorption

of quanta of light (now considered photons) and the ensuing release of electrons. The photoelectric effect helped promote the idea of light having dual properties where light exhibits characteristics of waves and partials at different times. In the next 50 years more experimental and theoretical work was performed in order to develop spectroscopic methods for surface analysis as well as high vacuum technologies. In 1954, Kai Siegbahn and co-workers developed a detector to distinguish slow electrons ejected from the surface when the surface is exposed to X-rays. Characteristic lines of different components of the solid could be clearly made out in the spectrum. The analytical information is only from the top most layers with a depth of only 3-5 nm. A few years later Siegbahn discovered that the same technique could additionally distinguish the oxidation state of metals and chemical states of nonmetal atoms by looking at the shift of the characteristic peak. For his development of the method for using electron spectroscopy Siegbahn was awarded the 1981 Nobel Prize in physics and during his Nobel Lecture called the method Electron Spectroscopy for Chemical Analysis (ESCA), now considered more of a historical name. The first commercial XPS was developed in the 1960's after improvements, such as new radiation sources emitting in the soft X-ray and UV regions and enhancement of the detector's focusing lens. XPS has a solid foundation in surface and material science as a primary instrument for elemental analysis and phase composition of solid surfaces that will only intensify particularly with the use of synchrotron radiation. [8]

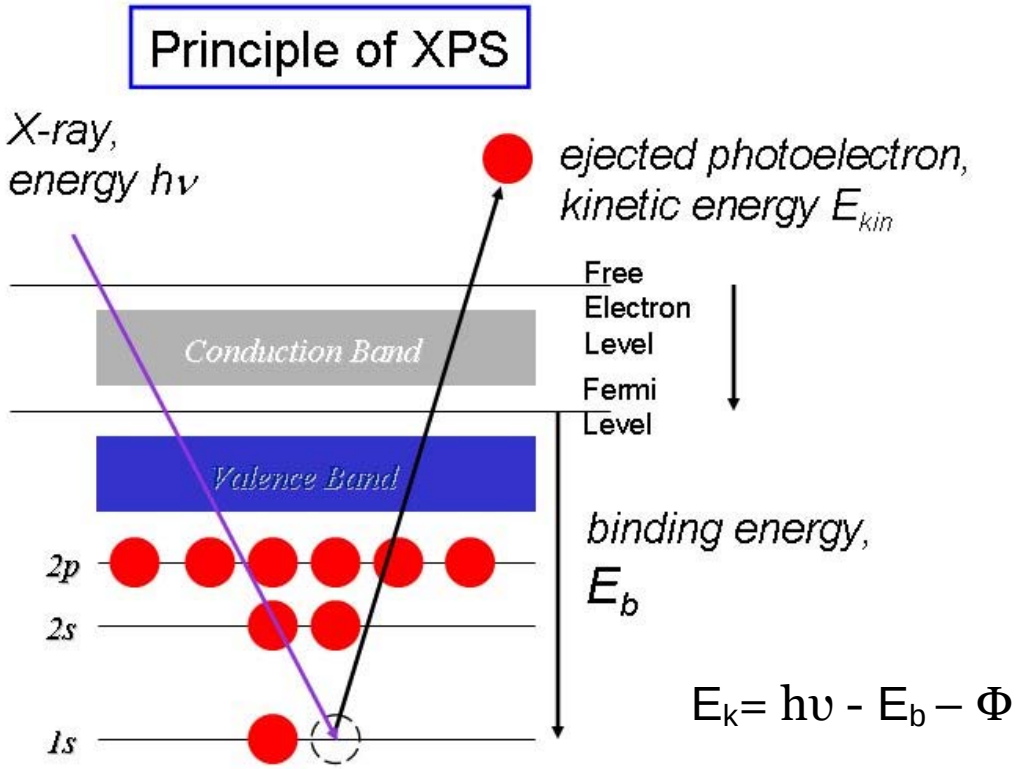

Figure 3: Energy diagram showing the theory of x-ray photoelectron spectroscopy.[9]

Theoretical Principles

The XPS works by irradiating a surface with electromagnetic radiation in the X-ray region. The impinging photons have an energy, hυ, greater than the binding energy of the core electrons. The photons strike the surface and core electrons are emitted from the solid. The core electrons are characteristic of the individual atom and do not participate in the bonding like valence electrons, thus bonding is not affected. To a first approximation the loss of core electrons does not alter the local environment and allows for elemental analysis. The kinetic energy of the emitted photoelectrons, measured by a detector, are used to calculate the binding energy through the relation:

$$E_k = h\upsilon - E_b - \Phi \qquad (1)$$

where E_k is the kinetic energy of the emitted core level electrons, hυ is the energy of the incident beam of electrons from the X-ray source, Φ is the work function of the spectrometer, and E_b is the calculated binding energy (figure 3). The binding energy is found by referencing all of the measurements to the Fermi level. Furthermore, this gives each element a unique a distinctive binding energy feature. Excluding helium and hydrogen, all of the elements can potentially be measured when utilizing proper procedures. Conducting materials have an electron cloud diminishing the effect of the reduction caused by the ejected photoelectron; however, non-conducting materials will become

reduced the longer they are in the beam. Low energy charge neutralization is necessary to prevent reduction that could cause an artificial peak shift. Each element has an individual fingerprint spectra and a typical binding energy survey scans the range of 1000 to 0eV. In order to save time during acquisition, which can take from minutes to hours depending on the concentration of the element being analyzed, the spectra recorded can be reduced to a specific range that concentrates around their primary peaks. This enables a closer view of particular peaks that can help analysis of the peak area and provide enhanced resolution.[1]

Instrumentation

The XPS used for all experiment therein were executed on a PHI 5500 XPS with a Perkin Elmer model 10-360 Precision Energy Analyzer. The separate components include the input lens, spherical capacitor analyzer (SCA), and the detector. The SCA consists of two metallic concentric hemispheres enclosed in a magnetic shield, additionally housing the detector. The small area lens has the ability to change the aperture size, depending on the size needed for the application, from 0.2 to 40mm. Additionally, along with the alteration in the aperture the lens has electronically variable lens magnification. This offers a wide range for the analysis area on the surface. The detector is a single channel detector with an exit slit followed by a channeltron electron multiplier. The

multichannel detector consists of a pair of channel electron multiplier plates followed by 16 discrete collector anodes.

Theory of Instrument Operation

The input lens accepts the electrons from the sample that has been exposed to x-ray radiation. The electrons are slowed in a retarding field to a range of kinetic energies able to pass through the analyzer. Next, the electrons are focused onto the entrance slit of the analyzer. The analyzer consists of two hemispherical, concentric biased electrodes. These electrodes allow charged particles of a specific energy to follow circular trajectories, which are focused toward the analyzer's exit slit. The trajectories are not affected by the magnetic fields due to the encasement of the analyzer in a magnetic shielding material. The electrons, which pass through the exit slit of the analyzer, are amplified by the channel electron multiplier and individually counted. The analyzer is stepped through the selected energy range and the number of particles are recorded for each step for a give amount of time (determined through settings in the accompanying software). A spectrum is produced through the computer interface showing the number of particles as a function of their binding energy. [12,19]

Auger Electron Spectroscopy (AES)

One of the most common surface science techniques used is AES. Positive aspects of AES include analysis without causing damage to the material and presenting quantitative and qualitative information on specific surface elemental composition of metals and metal oxides. A major disadvantage is the only materials that benefit are metals and other conducting materials.

The process by which AES works begins when an accelerated beam of electrons with a specific kinetic energy bombards the surface or occurs during the XPS process after impact of the incident photon ionizing and producing a core hole. Next one of two processes will occurs depending on conditions: X-ray fluorescence or Auger transition. Both competing processes help relax the system to a stable state and are utilized in different instances. In X-ray fluorescence, typically found in a conventional laboratory X-ray generator, the core hole is replaced by an electron from a higher energy shell and occurs when the initial incident electron energy is greater than 10keV. As presented in figure 4 the Auger process, discovered by Pierre Auger, shows the energy emitted due to replacing the core hole with an electron used in the emission of a second electron. The kinetic energy of the Auger process is calculated from the difference between the energy levels involved in the replacing the core hold with an electron from a lower energy level and the correlating relaxation process.

$$E_{KLM} \approx E_K - E_L - E_M - \delta E - \varphi \qquad (2)$$

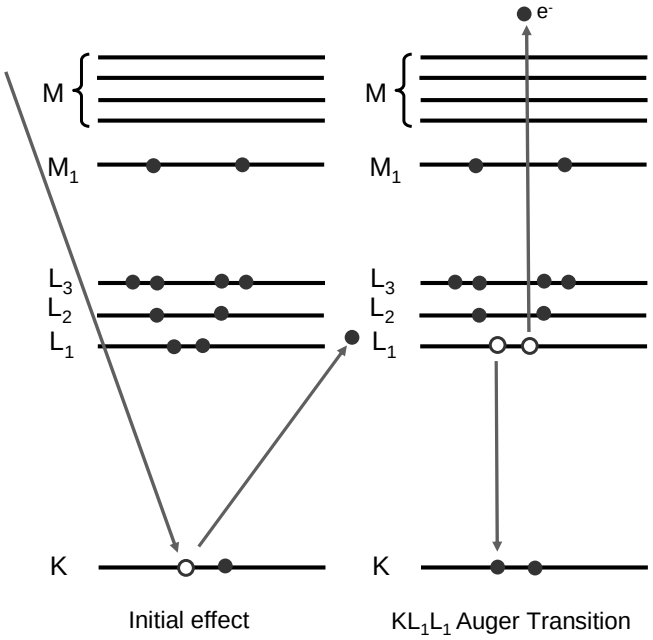

Figure 4: Diagram depicting the energy levels of the Auger emission process: Initial effect of the photoelectron and the following KL_1L_1 transition.

The kinetic energy of the Auger electron (E_{KLM}, E_K, E_L, E_M) is the BE of the electrons in the same named shells, δE denores the energy shift caused by relaxation effects, and φ is the work function of the material being analyzed. The kinetic energy measured is characteristic for each element and can be utilized to provide a means of differentiating between various elements. However, the AES signal is very low when compared to the background due in part to the emission of a secondary electron from the incidence of the initial high energy beam. Thus AES is plotted as the first derivative of the number of electrons detected at a particular energy. This gives characteristic sharp asymptotic peaks at different binding energies. Therefore, the actual AES curve presented, using the energies at the center of the asymptotic portion of the curve is the first derivative.

AES is considered a surface sensitive technique that probes to a depth of a few atomic layers from the surface of the metal. This is accomplished by the fact that the mean free path of electrons is extremely small, limited to a few nanometers, when excited by an Auger electron with an energy less than 1 keV. Additionally, AES is typically used to ascertain the thickness of a metal, when deposited on a dissimilar metal, or the growth of a metal oxide film grown on conductive surfaces. The thickness of the film can be determined using the attenuation of the AES signal of the underlying substrate as the film grows

$$I_s=I_s^o(\exp(-d/\lambda_i^s\cos\alpha) \quad (3)$$

where, I_s and I_s^0 are the intensities of the AES signals of the original metal and the grown film, respectively; d is the thickness of the film being measured; λ_i^s is the effective attenuation length of electrons in the film and α is the electron emission angle with respect to the surface normal. [1]

Low Energy Ion Scattering Spectroscopy (LEISS)

LEISS is a very effective tool when it is necessary to identify the composition of the top most atomic layer where reaction is known to have taken place. This technique involves impacting the surface with a beam of accelerated ions. After colliding with the atoms on the top-most layer some are scattered back. The energy of the backscattered ions is measured and related to the mass of the initial surface atoms. LEISS uses ions of inert gases such as helium, neon, or argon and is considered on of the most surface sensitive techniques. These inert gases are excited in the energy range from a few eV to keV during the process. Additionally, LEISS can be utilized to determine the structure of the surface and, when less than 1ML, can identify the atomic species shadowed by the upper layer.[20]

The scattering of the ions from the surface can be treated as a classical elastic two-body collision model due to the fact that the time of collision is small with respect to time period of phonon frequencies in a solid. Therefore,

conservation of energy and momentum principles are applicable for the system. This behavior can be quantified by the following equation:

$$\frac{E_1}{E_0} = \frac{1}{(1+A)^2}\left(\cos\theta \pm \sqrt{A^2 - \sin^2\theta}\right)^2 \quad (4)$$

where the incident ion with an energy of E_o and mass, M_o, collides with a surface atom of mass, M_1. The energy of the scattered ion is given by E_1, with a scattered angle of θ. A is equal to the ratio of the mass of the scattered electron to that of the incident ion. If A is greater than 1 the positive sign is used and vise versa.

Gas Chromatography (GC)

Introduction

Gas chromatography is used to separate components by running a mobile phase, an inert gas such as hydrogen, nitrogen, or helium etc., through a stationary phase. The components of the product are separated by attraction to the stationary phase, which is typically found as a packed column or capillary. Each column is designed to separate specific components with various packings, length, and width. The mobile phase flows through the column carrying the components to be separated, and the column is heated to a desired temperature to allow for proper separation of the peaks corresponding to each component. After the components have been separated they are then analyzed by separate

detectors. The two detectors used for the cyclotrimerization of acetylene to benzene reaction were the Thermal conductivity detector and the Flame ionization detector.

Thermal Conductivity Detector (TCD)

The TCD diagram is shown in figure 5. The two main advantages of TCD are (1) chemicals are not destroyed during analysis and (2) TCD is able to identify nearly any chemical compound. Although the TCD is very versatile, it possesses a major disadvantage at low concentrations where the sensitivity is greatly reduced.

The TCD contains four electrically heated tungsten-rhenium filaments in a Wheatstone bridge configuration, which allows for amplification of changes in the resistance. This change in the resistance is due to the difference in the temperature of the filaments. The flow of the mobile phase with the separated components across two of the filaments carries the heat away from the filaments at a constant rate. The other two filaments are maintained at a set temperature by flowing the reference gas with very high thermal conductivity, typically helium. The sample being analyzed, after leaving the column, removes less heat from the filaments and a peak forms if the conductivity is lower than Helium. The peak area depends on the temperature, and thus resistance, difference between the filaments with the reference gas and the separated analysis gas.

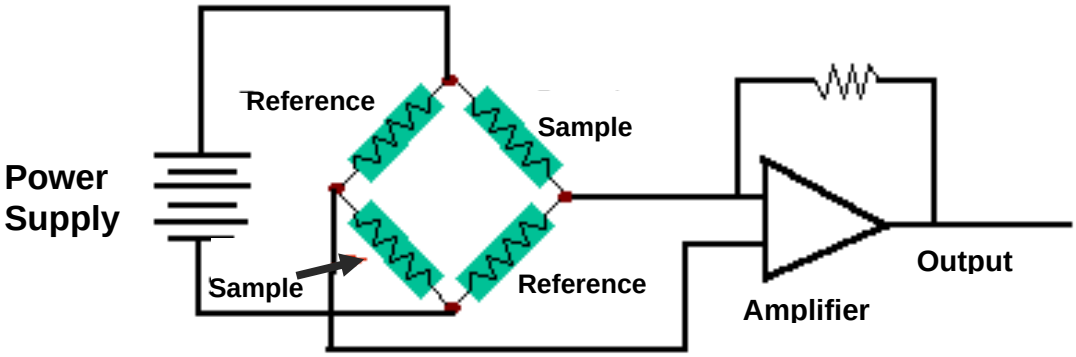

Figure 5: Detailed schematic of the different components of the thermal conductivity detector (TCD). [13]

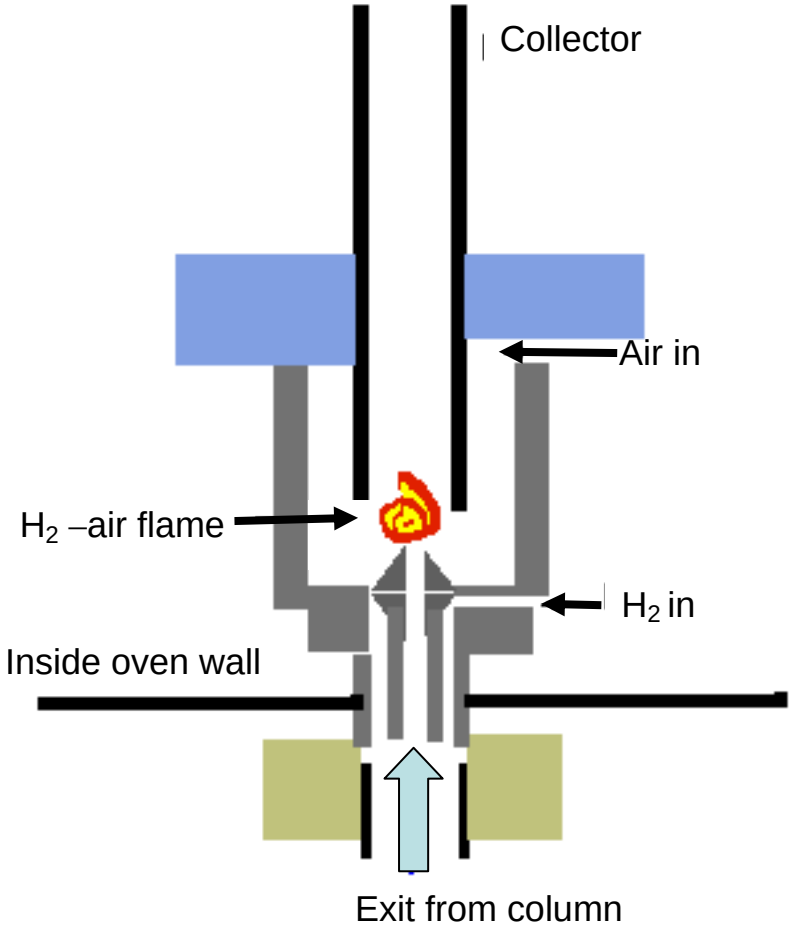

Figure 6: Detailed schematic of the flame ignition detector (FID).

The compounds are identified in the time it takes for them to exit the column. After the sample is analyzed by the TCD, the same sample can be then processed by an FID, allowing for a double analysis approach.

Flame Ionization Detector (FID)

It is possible to use a flame ionization detector independently or in conjunction with a TCD once the sample has been separated. As its name suggests this detection method involves combusting the chemical compounds in a small flame with H_2 in dry air as the fuel. The schematic in Figure 6 shows a minute jet of the sample gases located inside a cylindrical electrode where a few hundred volts is applied between the sample jet and the electrode. When the sample is combusted a current of electrons or ions develops and is collected at the cylindrical electrode. This current is then amplified and the analogue signal is sent to a recording device. The nature of this detection technique is limited to compounds that can be combusted such as hydrocarbons. However, the main advantage of the FID comes when analyzing extremely low concentrations. The low background signal is due to the ions or electrons from the fuel used to ignite the flame and is typically very small when compared to the strong signal of the compounds.

Experimental Configuration

The GC used for all experiments in the high pressure reactor is the Varian 3400 Cx series and is directly connected to the high pressure reactor via a liquid nitrogen trap and six way valve. The gases flowing through the GC were calibrated utilizing a bubble flow meter. The carrier gas was UHP (99.999%) Helium with a flow rate of 30ml/minute, UHP oxygen (99.999%) with a flow rate of 200ml/ minute, and pre-purified (99.995%) hydrogen flowing through the FID at 30ml/minute. The six-way valve allows the gases to flow from the reactor into a liquid nitrogen trap. This allows for a majority of the product gases to be trapped prior to transfer into the GC. After the product has been sequestered in the liquid nitrogen trap it is then allowed to flow through the GC column by turning the six-way valve. Closing off the flow from the reactor permits the carrier gas to flow through the liquid nitrogen trap and through the GC column, which is heated in the GC oven. Following separation the products go through, first, a TCD and secondly a FID to analyze the gases. [12]

CHAPTER III

Rh(111) OXIDATION AND CO OXIDATION ON Rh(111)

Pure Oxygen on Rh(111)

Rhodium, along with platinum and palladium, is a key late transition metals used in a plethora of reactions, the most important being automotive catalytic converters for pollution abatement. However, there has been limited study at higher pressures.[3, 24-61] A previous steady-state study at low pressures (less than 10 torr) on Rh(100) revealed high coverages of CO adsorbed on the surface suppressing CO_2 formation. [39] Kinetic studies of CO oxidation comparing single crystals of Rh and supported Rh/Al_2O_3 catalysts showed favorable agreement in both the apparent activation energies and the specific reaction rates. This argument supports the use of a single crystal model catalyst.[61] Chemisorbed O on Rh is considered to be an ideal candidate for CO oxidation than bulk oxides.[62-67] However, as *in situ* technologies improved and were able to be employed at higher pressures the focus turned to the intermediate oxides, those between the chemisorbed and bulk oxides, as a possibility for the most reactive surface for CO oxidation. Multiple studies were performed to understand the oxidation of Rh(111) and quantify the tri-layer Rh surface structure.[62, 63, 68-74]

The study of the tri-layer oxides opened debate as to the previous determination of chemisorbed oxygen as the dominate surface species during

CO oxidation on Rh and other Pt-group metals. The (9x9) tri-layer surface oxide is more stable than the chemisorbed oxygen surface. In figure 7 a bulk oxide was created by exposing a Rh(111) single crystal to high pressure (10 torr) oxygen at 800K.[75] The single crystal was then transferred to the XPS *in vacuo* via a gate valve and XPS spectra taken with an O 1s/ Rh 3d5/2 ratio of ~0.4 at a binding energy, ~529.7eV, indicative of bulk oxide.[71,74] The bulk oxide is then successively heated in vacuum to higher temperatures and maintained at that temperature while the spectra was recorded. At each temperature interval XPS spectra were taken after the sample was stabilized at that temperature. As low as 550K there is a peak shift (figure 8) and a significant decrease in the intensity of the peak (figure 7) indicating a change in the structure of the oxide. This correlates well with the stable (9x9) oxide described by Gustafson et al. who reported a DFT calculated binding energy for the O 1s peak of ~529.5eV.[76] The intensity and position remain constant until 700K where the peak area begins to diminish. Here the peak has not shifted to the higher binding energy in an intermediate state with a portion of the surface decomposing to chemisorbed oxygen and while the remainder maintains thin oxide character. After heating the single crystal to 800K there is a sudden shift to a higher binding energy correlating to the binging energy reported for the chemisorbed oxide with a coverage of $^3/_4$ML and a superstructure of (2√3 x 2√3) R30◦. At this point the kinetically stable (2√3 x 2√3) R30◦ dominates the surface filling the

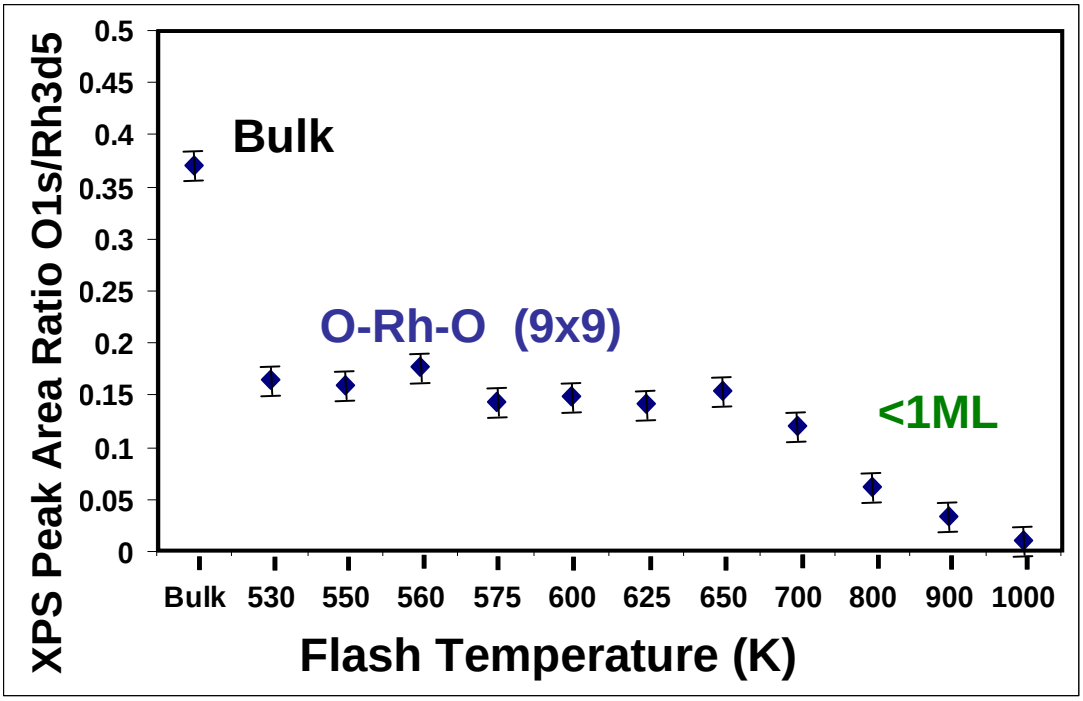

Figure 7: XPS peak area ratio of O/Rh as a function of the flash temperature.

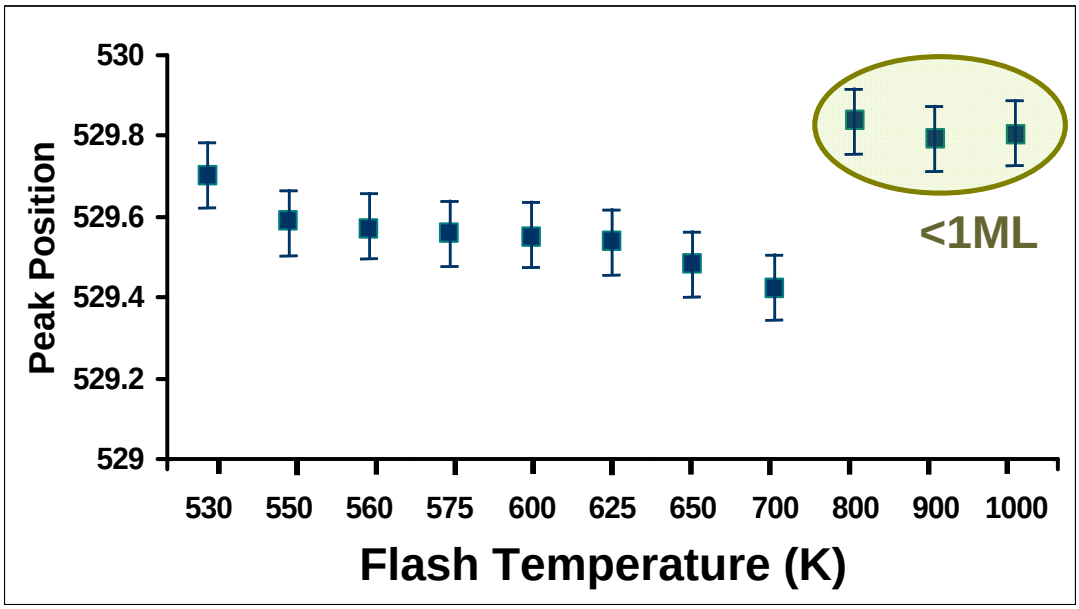

Figure 8: Peak position as a function of the flash temperature after formation of a bulk metallic oxide. The sudden shift at 800K is where the oxide devolves in to a chemisorbed oxygen layer.[75]

fcc and the hcp sites.[67] Subsurface oxygen is not found for this structure since the O 1s cannot be divided into two separate peaks as it can be for the tri-layer oxide. Subsequent to the densely packed chemisorbed surface the peak continues to attenuate while the binging energy remains constant and forms a p(2x1) chemisorbed O pattern at a coverage of 0.5 at ~900K.[64,66,67,71, 74,77-82] By 1000K there is no oxygen remaining as the XPS spectra matches the clean Rh(111) metal spectra.

Lundgren et al., showed the reactivity of the (9x9) Rh(111) tri-layer oxide comparing it to the chemisorbed p(2x1). [71] Utilizing XPS they were able to show the progression of spectra as a function of time when the surface was exposed to CO. The study concluded the 0.5ML chemisorbed O surface initially reacted faster with the impinging CO; however, quickly diminished as the amount of chemisorbed O was used in the reaction. During the oxide reduction by CO the (9x9) tri-layer oxide was not initially reactive and took approximately 1000 seconds before reduction began. The reduction started at CO uninhibited defect sites, as supported by STM images showing islands of the chemisorbed oxygen phase p(2x1) developing at defect sites and spreading out at the boundaries. Here the (9x9) oxide acts as a reservoir replenishing the oxygen for the chemisorbed O islands to sustain the reduction of CO for a longer period of time. As more of the uncoordinated Rh are exposed the number of adsorption sites for CO increases and the reaction propagates until the tri-layer oxide of O-Rh-O reduces to the p(2x1) chemisorbed phase. The reduction then continues at

the same rate until the surface is depleted of oxygen. The initial rate of reduction on the chemisorbed oxygen exceeded that of the (9x9) tri-layer oxide, which maintained a constant rate even when the surface became predominantly chemisorbed oxygen. However, the p(2x1) surface, with 0.5ML of oxygen, remained active only as long as the probability was high for a surface CO and O to encounter to occur.[71] It is clear from this study the (9x9) tri-layer oxide is less reactive than the chemisorbed O for reduction by CO at a pressure $1.5x10^{-8}$ torr.

To subvert the decline in yield the depleted oxygen will need to be recharged at the correct rate on the p(2x1) surface so a balance of O and CO is created on the surface. This entails increasing the oxygen in the reactants above the stoichiometric value and will be discussed further in the chapter.

Pure CO on Rh(111)

Before investigating CO oxidation on Rh(111) the interaction of CO with clean Rh(111) will be explored. Figure 9 shows the interaction of CO at a pressure of $1x10^{-7}$ torr at various temperatures. At 300K the CO saturates the surface with a maximum coverage, which remains saturated from 300K to 425K where the intensity begins to diminish. The amount of CO on the surface

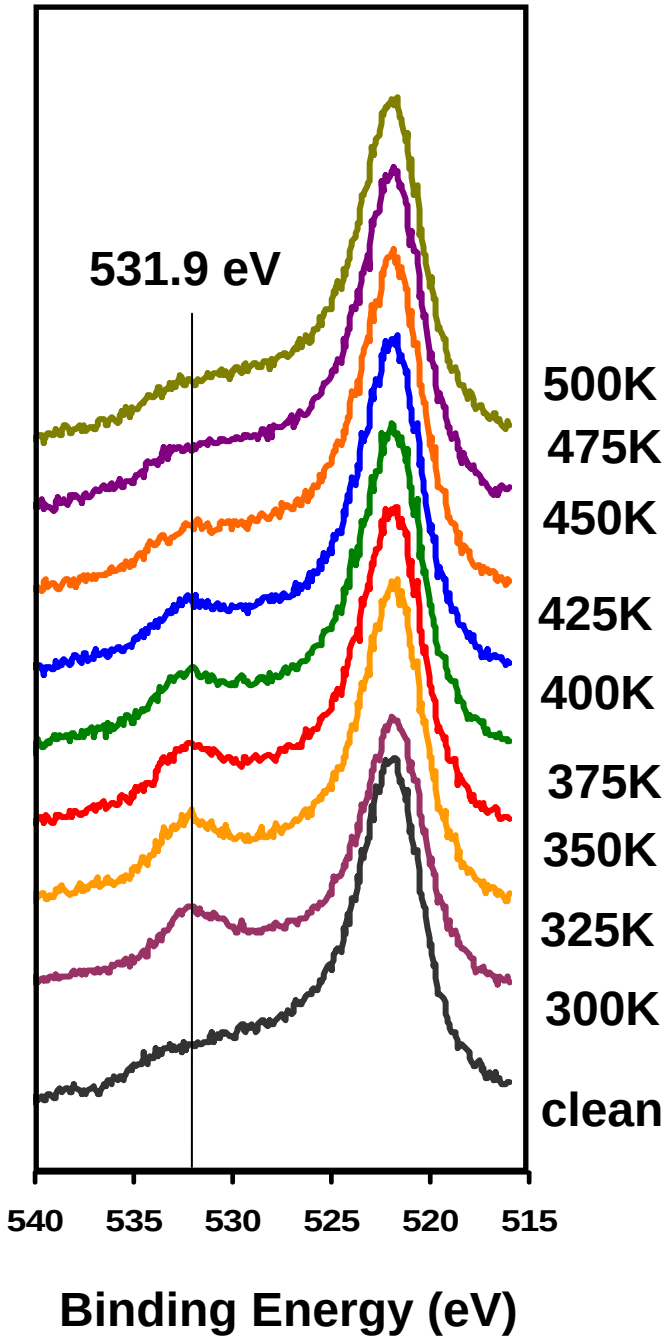

Figure 9: Pure CO adsorbed at 1x10^{-7} torr at various temperatures. The peak attenuation begins ~425K and vanishes by ~500K. Peak saturates at 300K and is correlated with 1/3ML.

decreases in the XPS spectra from 425K and completely disappears at 500K (figure 10). The binding energy of the O 1s peak (from the oxygen in CO) and the binding energy of the C 1s peak (not shown) remained consistent from 300K to 500K. These results correspond well with recent PM-IRAS results at a higher pressure of $1x10^{-5}$ torr revealing atop positions for CO alongside adsorption on three-fold hollow sites. [63, 75, 83-85] Above 425K, where the XPS peak begins to attenuate, the CO at the three-fold hollow sites begins to disappear as seen in figure 11. The atop CO feature at ~2060cm^{-1} are seen to shift toward a lower frequency and diminish as the temperature increased (figures 11 and 12). The highest intensity of the atop CO feature occurs at ~425K and comparing this result with that of previously published studies reveals a maximum CO coverage of $^1/_3$ ML.[75] The XPS spectra does not discriminate between the atop and three-fold CO adsorption sites as with the PM-IRAS data yet the coverage of both is similar and the maximum coverage of $^1/_3$ ML is used in figures 9 and 10.

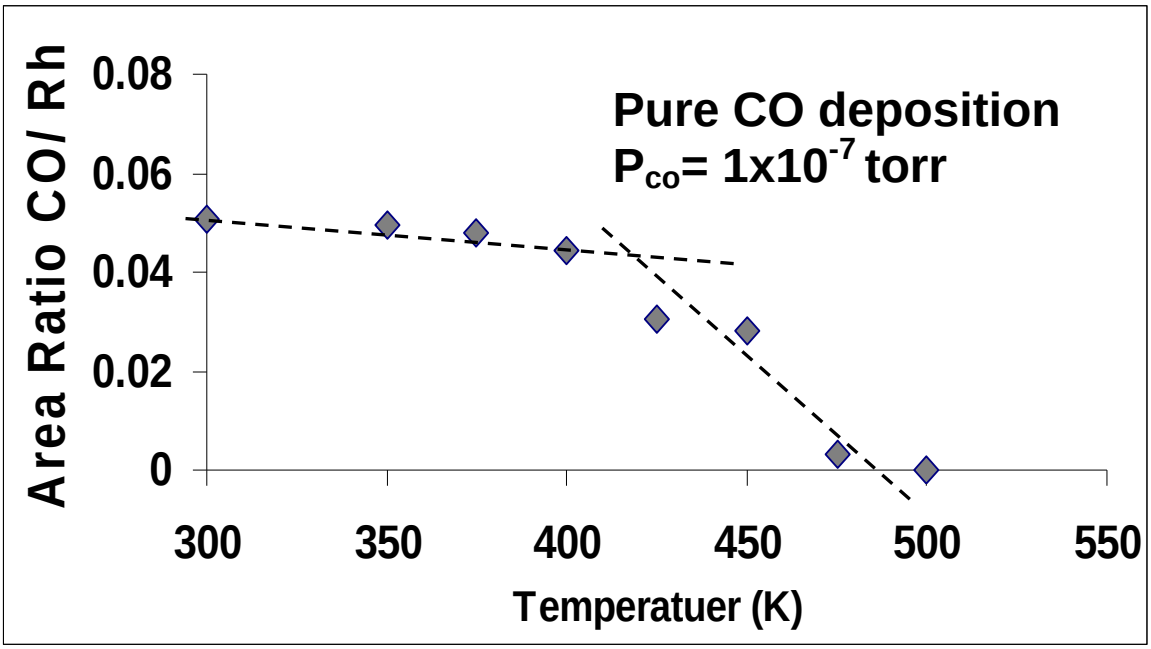

Figure 10: XPS spectra plot of pure CO adsorbed at 1x10^{-7} torr at various temperatures on Rh(111).

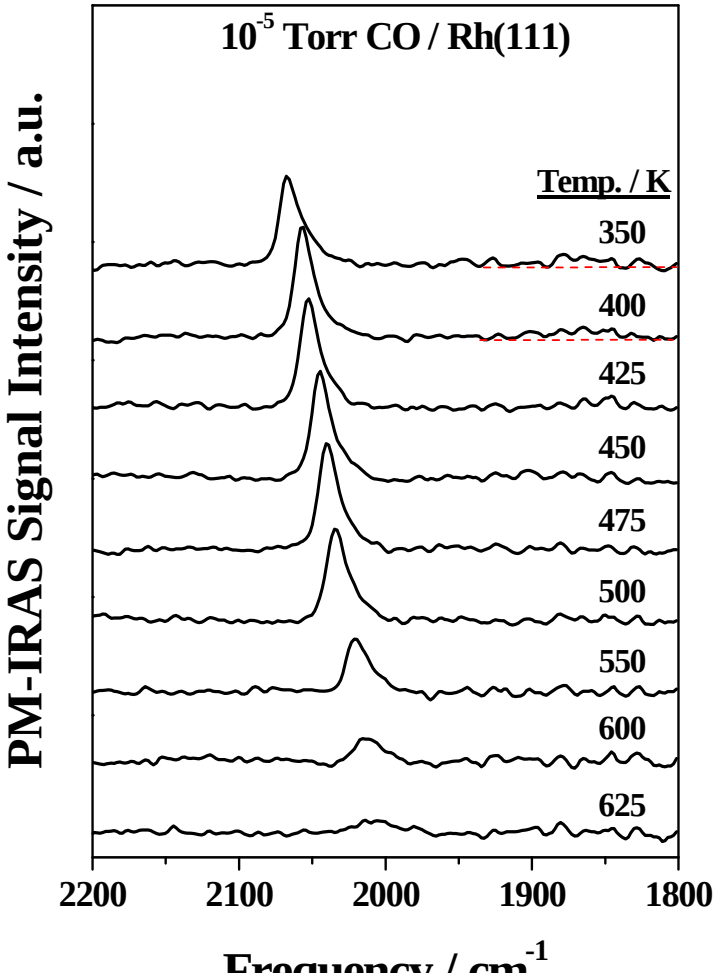

Figure 11: PM-IRAS spectra of 1x10^{-5} torr of CO on Rh(111) as a function of reaction temperature.[73]

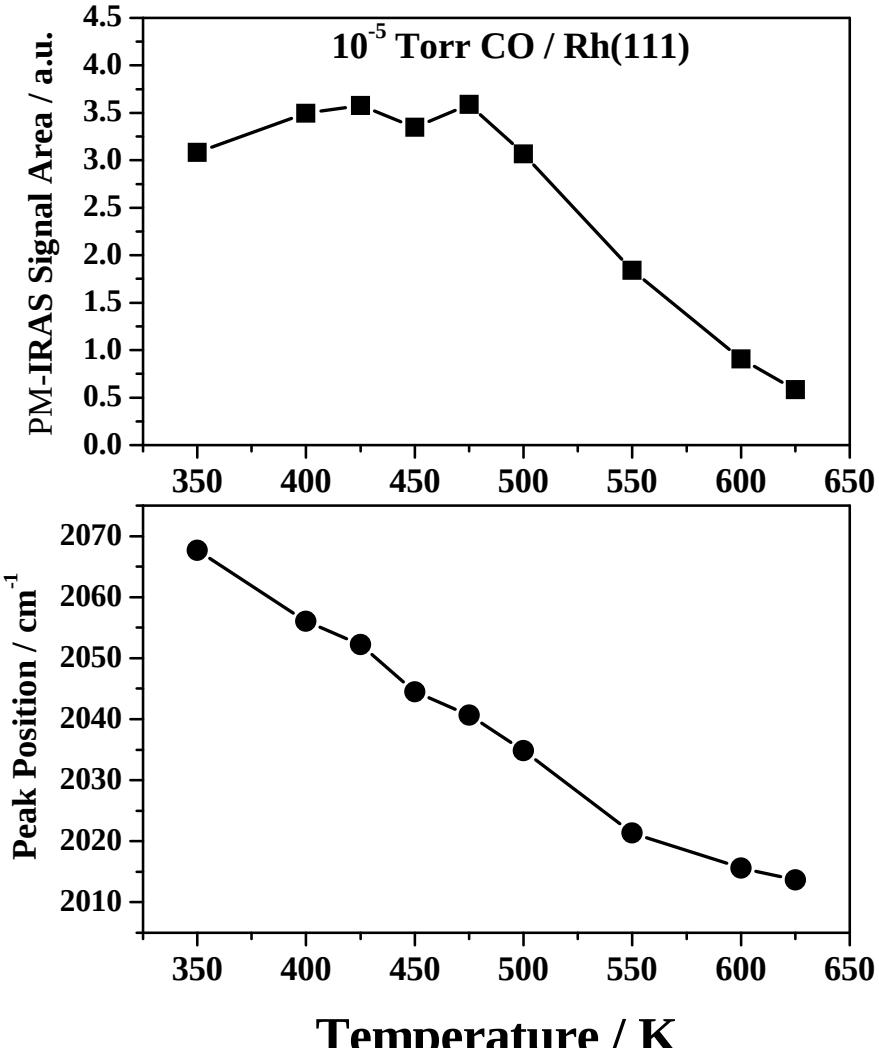

Figure 12: Integrated CO signal area and vibrational frequency of atop CO as a function of reaction temperature.[73]

Low Pressure Steady-State CO Oxidation over Rh(111)

In oxygen rich conditions, where a chemisorbed layer is formed on Rh, there is accelerated CO_2 formation. Rh oxidizes at lower oxygen partial pressures than both Pd and Pt due to a higher oxygen adsorption energy of 234kJ/mol. This makes Rh an excellent metal for forming oxide surfaces at low oxygen partial pressures.[34, 40-42] Under these oxygen rich conditions the surface displays unusual characteristics such as kinetic oscillations and bi-stability.[86-88] As previously mentioned, the actual surface for the optimal CO oxidation rate has been disputed with the advent of further Pt-group metal oxidation studies at elevated pressures. Low pressure steady-state reaction studies performed in typical UHV conditions reveal a bulk oxide of Rh metal is the most inactive followed by the thin (9x9) tri-layer oxide, and supporting evidence reveals the presence of a chemisorbed surface during CO oxidation.[9] Further investigations of steady state reactions at low pressures are presented here.

The experiments were set up by first preparing the mixed gases for a variety of compositions, in separate glass bulbs prior to introduction into the chamber, to insure proper mixing. The gas mixtures were then introduced into the preparation chamber via a leak valve positioned in the preparation chamber. Each experiment maintains a specified pressure and $CO:O_2$ ratio in the chamber while the temperature is altered and XPS taken *in situ*. An XPS spectrum is taken at the designated temperature after waiting five to eight minutes to

achieve steady-state and takes four minutes to complete once started. When all of the spectra are finished the background is subtracted and the area under the O 1s curve is analyzed by defining two separate symmetrical Gaussian curves for CO and O. The area of the separated peaks is then compared with the Rh $3d^5/_2$ peak area to create a comparative ratio as a function of the surface temperature at various pressures and composition mixtures. Once plotted, as in figure 13 for the 1:1 $CO:O_2$ ratio, the surface coverage of CO and O_2 as a function of temperature can be compared by increasing the partial pressure of the oxygen or changing the pressure in the chamber. From these plots and kinetic measurements, performed with a mass spectrometer, the ratio of CO and O on the surface during the highest CO_2 formation rate can be deduced. [73]

As seen in figures 13-17 the total surface coverage remains constant with minute changes of the O 1s peak area, well with in an error range, showing the surface maintains a consistent coverage as the temperature is increased. However, as the temperature is increased, the surface transforms from a CO uninhibited surface to that of an oxygen dominated, CO inhibited surface. The oxygen on the surface is known to weaken the CO-Rh bond in comparison to that of pure CO on clean Rh metal.[63,65,70,71,78,85,89,90] The CO deconvoluted peak disappears at a lower temperature for the 1:1 $CO:O_2$ ratio and at even lower temperatures for the more oxygen rich mixtures of 1:5 and 1:10 than the deconvoluted O peak.

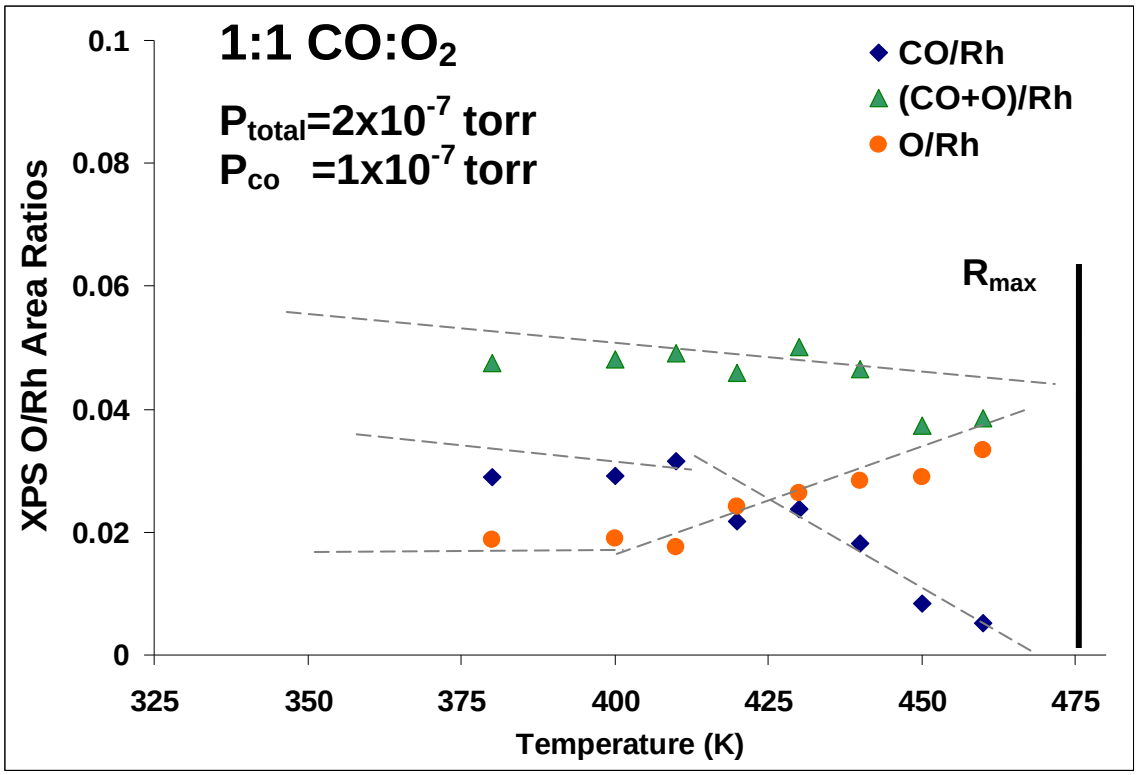

Figure 13: XPS peak area O/Rh ratio as a function of temperature of a clean Rh single crystal exposed to 1:1 $CO:O_2$ at a total pressure of $2x10^{-7}$ torr. R_{max} denotes the temperature with the highest CO_2 formation. There is an error of ± 0.01 in each of the datum points.

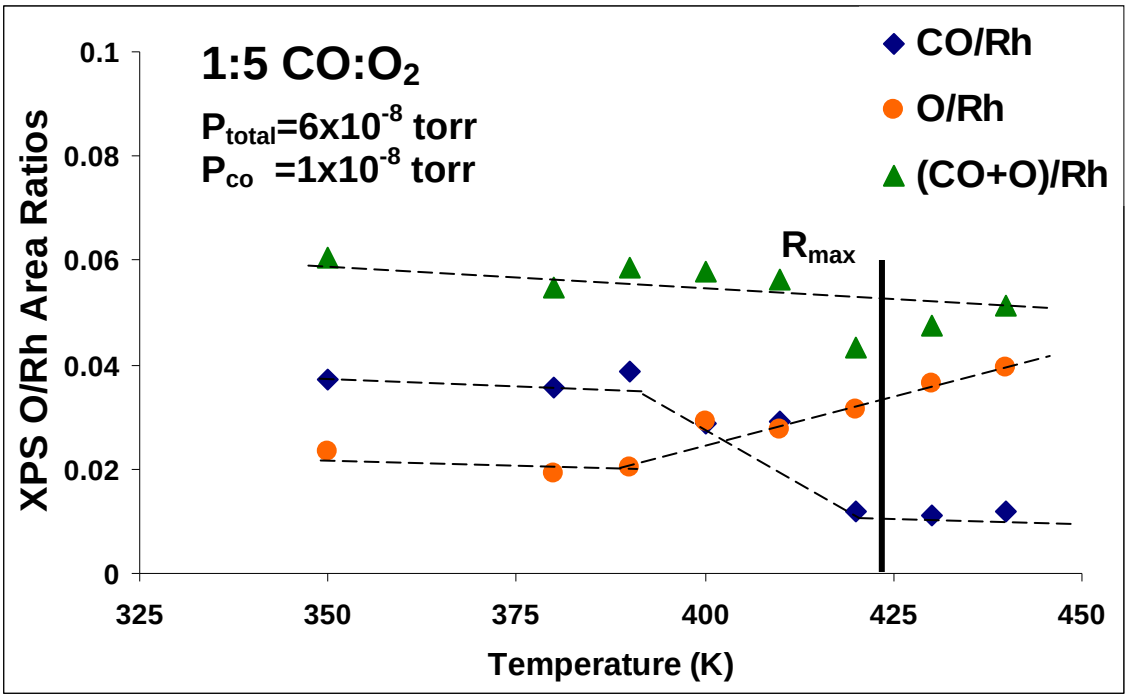

Figure 14: XPS peak area O/Rh ratio as a function of temperature of a clean Rh single crystal exposed to 1:5 $CO:O_2$ at a total pressure of $6x10^{-8}$ torr. R_{max} denotes the temperature with the highest CO_2 formation. There is an error of ± 0.01 in each of the datum points.

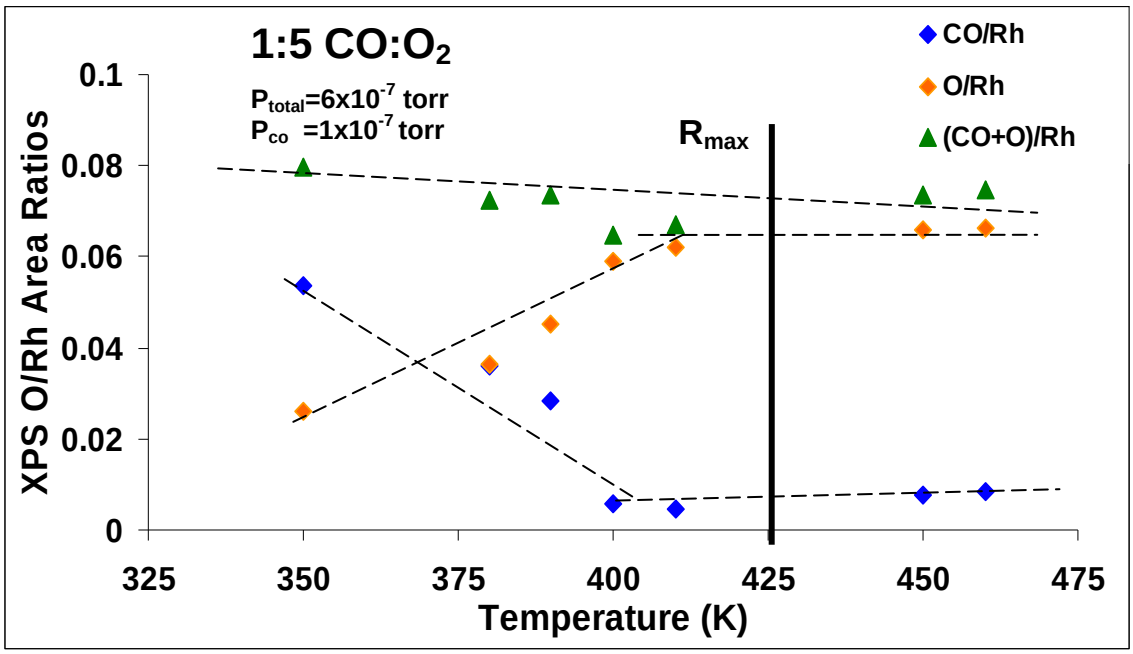

Figure 15: XPS peak area O/Rh ratio as a function of temperature of a clean Rh single crystal exposed to 1:5 $CO:O_2$ at a total pressure of $2x10^{-7}$ torr. R_{max} denotes the temperature with the highest CO_2 formation. There is an error of ± 0.01 in each of the datum points.

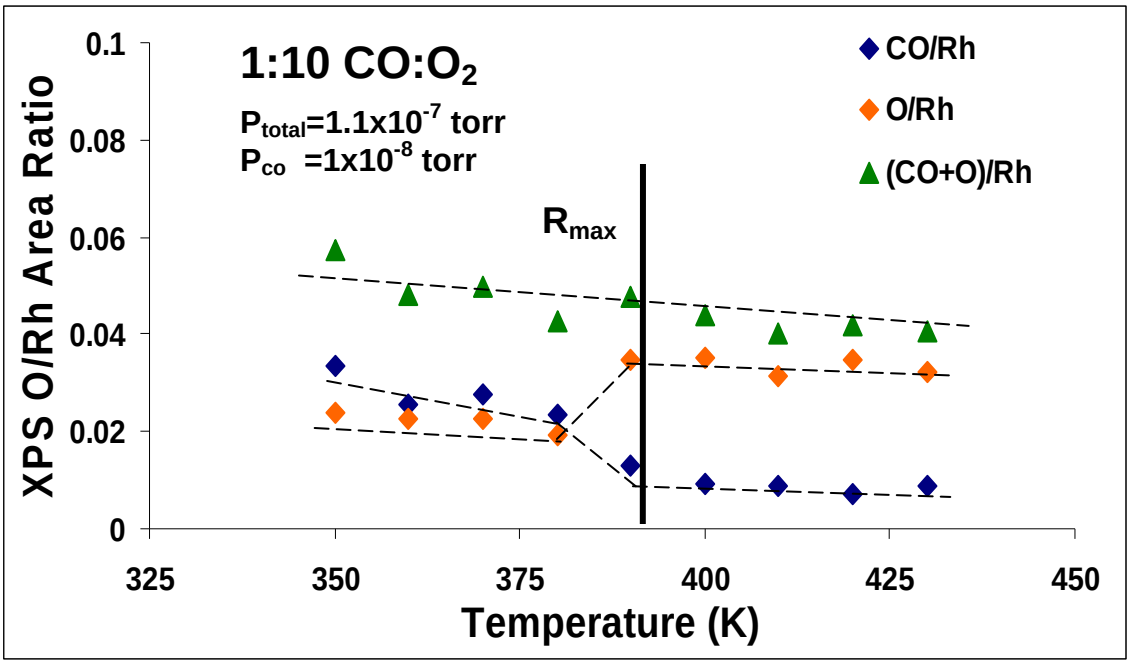

Figure 16: XPS peak area O/Rh ratio as a function of temperature of a clean Rh single crystal exposed to 1:10 $CO:O_2$ at a total pressure of $2x10^{-7}$ torr. R_{max} denotes the temperature with the highest CO_2 formation. There is an error of ± 0.01 in each of the datum points.

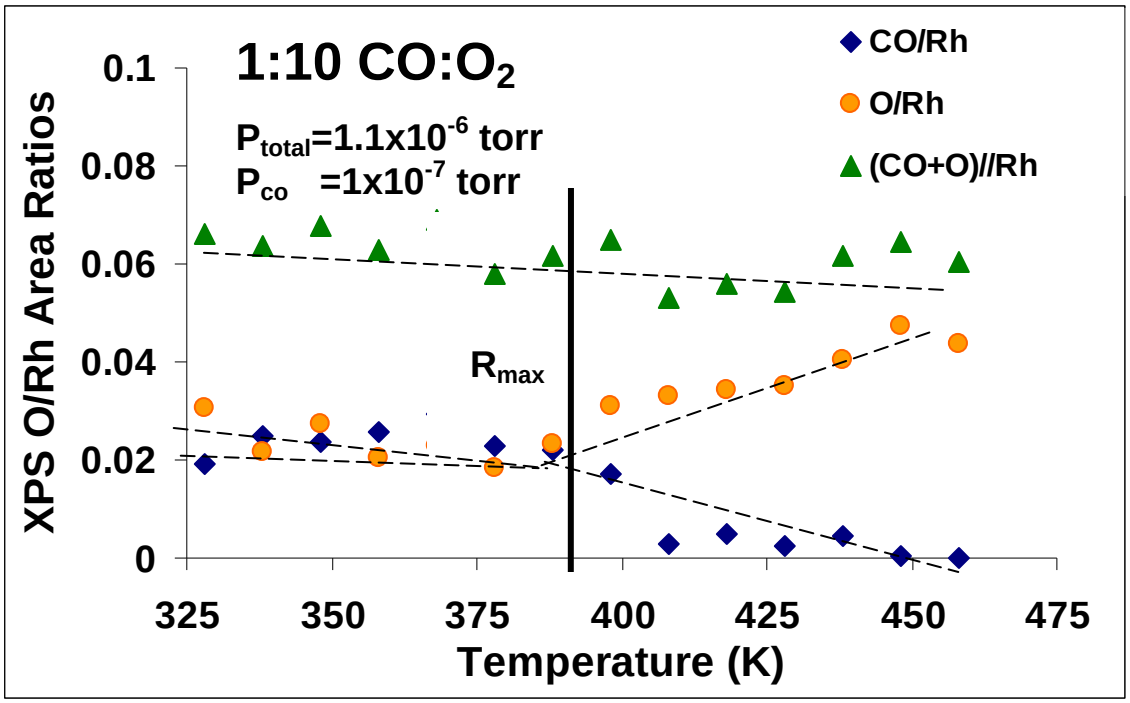

Figure 17: XPS peak area O/Rh ratio as a function of temperature of a clean Rh single crystal exposed to 1:10 $CO:O_2$ at a total pressure of $2x10^{-6}$ torr. R_{max} denotes the temperature with the highest CO_2 formation. There is an error of ± .01 in each of the datum points.

At each individual ratio and pressure the surface, during the highest CO_2 production, is dominated by oxygen. For the 1:1 ratio the peak CO_2 formation occurred at ~475K as shown in figure 13 as R_{max}. These results are in agreement with PM-IRAS studies showing a CO inhibited surface. [73] Increasing the amount of oxygen in the mixed gas while maintaining a CO partial pressure, producing a $CO:O_2$ ratio of 1:5, lowered the temperature at which the highest CO_2 formation, R_{max}, occurred. Additionally, the surface composition for the 1:5 $CO:O_2$ ratio maintained an oxygen dominated/ CO inhibited surface at the maximum of CO_2 formation. The temperature for $R_{max,}$ at a $CO:O_2$ ratio of 1:10, continued to decrease and became close to crossing the junction from a O dominated surface to one where the fraction of CO is nearly equivalent to O on the surface as can be seen in figures 16 and 17. A slightly lower R_{max} is found, for identical ratios (1:1, 1:5, 1:10) at lower CO partial pressures. The major trends are reiterated in figure 18 using IRAS. The fraction of O coverage on the surface at $R_{max,}$ shown in figure 18, decreases as the partial pressure of O_2 is amplified. Thus, as more O_2 is added to the surrounding environment the amount of O needed on the surface for maximum CO_2 formation, is reduced. As the fraction of O_2 in the reactant gas increased (1:1, 1:5, 1:10), while maintaining a partial pressure of CO (i.e. $1x10^{-7}$ torr), the temperature at which R_{max} occurs decreases. Additionally, figure 18 shows an increase of O_2 in the reactant gas mixture directly correlates with the maximum CO_2 formation (R_{max}) occurring at a higher CO surface coverage.

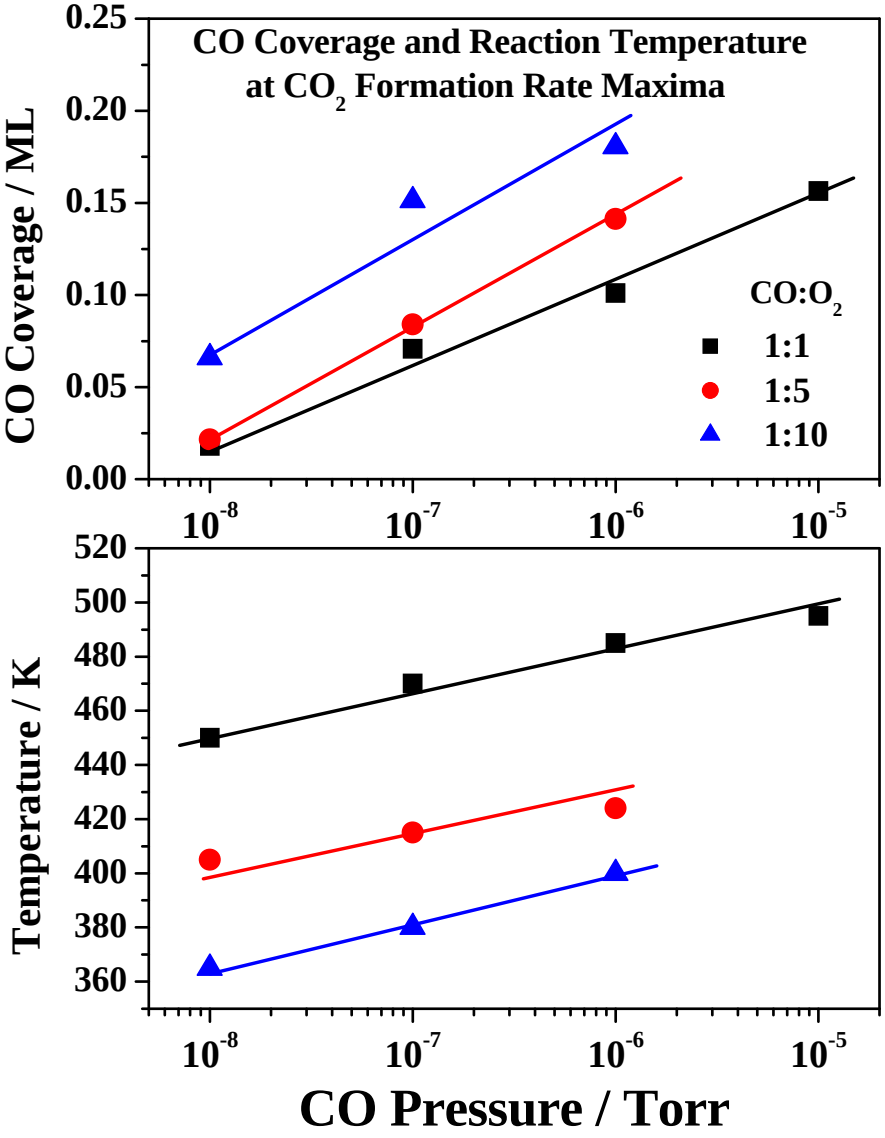

Figure 18: Using IRAS peak area ratios at the maximum CO_2 formation rate the temperature versus CO pressure (Torr) and the CO coverage versus CO Pressure are plotted.

Under low pressure conditions ($P<2x10^{-6}$ torr) XPS and mass spectroscopy are used for determination of surface CO and O coverages and the TOF under various the reaction conditions. The maximum CO_2 formation rate changes with the ratio of $CO:O_2$ and pressure, consistent with previous studies and reflecting a Langmuir-Hinshelwood mechanism.[73] The CO blocks adsorption and dissociation of oxygen. Therefore R_{max} occurs a lower oxygen surface coverage when the partial pressure of oxygen is increased. Thus, with the total surface coverage constant and not dependent on temperature, the lower oxygen coverage means a high CO coverage. After R_{max} is reached it is likely that the surface oxygen begins to penetrate into the sub-surface.[91] The chemisorbed oxygen surface is the most beneficial for CO oxidation; however, it becomes a deactivating agent when the surface coverage extends beyond where thermodynamics favor subsurface oxygen.[73] Even at low coverages (~0.5ML) the oxygen favors the sub-surface position, typically occurring between 390K and 800K.[92] At 400K and $2x10^{-8}$ torr of 1:1 $CO:O_2$ Rh(111) XPS showed oxygen penetration. This is confirmed by previous XPS studies at 400K with pure oxygen. [93] Additionally, the poisoning of the catalyst by sub-surface oxygen gives further verification that the reactivity for CO oxidation follows the trend of chemisorbed oxygen> tri-layer oxide> bulk oxide.

In conclusion, chemisorbed oxygen on Rh(111) has been determined to be the most active surface in the low temperature regime. During CO oxidation no

CO is detected on the surface by XPS or PM-IRAS.[73] XPS was able to confirm that the surface does not lose coverage as the temperature is increased; however, the fractions of CO and O_2 on the surface do change. The R_{max} for increasing oxygen partial pressures (1:1<1:5<1:10) occurred at lower oxygen coverages and R_{max} for 1:1 and 1:5 was greater than the 1:10 with the most oxygen. This trend is explained by the deactivation caused by sub-surface oxygen, which continues to intensify as more oxygen displaces the Rh atoms eventually creating the tri-layer oxide and bulk oxide.

CHAPTER IV

Pt(100) METAL AND CO OXIDATION

Pt(100) Oxidation

Industrial platinum catalysts are responsible for a plethora of reactions from automotive catalytic converters to oxidation of NH_3 in nitric acid synthesis.[94,95] Additionally, Pt single crystals are a preferred model system for heterogeneous catalysis studies for CO oxidation. Large numbers of studies have been carried out under UHV conditions, providing a vast majority of our present-day understanding of this system.[95,96-105] Platinum is a well-known metal used for CO oxidation and possesses superior CO oxidation rates under oxygen rich conditions. Furthermore, it is the most difficult of the Pt-group metals to oxidize, with an oxygen adsorption energy of 188kJ/mol.[95,100,103]

Clean Pt(100) is known to relax into a "hex" phase, first denoted as a (5x20)[100], considered less reactive toward O_2 adsorption than the more difficult to obtain metastable (1x1) phase.[99,100,106, 107] Oxygen adsorbs initially without structural alteration below a coverage of 0.1ML. However, at a coverage of ~ 0.3ML the surface structure quickly changes, as determined by a (1x1) LEED pattern with a high background intensity. This is typically referred to as a disordered (3x1) surface due to the surface patches of various mixed phases. The slow start followed by quick uptake is indicative of nucleation sites

trapping the incoming gas O_2 molecules, thus speeding up the adsorption process.[108] Further confirming the island growth is the development of a "complex" surface structure with a LEED pattern of various groups of spots. This pattern is characteristic of the saturated oxygen over layer of 0.63ML found while cooling the platinum surface below 630K in $3.9x10^{-2}$ torr of oxygen.

A (3x1) phase is formed when Pt(100) is exposed O_2 at 300K corresponding to an oxygen coverage of 0.44ML. This same experiment was reproduced in the analysis chamber of the XPS by dosing ~10,000L of O_2 at 300K (figure 19). Since the O 1s/ Pt 4f7 ratio increases linearly with oxygen coverage and the ratio at 10, 000L is equivalent to a coverage of 0.44ML this relationship can be used to determine surface oxygen coverage in the low pressure regime. [97,98]

A primary obstacle to studying Pt oxidation in a UHV system is the clean off reduction reactions by background CO and H_2 found in a typical UHV chamber.[100] The low reactivity of Pt toward O_2 limits the coverage to a chemisorbed oxygen surface in UHV studies. To overcome this hurdle, techniques are used to replicate the formation of an oxide during high

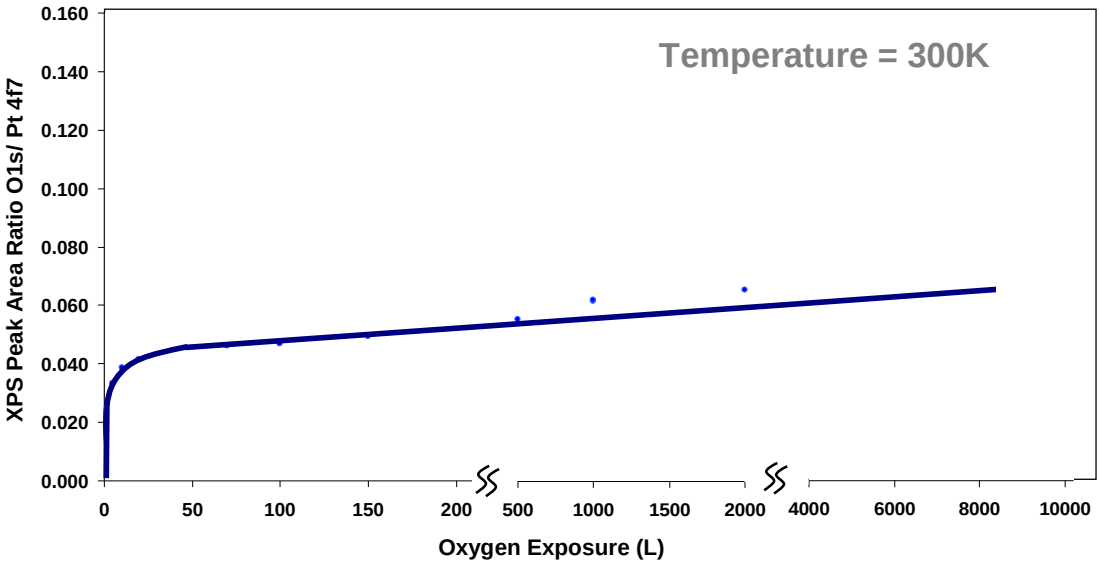

Figure 19: Formation of a chemisorbed surface. Exposed clean Pt(100) to ≤5x10^{-2} torr at 300K for a oxygen coverage of 0.44ML.

pressure conditions such as employing ozone (O_3) as the oxidant [95] or atomic oxygen from a microwave plasma source [99]. These techniques assist in modeling surface conditions during oxidation occurring at higher coverages in UHV; however, utilizing high pressures by means of a high pressure reactor allows for a more complete understanding of metal oxidation and reactions such as CO oxidation on platinum single crystals.[101,108]

XPS was used in combination with the high pressure reactor to develop a thick oxide film. First, the surface was cleaned by sputtering with Argon for 30 minutes E-beam heated to 1200K for 5 minutes and an XPS spectra taken to determine cleanliness. The probe then was moved into the high pressure reactor, which was pressurized with O_2 to 500 torr for 10 minutes and heated to the desired temperature. This procedure was repeated for each temperature (400-700K) and plotted in figure 20 with O 1s/ Pt 4f7 ratio as a function of oxidation temperature. The ratio increases linearly until ~600K, at which point it levels off. Previous studies have shown that the formation of the surface chemisorbed oxygen is found below 450K where the ratio is ~ 0.065 corresponding to a coverage of ~0.44ML.[95,99,100] Below 550K the coverage (~0.63ML) is identical to the previously described complex saturated surface.[97,100] Heating above 600K creates the PtO_2 oxide, as seen previously.[95, 100]

Active Surface for CO Oxidation

One technique to alleviate the challenge of contamination during Pt oxidation is to develop experiments that allow high pressure operation while maintaining the majority of the chamber in UHV. Hendriksen et al., [108] developed a high pressure and high-temperature scanning tunneling microscope (STM) with a flow reactor system. STM is an excellent instrument to use in determining surface structure at the atomic scale. Combining this capability with a high pressure flow reactor and a quadrupole mass spectrometer measuring the gas leaving the reactor the surface structure change and the reactant gas composition can be documented *in situ* under a variety of conditions. However, the composition of the surface can only be analyzed during the preparation of the surface, pre reaction, and post reaction. An STM image can only provide information on surface structure and does not provide a definitive analysis of the composition, as supplied by spectroscopic techniques. Thus the *in situ* measurement is not complete and the surface composition is an assumption. Initially, the Pt(110) surface is cleaned and CO introduced into the reactor at 475K and 375 torr. The flow was held constant at 3.0 ml/min during the entire reaction with only the ratios of CO and O_2 altered to change the reaction conditions. After the initial pure CO flow was changed to pure oxygen, no alterations were seen in the smooth surface.

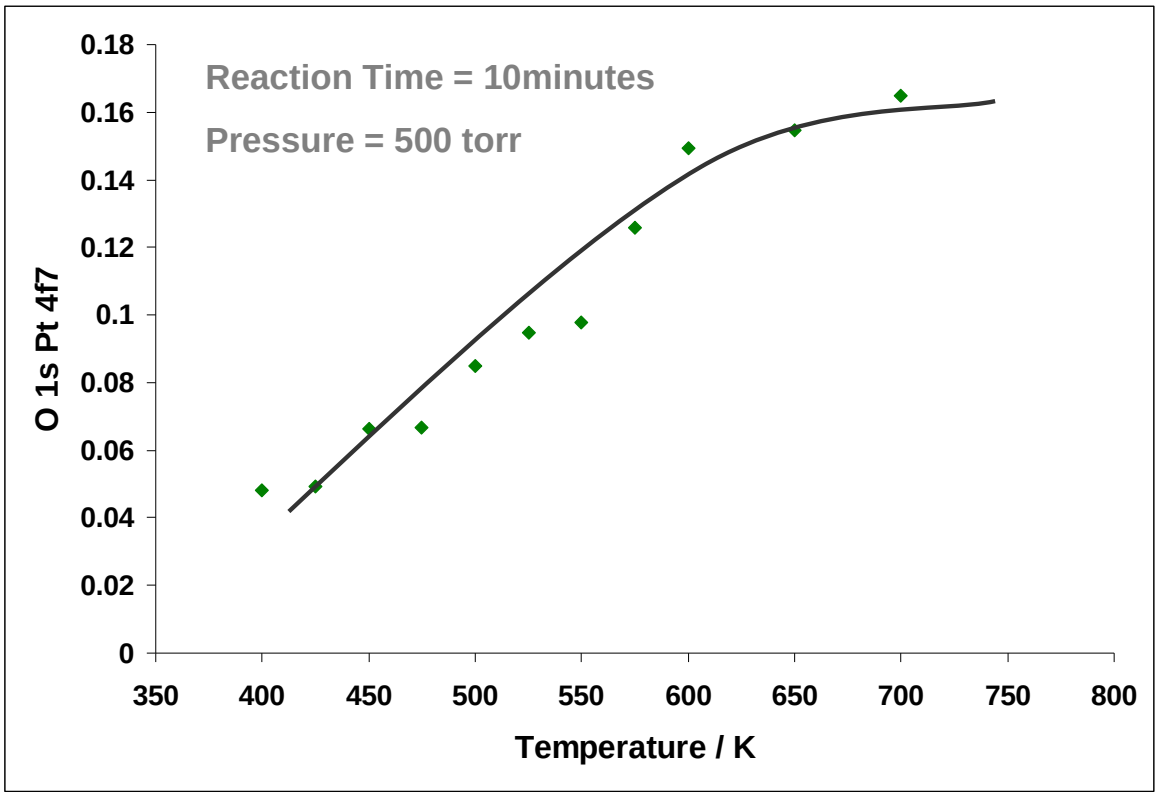

Figure 20: High pressure Pt(100) oxidation. O_2 at 500 torr for 10 minutes and heated to the desired temperature from 400K to 700K. Probe transferred *in vacuo* to analysis chamber.

Conversely, the formation of CO_2 began almost immediately after the CO flow was turned off and the O_2 flow was started. Immediately after, CO began a rapid decline quickly deteriorating into a languid decay of the partial pressure of CO. Once the ratio of $CO:O_2$ reached ~1:37 the rate of CO_2 formation tripled. The surface developed a rougher texture as proven by STM images scanned after the sudden increase in the CO_2 formation. [108]

In order to test this conclusion a Pt single crystal was exposed to 10 torr CO in the high pressure cell with the CO mechanically pumped before adding 500 torr O_2 for 10 minutes while maintaining a temperature of 475K during the entire process. This surface was then compared to the previously described saturated chemisorbed oxygen layer with a coverage of 0.44ML[95] Figure 21 depicts the oxygen coverage after the exposure in 500 torr at 475K along with the formation of the chemisorbed oxygen. This figure clearly shows a surface composed of <1ML of oxygen rather than the oxide surface proposed by studies performed with only a STM. Hendriksen et al. explained, after an increase in catalytic activity, the surface roughness reveals an active surface primarily composed of a thin Pt oxide.[109] However, this surface roughness develops ~400 seconds after the increase in activity and during the decline of in CO_2 formation. Thus the rough surface can be interpreted to inhibit the reaction. More accurately, the highest CO_2 formation is seen directly after the most active surface develops, corresponding to the smooth surface.

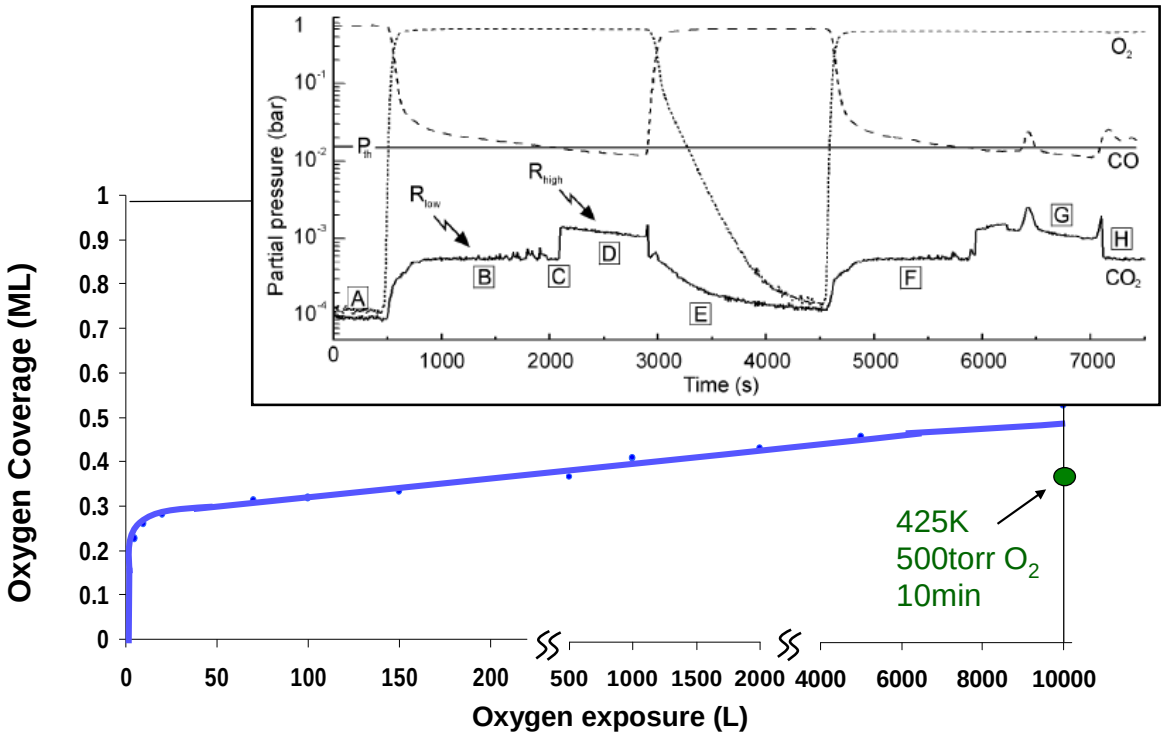

Figure 21: Oxygen coverage after the exposure in 500 torr at 475K for 10 minutes along with the formation of the chemisorbed oxygen. Inset [109] shows the partial pressure of O_2, CO and CO_2 as a function of time.

CO Oxidation on Pt(100) at $CO:O_2$ ratios of 1:1. 1:5, 1:10

Under certain conditions CO oxidation on Pt(100) undergoes oscillations related to the hex to (1x1) transition. [95,100,101] The oscillations are seen at low pressures between a CO partial pressure of ~$3x10^{-6}$ torr and $1x10^{-3}$ torr at ratios far exceeding stoichiometric ratios. [105,106] The temperature at which these oscillations occur depends on the partial pressure of CO, with an upper limit at the CO desorption temperature. [105,110-112] Although the oscillations are not observed under the conditions reported here, the switching back and forth lends credence to a Langmuir-Hinshelwood mechanism for CO oxidation on Pt(100) and oxygen island formation during CO oxidation on Pt(100). [103,105, 106, 113-116]

XPS was used to determine the surface composition during titrations on a clean Pt(100) surface with various ratios of $CO:O_2$. Combined with kinetic studies the surface composition during maximum CO_2 formation can be elucidated. For the $CO:O_2$ ratio of 1:1, an increase in pressure of an order of magnitude, from $2x10^{-8}$ to $2x10^{-7}$ torr, did not alter the temperature at which the O 1s peak disappeared by an appreciable amount and falls within the margin of

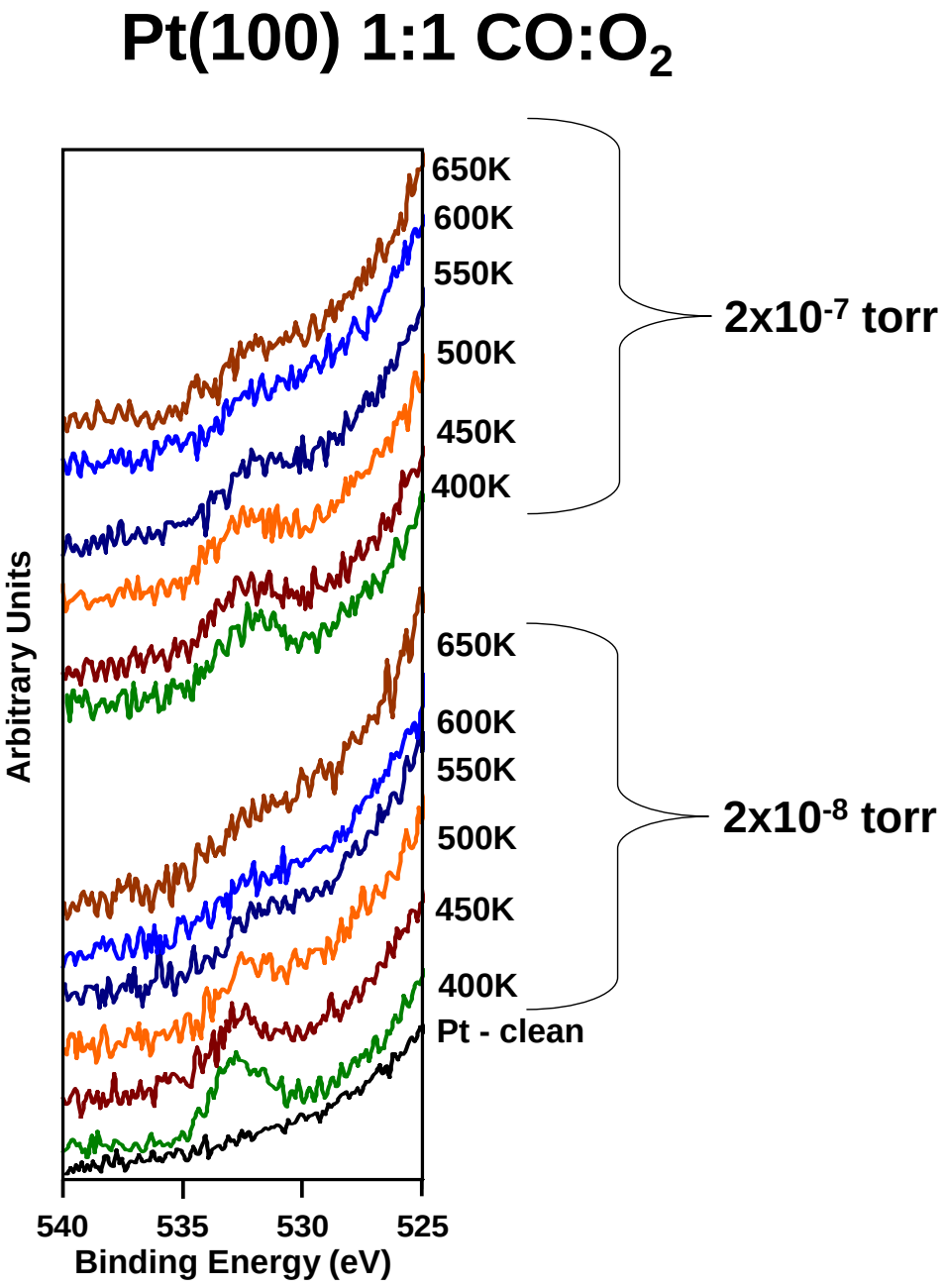

Figure 22: Determination of surface composition. *In situ* XPS used during low pressure CO oxidation reactions. Pt(100) single crystal exposed to $CO:O_2$ ratio 1:1 at $2x10^{-7}$ torr and $2x10^{-8}$ torr.

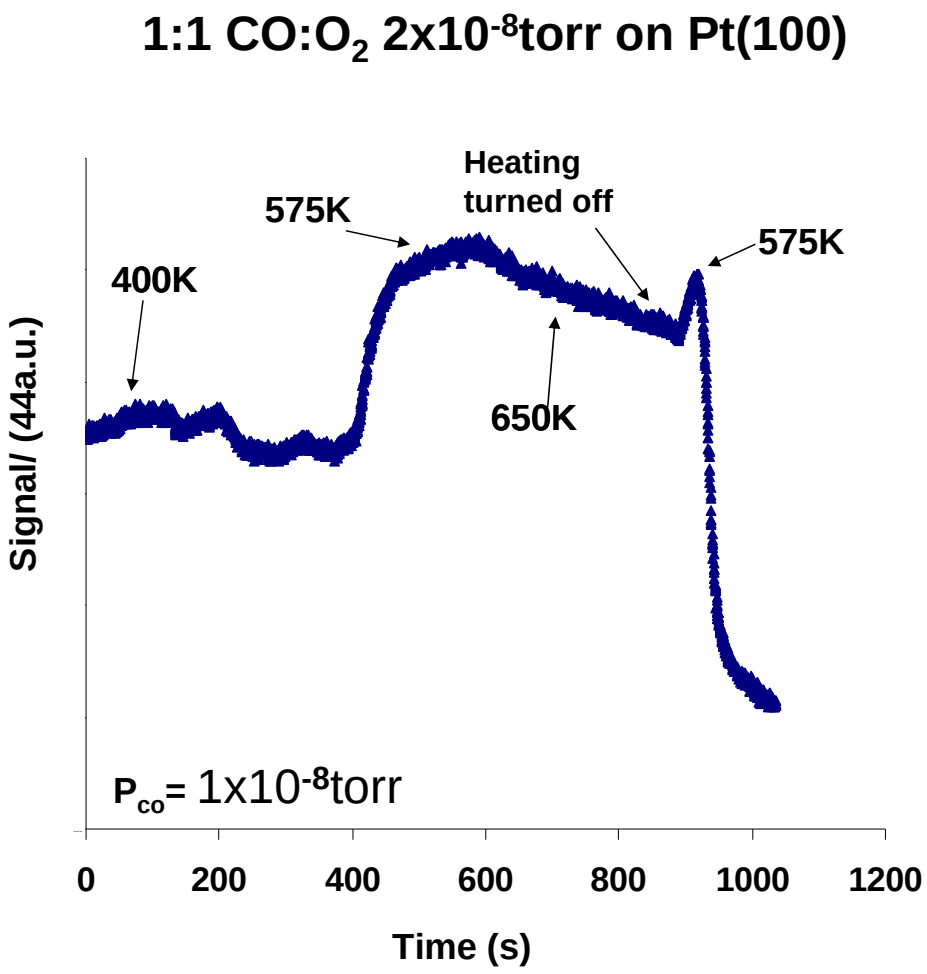

Figure 23: Mass spectrometry used during low pressure CO oxidation reactions to determine the highest relative CO_2 formation. Pt(100) single crystal exposed to $CO:O_2$ ratio 1:1 at $2x10^{-7}$ torr and $2x10^{-8}$ torr.

error for the XPS. Figure 22 shows the XPS spectra for the 1:1 ratio at increasing temperatures. The O 1s peak arises from both the dissociated oxygen and the CO bound to the surface. The CO peak shifts to a slightly higher binding energy than O on Pt, thus the O 1s peak is a combination from both components. The highest turn-over-frequency (TOF) for the $CO:O_2$ ratio of 1:1 is at 575K , unambiguously disputing the assumption that a thick oxide is the most active for CO oxidation (figure 23). By increasing the amount of oxygen by a factor of five in the feed stream from 1:1 to 1:5 (figure 24) there was a very small change in the attenuation of the O 1s peak area. The maximum CO_2 formation occurred at a slightly lower temperature, 550K as seen in figure 25. This result follows the trend on Rh(111) where there is a direct correlation between the decreasing oxygen partial pressure in the feed stream and the temperature at which CO_2 formation peaks exists. The 1:10 ratio (figures 26 and 27) maintains the same relationship with identical XPS spectra and a lower temperature, 525K for the greatest amount of CO_2 formation. Unlike the Rh(111) spectra the Pt(100) O 1s peak cannot, with enough certainty, be separated into CO and O peaks due to the diminished peak area with the thin chemisorbed layer on Pt single crystals in UHV. However, combining XPS with the PM-IRAS can provide a well defined depiction of the Pt surface during CO oxidation at low pressures.[111, 114] Figure 28 is a plot of the XPS spectra summarized showing the attenuation of the O 1s peak as a function of $CO:O_2$ ratio and temperature.

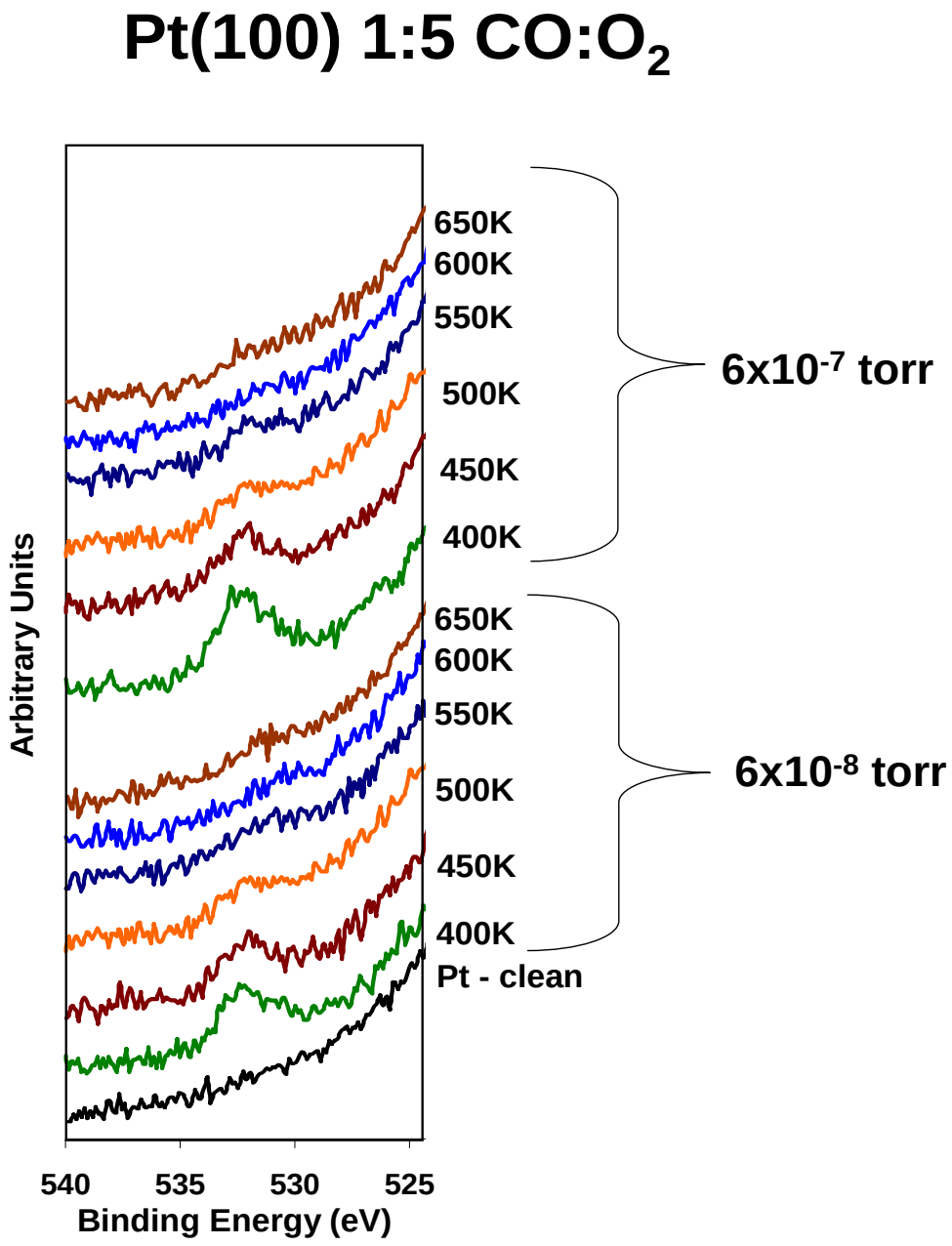

Figure 24: Determination of surface composition. *In situ* XPS used during low pressure CO oxidation reactions. Pt(100) single crystal exposed to $CO:O_2$ ratio 1:5 at $6x10^{-7}$ torr and $6x10^{-8}$ torr.

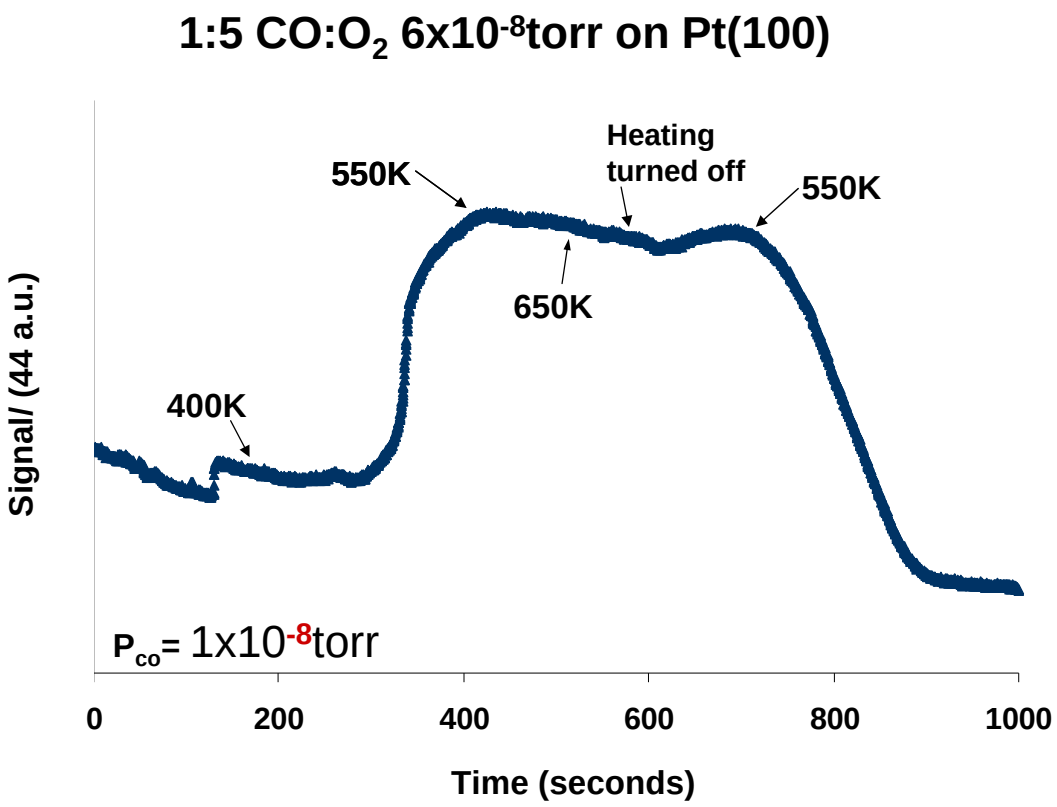

Figure 25: Mass spectrometry used during low pressure CO oxidation reactions to determine the highest relative CO_2 formation. Pt(100) single crystal exposed to $CO:O_2$ ratio 1:5 at $6x10^{-7}$ torr and $6x10^{-8}$ torr.

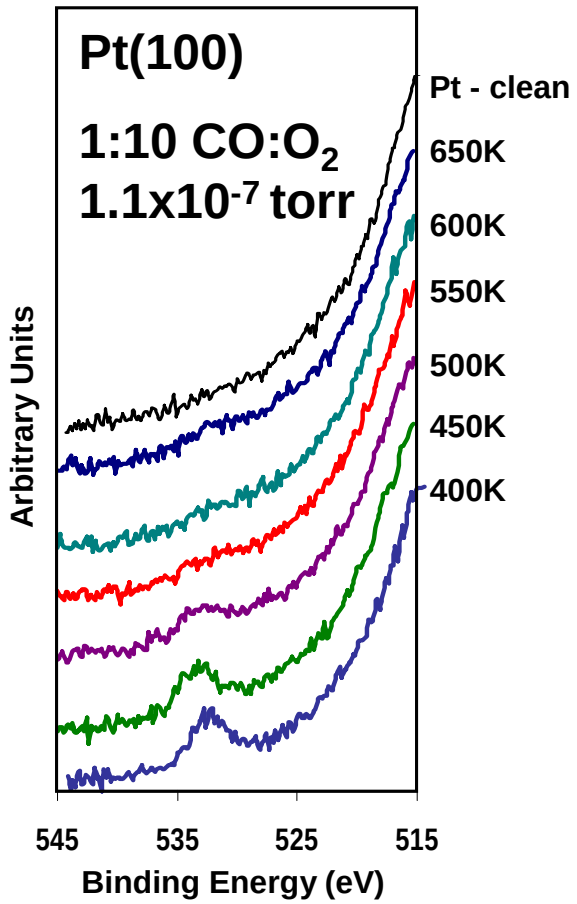

Figure 26: Determination of surface composition. *In situ* XPS used during low pressure CO oxidation reactions. Pt(100) single crystal exposed to $CO:O_2$ ratio 1:10 at $1.1x10^{-7}$ torr.

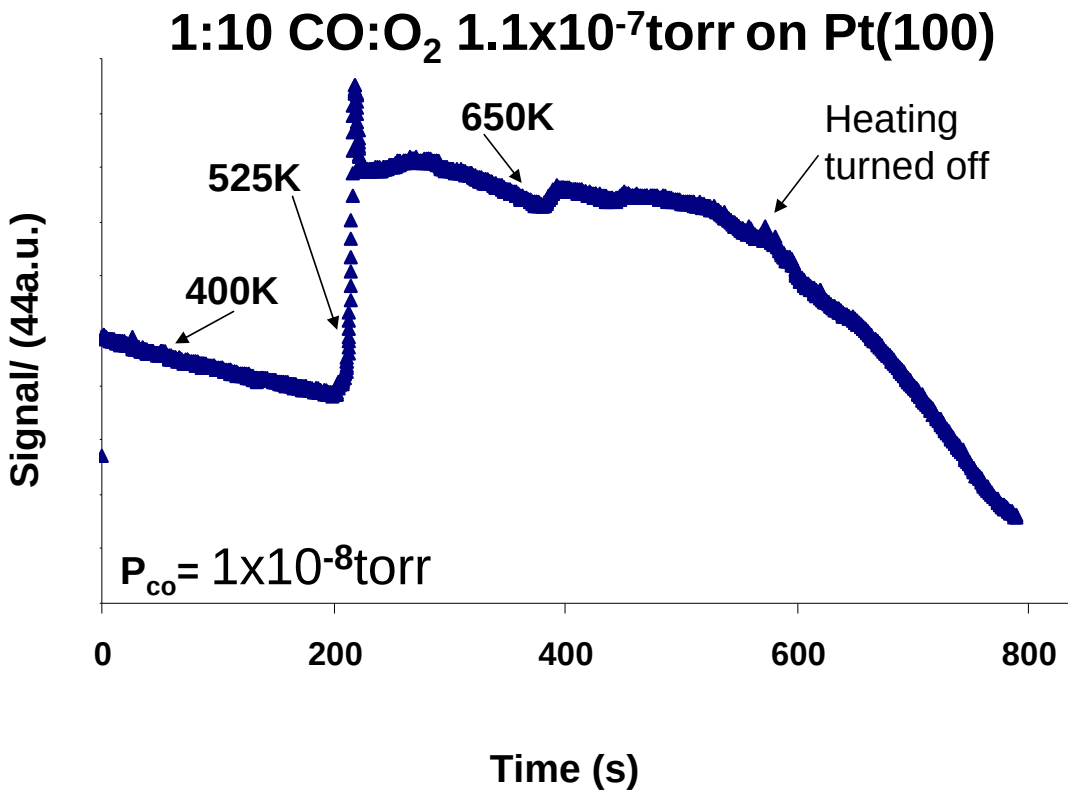

Figure 27: Mass spectrometry used during low pressure CO oxidation reactions to determine the highest relative CO_2 formation. Pt(100) single crystal exposed to $CO:O_2$ ratio 1:10 at $1.1x10^{-7}$ torr.

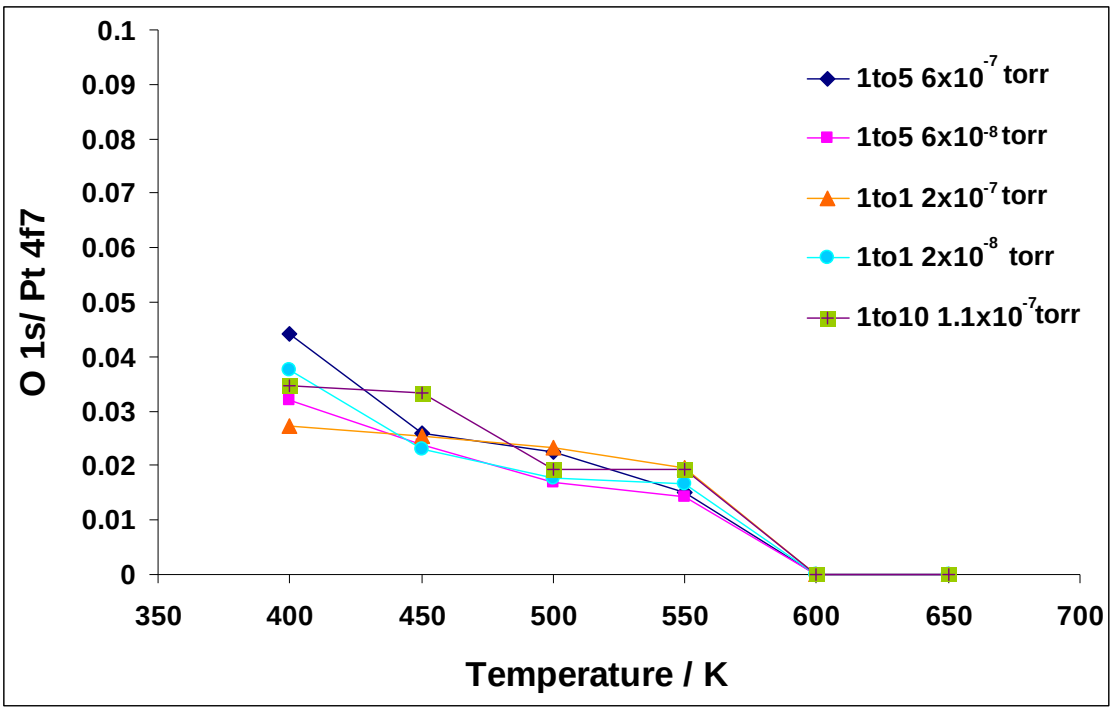

Figure 28: Summary of low pressure reactions with $CO:O_2$ ratios of 1:1, 1:5, 1:10. O 1s/ Pt 4f7 Oxygen.

Although not able to operate at higher pressures, XPS is an excellent tool for determination of surface composition. Low-pressure studies have been proven to scale-up well to higher pressures[111]. Previous studies conclude that during CO oxidation at low and high pressures on Pt the most active surface coverage is a thin Pt oxide rather then the chemisorbed oxygen surface.[111-113, 117-120] However, through simple, well-designed experiments, combining various techniques such as XPS, IRAS, and mass spectrometry we were able to prove the existence of a chemisorbed oxygen >1ML during maximum CO_2 formation, similar to the results found for Rh(111).

CHAPTER V

Pd(100) OXIDATION AND CO OXIDATION ON Pd(100)

Introduction

Palladium metal is used in a plethora of applications including catalytic oxidation of hydrocarbons in catalytic converters for automobiles and is considered the most efficient metal for catalytic methane combustion.[37, 40, 48, 59, 121-139] Although, it is considered one of the most important catalytic reactions, the atomic scale process responsible for the oxidation of Pt-group metals is not completely understood. One consideration is the lack of studies covering the metal-oxide equilibrium states in the high (~1atm) pressure and high temperature regime needed to oxidize the metals, since the instrumentation able to differentiate between the different oxidation states does not typically work in under these conditions.[124]

Pd(100) Oxidation

Background

The oxidation of palladium is a complex reaction involving diffusion, ordering, reconstruction, and nucleation.[27-29,31] Initially low energy electron diffraction (LEED) and temperature programmed desorption (TPD) were used to discern the various phases of oxygen adsorption. After new technologies were

developed the oxidation reaction was studied at a greater depth with *in situ* XPS, STM, and calculations of the thermodynamically stable surface.[43,44]

The first stage of the reaction is the rapid chemisorption of the oxygen as overlayers followed by island formation and dissociation of the oxygen into the bulk via reconstruction and diffusion.[27-35, 40-43, 54-60] For Pd(100) the oxidation is similar to the highly studied Pd(111), with a deviation in the steps to form an oxide layer. Both surfaces begin with the chemisorbed O_{ads} atoms <0.05ML. As oxygen is chemisorbed on Pd(100) it begins to form a p(2x2) structure at room temperature starting as small islands of higher adsorbed oxygen concentration and growing until the oxygen coverage reaches ~0.25ML.[27, 40, 47-53] Before the entire surface has converted to chemisorbed p(2x2) oxygen, islands of higher coverage with a c(2x2) overlayer forms in adjacent patches on the Pd(100) surface. By the time the coverage reaches ~ 0.25ML the surface is completely converted to a p(2x2) structure. Further exposure to oxygen at room temperature allows the more dense c(2x2) overlayer to continue grow similar to the growth of the p(2x2). Once the coverage reaches ~0.5ML the oxygen atoms begin to slowly accumulate in the sub surface; however, if the temperature is above 500K allows the surface to reconstructs and regions of the Pd(100) alter their configuration to p(5x5) islands one palladium atom high. This is accompanied by substantial mass transfer between the Pd and the oxygen surface overlayer.[47] This

reconstructed surface oxide must have stronger metal-oxygen bonds in order to overcome the oxygen-oxygen repulsion.[2-3]

The phase change, at 500K, resulted in a slower oxygen uptake and new desorption peaks between the bulk desorption temperature and the chemisorbed desorption temperature.[27-32] After initial nucleation of p(5x5) islands on a c(2x2) surface there is continued island growth while the surface periodicity remains unchanged. [49-51] At temperatures greater than 573K the islands reconstruct to a $(\sqrt{5}x\sqrt{5})R27^{o}$ phase similar to epitaxial PdO(001). Here the Pd-O bond strength is intermediate between the chemisorbed oxygen and bulk PdO.[27-32, 47, 52,122-124] The final phase for the oxidation of Pd(100) is a rough oxide surface with 3D clusters of PdO dominating the surface.[27-32, 47-50]

High Pressure Pd(100) Oxidation

XPS is able to determine the degree of oxidation of a metal by detecting the change in the binding energy between states.[74] In figure 29 a Pd(100) single crystal was oxidized in the high pressure reactor 10 torr for 10 minutes at increasing temperatures from 300K to 700K. The O 1s peak at ~530.0eV overlaps with the Pd 3p3 peak occurring at 532.0eV, thus when making a determination of the integrated peak area for oxygen and the position of the peak for various Pd oxide species the Pd 3p3 peak is taken into consideration.[10] At 700K a bulk oxide forms and the Pd peak shifts from

335.1 for bulk metallic Pd to 336.6eV.[27, 45, 46, 124, 138] Similarly, the Pd 3p peak at 532eV shifts 1.5eV to a higher binding energy, while the O 1s peak develops at a lower binding energy, 530.5eV.

As previously described, there is a distinct shift in the binding energy of the Pd 3d5 and the O 1s/ Pd 3p3 between the spectra taken at 500 and 525K: this is due to the change from a chemisorbed oxygen surface to an oxide tri-layer (O-Pd-O), in which O penetrates into the top-most Pd layers and displaces Pd atoms from of the bulk.[45,46, 122-131] Figure 29 defines the different oxides on Pd and is used to aid in the assigning of peaks for CO oxidation experiments.

CO Oxidation on Pd(100)

Background

Palladium is commonly used for industrial reactions such as with volatile organics and CO oxidation for pollution control for automotive exhaust. Under realistic operating conditions, the catalyst is exposed to atmospheric pressures at various temperatures as the exhaust flows through the catalysts. In recent years more emphasis has been placed on experiments that mimic realistic

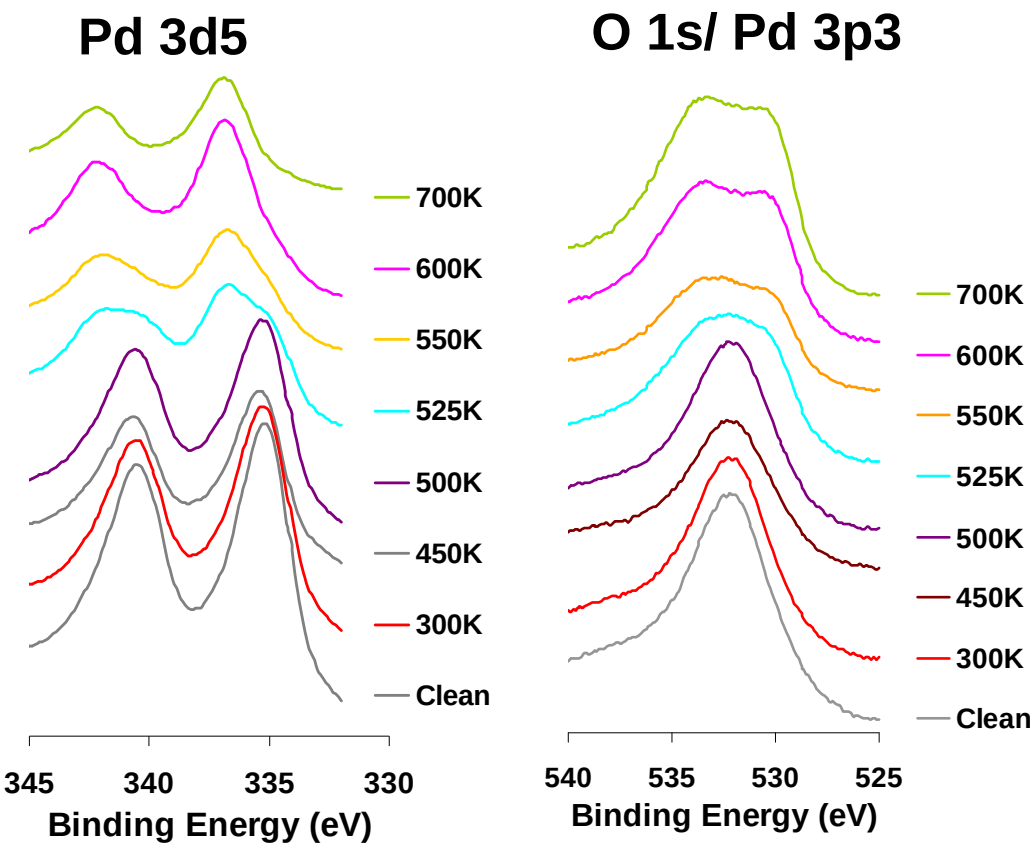

Figure 29: High pressure oxidation of Pd(100). XPS Pd3d5 and O1s/Pd3p3 spectra taken after oxidation in 10 torr of O_2 for 10 minutes at temperatures from 300K to 700K.

conditions as opposed to laboratory UHV conditions. The majority of CO oxidation experiments on Pt-group metals performed in the past have been under UHV conditions whereas CO oxidation occurs on a chemisorbed surface and bulk oxides do not readily form.[121, 137-139]

High Pressure CO Oxidation

High pressure CO oxidation was investigated over Pd(100) employing the high pressure reactor and XPS. The Pd(100) was cleaned by oxidizing for 10 minutes at $4x10^{-6}$ torr O_2 at 600K and then annealed to 1200K, XPS used to confirm a clean sample. [133] Once the sample was isolated in the high pressure cell, it was heated to 525K in 40 torr of a $CO:O_2$ gas mixture ratio of 1:5. The rate of CO_2 formation can be calculated by monitoring the pressure drop, where each torr lost produces two torr of CO_2. Figure 30 shows the pressure drop as a function of time. Once the pressure drop was well documented, the reaction could be quenched at specific points to ascertain the composition of the surface during the reaction. As the reaction proceeded the ratio of CO to O_2 decreased linearly due to a CO consumption twice that of O_2. Once the reaction proceeded to a particular ratio (seen in figure 30 at ~140 seconds) the pressure change increased exponentially indicative of a highly active surface.[34]

The prevailing concern relates to the nature of the oxygen species (chemisorbed or tri-layer oxide) that is on the surface during the period of high activity. The reaction was quenched at three pre-specified: (1)prior to obtaining

a highly active surface, (2)during the increased activity, and (3)after the reaction has completed. Previous peak measurements, peak assignments from literature, and deconvolution of the Pd 3d5/2 peak are used to assign the peaks and to determine the relative surface composition. [10] The single XPS peak shown is the Pd 3d5/2 peak, the largest peak in the Pd and PdO spectra. The Pd 3d5/2 XPS peak was separated into metallic Pd (334.75eV), two Pd coordinated to a surface oxygen (335.38eV), and four Pd coordinated to sub-surface oxygen (336.38eV). At the start of the reaction prior to the accelerated pressure drop the composition is comprised mostly of bulk metallic Pd and a small amount of surface chemisorbed oxygen (figure 31). The surface chemisorbed peak is small in comparison to the bulk Pd; however, this is misleading since the XPS signal includes a depth of up to 10nm from the surface.[10] During the accelerated pressure drop has begun, where the CO_2 formation increases by 2-3 orders of magnitude, the metallic Pd peak attenuates as the surface chemisorbed oxygen peak saturates. [91] The sub-surface oxide peak remains smaller than the

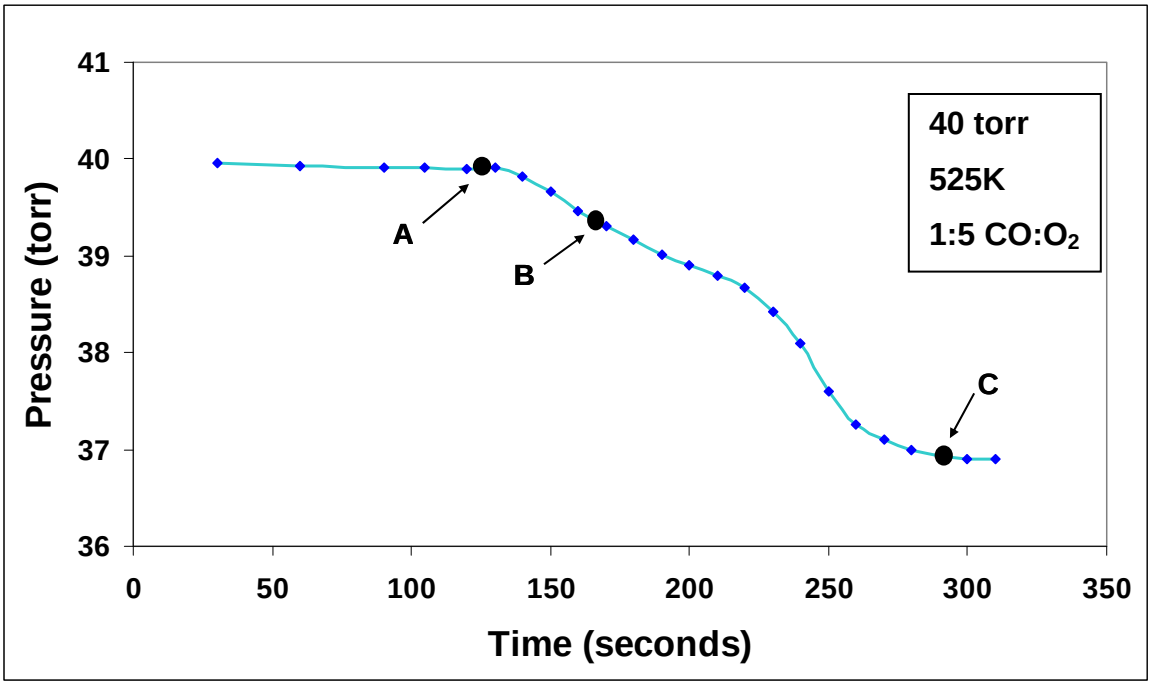

Figure 30: CO oxidation reaction performed in the high pressure reactor and transferred *in situ* to the analysis chamber. Pressure measured to determine CO_2 formation rate. A, B, C are points where separate reaction runs were stopped and the surface composition analyzed with XPS.

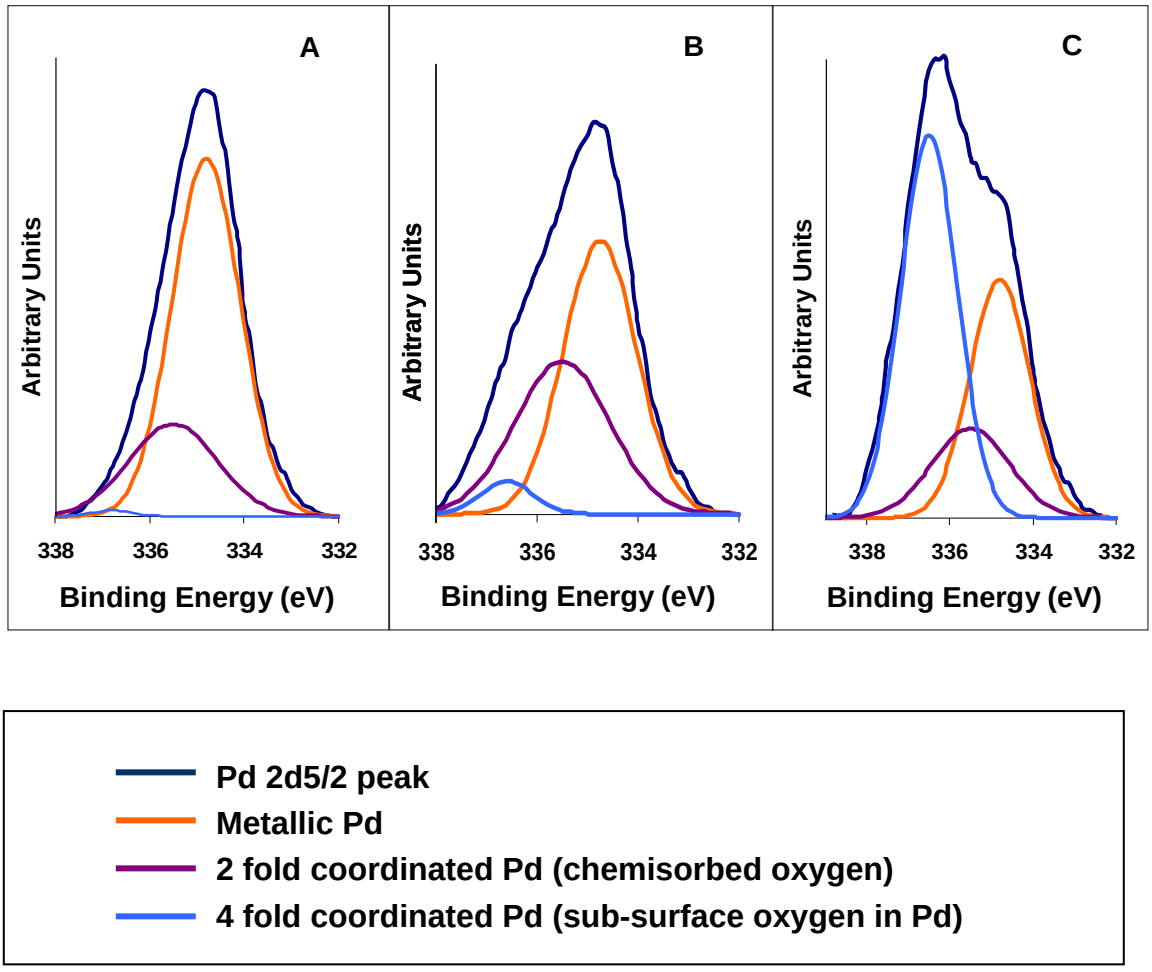

Figure 31: XPS measurements to compare the composition of the top most layers of the Pd(100) single crystal as the reaction (Figure pd2) proceeded. A: Before highly active surface developed noted by an increase in CO_2 formation rate. B: Composition of surface during highly active state. C: Post reaction where CO has been completely consumed.

chemisorbed surface, thus the amount of sub-surface oxygen is an insignificant amount when compared to the surface oxygen. After the reaction is complete, and the CO is completely depleted, the Pd begins to oxidize and the sub-surface oxygen peak dominates over the chemisorbed surface oxygen and metallic Pd peaks.

The high pressure results agree with the previous results from Pt(100) and Rh(111) presented herein. Hendriksen et al, using the STM system detailed in Chapter V, proposed that the highly active surface is a rough oxide surface.[121, 137-139] However, as with the Pt(110), the surface described as the active surface occurs after the increase in the CO_2 formation rate. XPS provide a definitive composition when compared to literature values and spectra taken of know compositions.

CHAPTER VI

ACETYLENE CYCLOTRIMERIZATION TO BENZENE ON Pd-Au/Mo(110)

Cyclotrimerization of Acetylene to Benzene

Introduction

Cyclotrimerization of acetylene to benzene was discovered in 1866 by Berthelot and coworkers, [140-142] since then there has been much interest experimentally and theoretically [142,143-149] due to its simple, archetypal thermally allowed cycloaddition. [142] This addition reaction takes place without the carbon-carbon bonds completely breaking, yet rather the π-bonds translate into carbon-carbon σ-bonds as shown in figure 32.

Mechanism on Pd(111)

The cyclotrimerization of acetylene to benzene has been studied from UHV to atmospheric conditions on single crystals. [150-155] Benzene formation is very sensitive to surface crystallography with Pd(111) shown to be the most efficient crystal face. Cyclotrimerization is often carried out over dispersed Pd catalyst. [157]

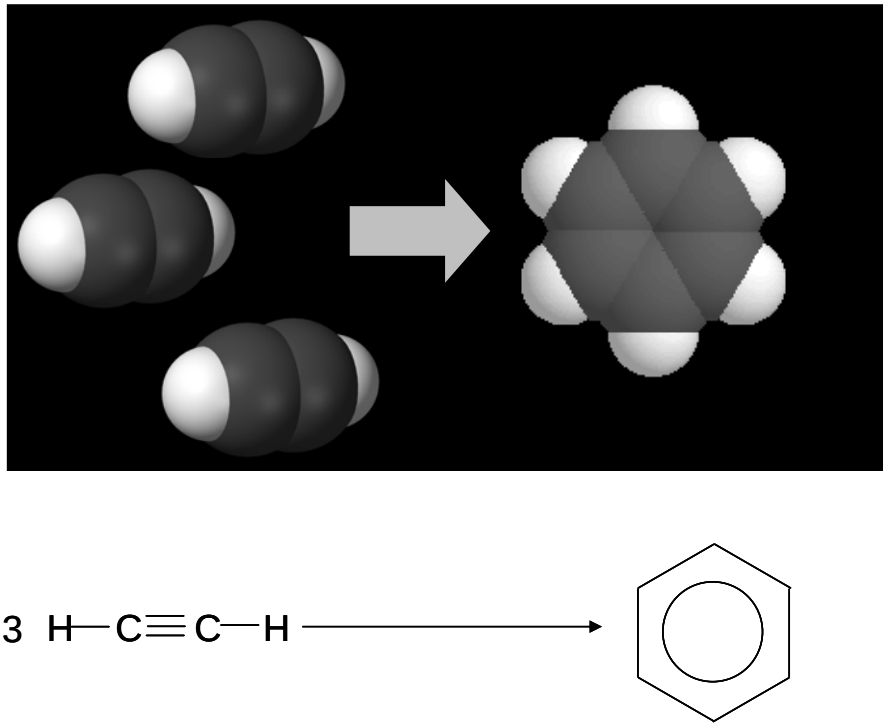

Figure 32: Representative stoichiometric reaction for acetylene cyclotrimerization to benzene.

The process can be separated into three discrete steps [152]:

$$Pd_{site} + 2C_2H_2 \rightarrow Pd_{site}(C_2H_2)_2 \rightarrow Pd_{site}(C_4H_4) \quad (1)$$

$$Pd_{site}(C_4H_4) + C_2H_2 \rightarrow Pd_{site}(C_4H_4)(C_2H_2) \rightarrow Pd_{site}(C_6H_6) \quad (2)$$

$$Pd_{site}(C_6H_6) \rightarrow Pd_{site} + C_6H_6 \quad (3)$$

The C_4H_4 metallocycle forms from two free acetylene molecules adsorbing on the surface and arranging into a tilted conformation from the surface normal. Then a third acetylene rapidly incorporates to form benzene. [153] During the formation of the metallocycle there is no C-C bond scission and the acetylene molecules adsorb to the surface via two σ-bonds and a π-bond with the palladium surface. Benzene desorption from the Pd(111) surface is the overall rate limiting process. There are two desorption temperatures revealing two different benzene configurations. The first configuration lying flat desorbs at ~500K parallel to the surface while the second, in a tilted conformation, desorbs at ~300K. [153] The latter desorbs at a lower temperature due to the crowding on the surface, forcing a tilted conformation at high pressures. The former is mostly seen at lower pressures, at which there is room for a benzene molecule to lay flat.

The sites for acetylene adsorption are the 3-fold hollow sites which has been shown by both experimental [157] and theoretical methods[158]. Although only three Pd atoms make up the acetylene adsorption site, three of these sites

collectively in a circular configuration are necessary to form the benzene ring. The honeycomb structure of the Pd(111) is the ideal surface with three 3-fold hollow sites utilizing the center Pd as a focal for the three acetylene molecules. Results from previous experiments have shown that the critical ensemble for benzene formation is seven palladium atoms. [159-161]

Pd/MgO Model System

Abbet et al., revealed that acetylene cyclotrimerization does not take place on a single free Pd atom. This was confirmed by determining the bond length of the third acetylene molecule, which has a stretched and weakened Pd-C bond preventing activation.[172] However, a single Pd atom atop an oxygen vacancy of MgO produces a Pd atom active for benzene formation. The MgO oxygen anions, acting as centers of electron density, donate electron density to the single Pd atom allowing it to maintain a net negative charge. The charge can then flow from the supported Pd atom to the adsorbing molecules permitting the adsorption of all three acetylene molecules around a single Pd atom. The desorption of benzene from the single Pd atom on MgO was completed at the lower temperature (~300K) even at higher pressures unlike Pd(111), which needs higher temperatures to desorb all the benzene.

Bimetallic Model System

Introduction

Bimetallic systems have been employed by industry since the 1960's and 70's for hydrocarbon reforming. These special materials continue to influence catalysis, electrochemical applications such as fuel cells, and are considered the next step in the development of semiconductors. [174] This is due to the extensive use and continued interest for "designer" surfaces as modern scientists strive to understand these complex systems. Several investigations have made a considerable efforts to discern the electronic, physical and chemical properties of these systems.[166-182]

Typically two methods are used to produce bimetallic systems. [166] The first method involves cutting and polishing a bimetallic alloyed single crystal followed by cleaning in UHV. The second method involves utilizing vapor deposition of one metal onto another in UHV or depositing both metals with vapor deposition onto another metal with a well defined single crystal surface that is immiscible with both of the metals under study. This second method is the more popular process and can be easily tailored by altering the composition of the alloy. By understanding the composition and how the metals mix in these systems one can then correlate the atomic structure with the electronic and chemical properties creating a structure-function relationship, which can be employed to design surface for specific purposes.

Surface Structure

For these bimetallic systems the reactivity of the metal surface is a critical function of the composition and structure with very unique properties when evaluated against the corresponding individual component metals. When taking into consideration the mixture of Pd and Au it is necessary to consider the individual metals. Pd is a well known catalyst used for many industrial reactions and Au is relatively new as an industrial catalyst previously considered inert. However, when Au is added to Pd the selectivity, stability, and activity for specific reactions are enhanced. The promotion of Pd by Au is used as a catalyst for numerous applications such as hydrogen fuel cells [174] and pollution control [175].

Understanding the nature of the interaction between Au and Pd is fundamentally important toward understanding the promotional effects. Au and Pd are completely miscible with the Pd-Au alloy possesses negative heat of formation at 300K. The maximum stability of the alloy occurs when the ratio of Au to Pd is 60/40. The Au-Pd system has a tendency to order with attractive interactions between the two components, which is an indicator of large negative enthalpies observed experimentally.[176] The lattice parameters of the individual parts of the alloy at 300K are 0.389nm and 0.408nm for pure Au and Pd, respectfully. The close lattice parameters show only a small deviation from Vagard's law, in which there is a linear relation between the crystal lattice constant and the concentration of the constituents.

It has been observed through experimental and theoretical study that the surface composition is of much higher significance than the bulk electron structure for adsorption and catalyst performance. [184-188] This is important since the surface composition can differ to a great extent from the bulk leading to considerable uncertainty in the interpretation of the catalytic properties. Theoretical calculations by Mavrikakis et al. have revealed a strong correlation connecting surface strain, adsorption energy, and the activation barriers for catalytic reactions. [181]

A large number of studies have proven the surface composition to not only deviate greatly from the bulk composition, but have a Au rich surface.[182,183] AES studies evaluating various bulk compositions, and confirmed by LEISS, illustrate that even at these different compositions Au has a significant proclivity toward surface enrichment.[182] This is consistent with Au having a much lower surface free energy compared with Pd. Additionally, rather then using bulk Pd-Au alloy investigations 5ML Pd/5ML Au on Mo(110) and 5ML Au/5ML Pd on Mo(110) can be used. Thus the effect of mixing can be studied when the alloy is annealed to various temperatures.[182, 183] When the alloy is annealed to high temperatures (700-1000K) the inter diffusion is evident; e.g., after annealing to 800K for 20 minutes the surface becomes Au rich, independent of which metal was deposited first. Between 700K and 1000K a stable alloy with composition of 20% Pd and 80% Au, denoted as $Pd_{0.2}Au_{0.8}$, formed using a 50/50 elemental mixture of the Pd and Au.[183]

Further surface composition information was obtained using LEISS at differing ratios of Pd and Au and XPS to determine the bulk concentration. This made possible a surface composition phase diagram developed with the surface composition as a function of the bulk ratios. The phase diagram presented in figure 33 for Pd/Au thin films deposited on Mo(110) surface is in exceptional agreement with previous results obtained from bulk alloys. [183-186] Similarly, Pd-Au/SiO_2 model catalysts show enrichment in the surface concentration of Au for different bulk ratios of Pd and Au. It is evident from LEISS studies that surface segregation of Au is more considerable for Pd-Au planer surfaces. [183] Nonetheless, this study demonstrates that properties related to the surface makeup can be studied using both model catalysts and supported catalysts when they have comparable surface compositions to thin film model catalyst.

Segregation is unexceptional in Au alloys with the Au exhibiting preferential surface segregation. The surface is shown to consist primarily of a Au layer with an increased concentration of Pd in the second layer. [187, 188] Only a few studies employing atomic surface-layer sensitive techniques such as LEISS have been completed and encompass various surface including $Au_3Pd(113)$[190] and $Au_3Pd(100)$ [180].

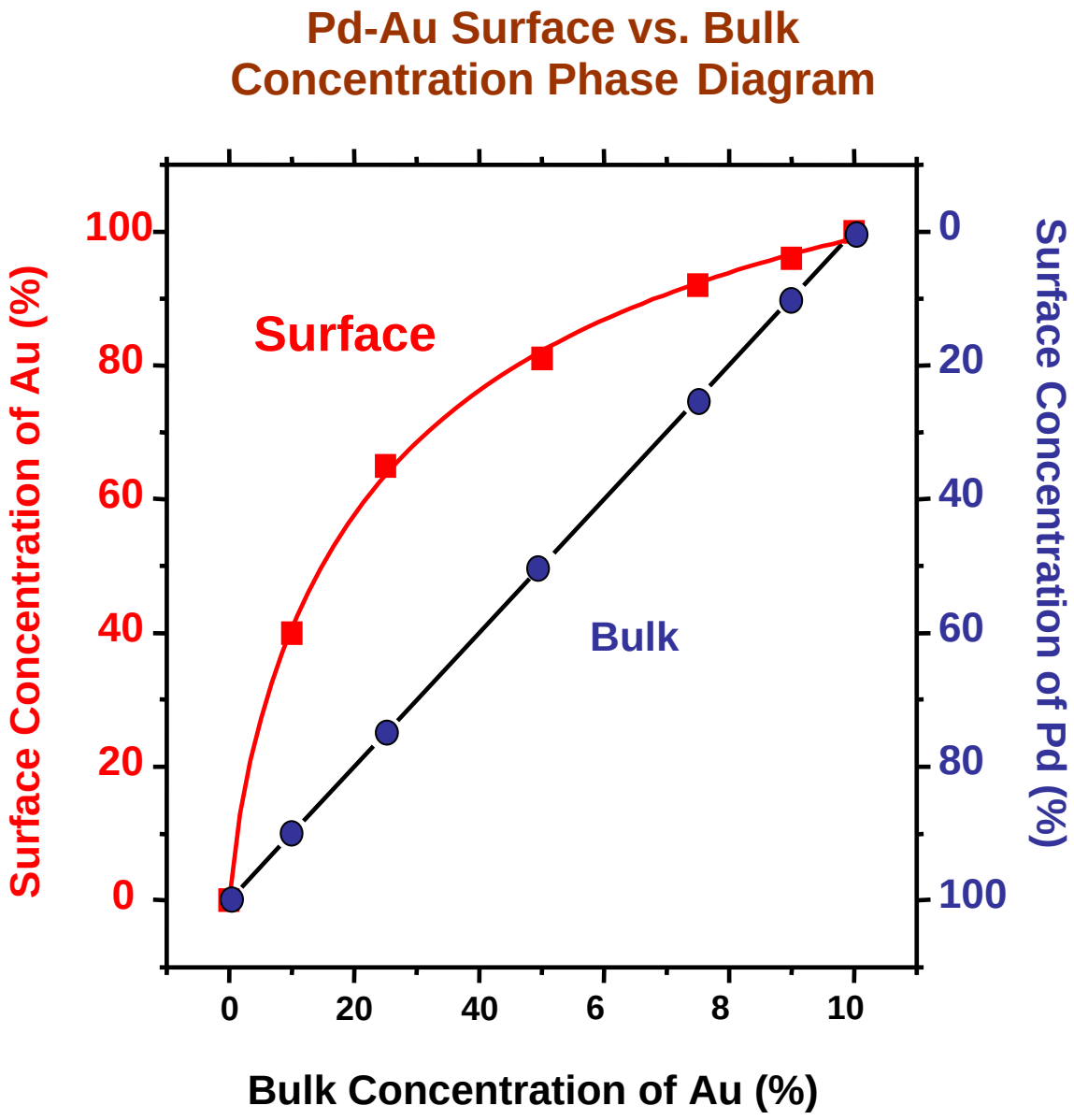

Figure 33: Surface concentration of various Pd-Au alloys on Mo(110) measured by LEISS compared to the corresponding bulk concentration. Sample annealed at 800 K for 20 min.[183]

The epitaxial growth of a vapor deposited monolayer of Pd on Au(111) is thermodynamically unstable, based on the surface composition of the Au-Pd. Koel et al. preformed detailed investigations of Pd overlayers on Au(111) using AES to determine the bulk concentrations and LEISS for the top surface layer. [191] After deposition at temperatures as low as 150 and 300K layer-by-layer growth (van der Merwe growth) is seen. However, when the alloy is annealed to 500K the Pd AES signal becomes much smaller while the Au AES intensity grows in comparison to the corresponding values at 150K and 300K. This qualitatively indicates further alloying or inter-diffusion of 1 monolayer of Pd at 500K.[186] Lambert et al., concentrated on sub-monolayers of Pd on and Au(111)-(2√3x2√3) where, due to the surface edge dislocations in the Au herringbone reconstruction, Pd islands initially nucleated and developed. As the Pd coverage is increased evolution of Pd islands is observed and provides an explanation for the exceptional catalytic behavior. Maroun et al., in figure 34, used STM to produce high resolution images of Pd-Au alloy surfaces prepared from electrochemically co-depositing Pd and Au on Au(111).[173] These STM images are shown in figure 34 with two clearly distinguishable types of atoms with well resolved and separated heights and shapes, arranged in a

hexagonal lattice and a spacing equivalent to that of Au(111). A single uniform Au-Pd alloy phase with an extremely unordered metal-atom arrangement is formed without phase separation in to the disconnected Pd and Au domains.

Using CO as a probe molecule, previous studies in the Goodman laboratory clearly demonstrate the formation of isolated atomic Pd surface sites surrounded by Au on Au-Pd films supported on a Mo(110) surface[173, 183, 187-196] The IRAS spectra in figure 35 reveal the CO adsorption as a function of annealing temperature and Au surface structure at 90K onto a 5MLPd/5ML Au/Mo(110) surface. To determine the assignments of CO adsorption on a Au-Pd alloy separate assignments were needed for the separate metals. On Pd(111) previous assignments include features at 2110-2080cm^{-1} for linearly bound CO, 1965~1900 cm^{-1} for two-fold bridging of CO, and 1900~1800 cm^{-1} for three fold bound CO species. Vibrational features of CO on Au(111) on atop sites are typically seen between 2100 cm^{-1} and 2120 cm^{-1} of which vanish below 200K whereas the atop feature on the Pd(111) disappears at a higher temperature.[175] After a low CO coverage less than 0.10L is deposited on the Au-Pd alloy two prominent stretching features related to the linearly and bridged bound CO on the alloy surface appear at 2087 cm^{-1} and 1940 cm^{-1}, respectively. These

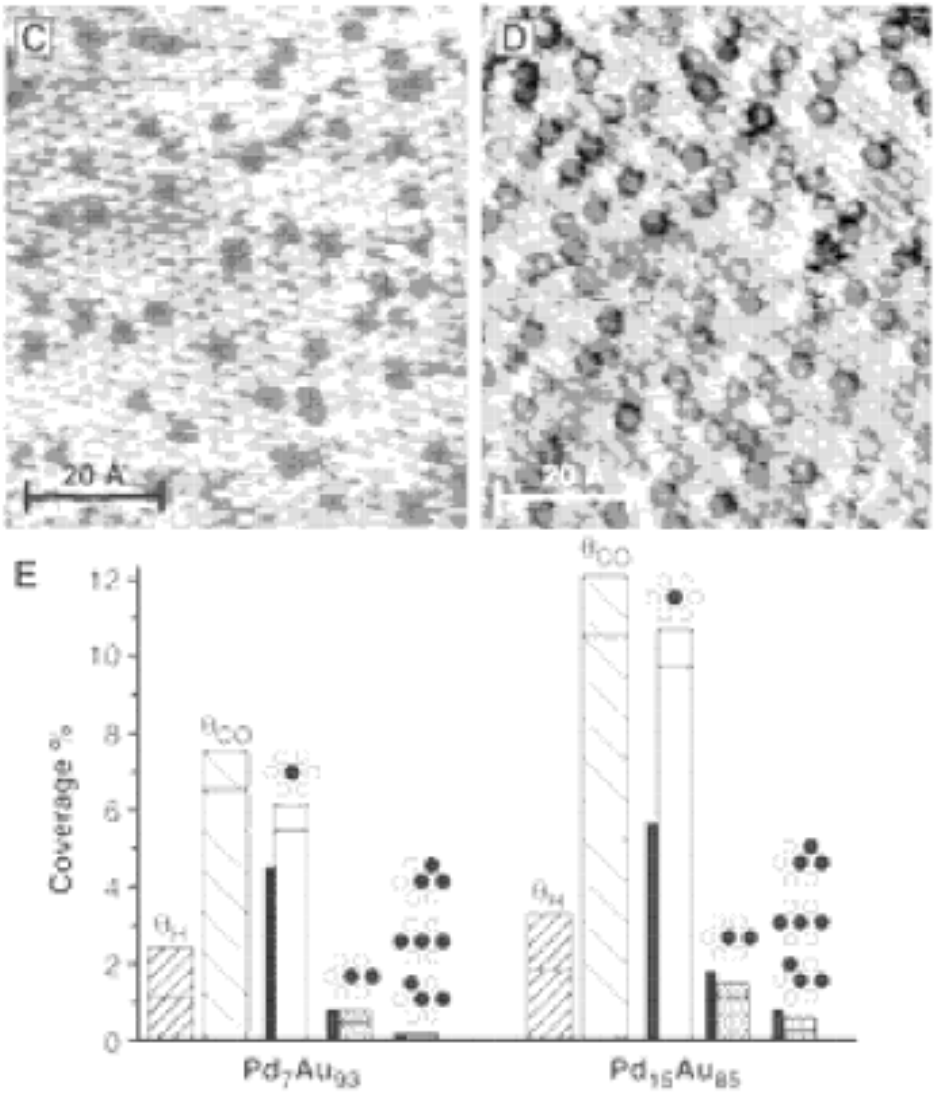

Figure 34: *In situ* STM images of PdAu alloys electrodeposited on Au(111) for (A) Pd_7Au_{93}; and (B) $Pd_{15}Au_{85}$. Pd atoms appear bigger, depending on tunneling conditions. (C) Surface coverages of Pd monomers, dimmers, and trimmers as obtained from the above STM images. [173]

features closely resemble assignments seen by Koel et al. for Pd deposition on Au(111) for atop sites (2090 cm^{-1}) and for CO bridged bound sites (1910 cm^{-1}).[144] When the CO coverage is increased above 0.02L a new feature is develops at 2105 cm^{-1} and saturates at a CO exposure of 0.5L. The adsorption features of CO on the 5MLPd/5ML Au/Mo(110) annealed to 800K for 20 minutes is shown in figure 35. Here the distinct feature at 2087cm^{-1} corresponds to CO atop Pd when the CO coverage is below 0.10L. After the CO exposure has been increased a second feature is observed at 2112cm^{-1} in line with a CO atop Au. Both of these features are associated with linearly bound CO on Pd(111) and show no indication of bridge bound or 3 fold adsorption sites indicative of Pd atoms isolated by Au atoms. These results further strengthen the observation that the majority of the Pd atoms diffuse into the bulk of the deposited metals. The surface, after annealing, of the Pd-Au alloy catalyst with fewer Pd thus forms Pd monomers surrounded by Au, Au_6Pd on Au(111) and Au4Pd on Au(100). Considering the LEISS results in figure 36, this suggests that the concentration of the surface Pd is <20% after annealing 5Pd/5MLAu/Mo(110) to 800K for 20 minutes.

Additionally, TPD is used to support the theory of a single Pd atom CO adsorption site. Using CO adsorbed on Pd-Au/Mo(110) two distinct TPD peaks are seen at 100K and 300K, which are characteristic of CO atop adsorption on Au and Pd, respectively. However, on the Pd/Mo(110) surface CO adsorbed on

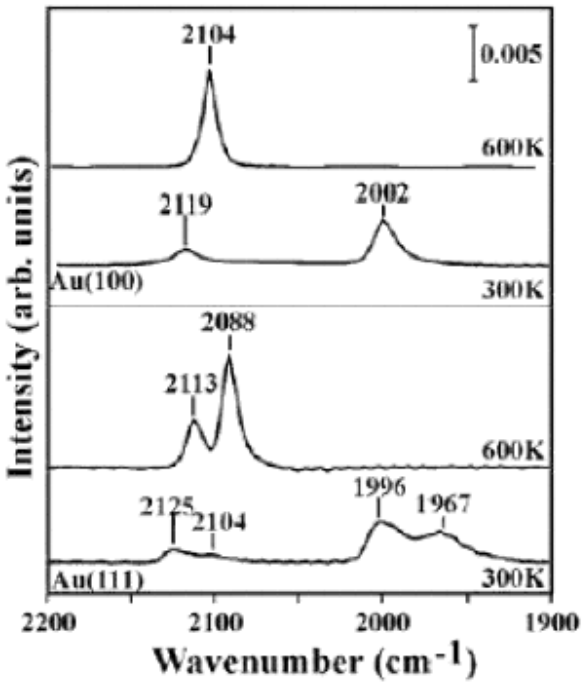

Figure 35: IRAS spectra after CO adsorption at 90K on 4ML Pd/Au(100) and Au(111) at 90K and subsequently to 300 and 600K for 10 minutes each. [183]

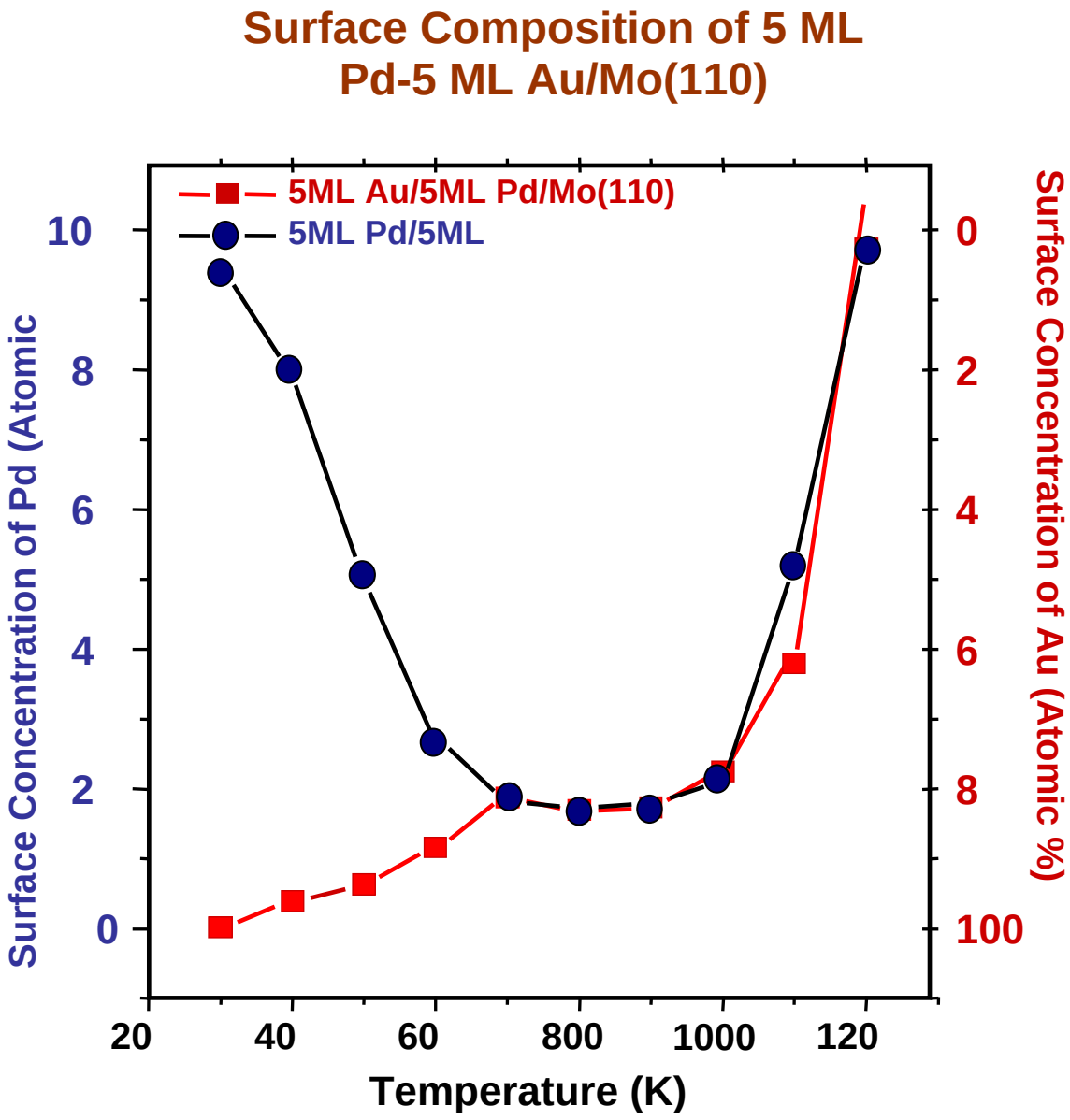

Figure 36: Surface concentration of Au and Pd of 5 ML Pd/5 ML Au/Mo(110) (●) and 5 ML Au/5 ML Pd/Mo(110) (▪) as a function of annealing temperature. Sample annealed at each temperature for 20 min. [183]

the bridge site desorbs at 400K and 3 fold hollow sites at desorbs 500K, both at a higher temperature than the alloy.

Acetylene Cyclotrimerization

As previously stated acetylene cyclotrimerization to benzene on pure Pd(111) is a well understood process and has been studied under a wide range of conditions.[164,165] The rate limiting process is the desorption of the benzene molecule for the pure Pd. The two temperatures at which benzene desorbs are ~500K for the flat-lying, strongly bound species and ~200K for the tilted, weakly bound species. By the addition of another metal the catalytic activity and selectivity is able to be altered and more can be learned about the process. From *ab initio* theoretical calculations preformed by Pacchioni et al. the d-π interactions of the benzene molecule with the metal surface is diminished when Au is added, when compared to the Pd_7 ensemble. [166]

Bimetallics can aid in the discovery of the chemically active ensemble in the same manner dispersed metals on oxides portend active ensemble, as previously elucidated with Pd on MgO. When Pd was deposited on the MgO it was found that the ensemble for highest activity was seven Pd in an arrangement with six Pd atoms surrounding a central Pd atom in a closed packed arrangement. As previously mentioned, Abbet et al., discovered only one Pd is necessary for the acetylene to cyclotrimerize and form benzene. [161]

Model planer catalysts offer a simplified method to investigate reactions on bimetallics and Baddeley et al. used this method to study Pd deposited on Au(111) and the inverse, Au deposited on Pd(111).[152] Both the Au(111)/Pd and Pd(111)/Au were a more effective catalyst than the pure Pd(111) for acetylene cyclotrimerization to benzene. In the former case a $(\sqrt{3}x\sqrt{3})R30^{\circ}$ surface alloy with well defined structures had a composition of Pd_2Au. However, in this system the controlled alteration of the surface composition is difficult to accomplish. The alternative Au/Pd model, with Pd as the support and deposited Au behaves much differently and does not form ordered alloys, but rather forms a disordered surface with continuously varying composition. The variation of mobilities of Au in Pd and vice versa accounts for the difference in behavior. This provides the possibility of studying the reaction at various concentrations. Nevertheless, in order to predict the surface with optimal activity the surface composition needs to be accurately ascertained.

Baddeley et al. used AES, TPD (with CO as the desorption molecule), and HREELS to determine the surface sites of the Au/Pd alloy. [177] Koel et al. and Yi et al. used LEISS to determine the surface concentration of Au and Pd.[183, 191] AES is not an advantageous technique for determining the top most atomic layer where adsorption/desorption takes place; however, it does provide a

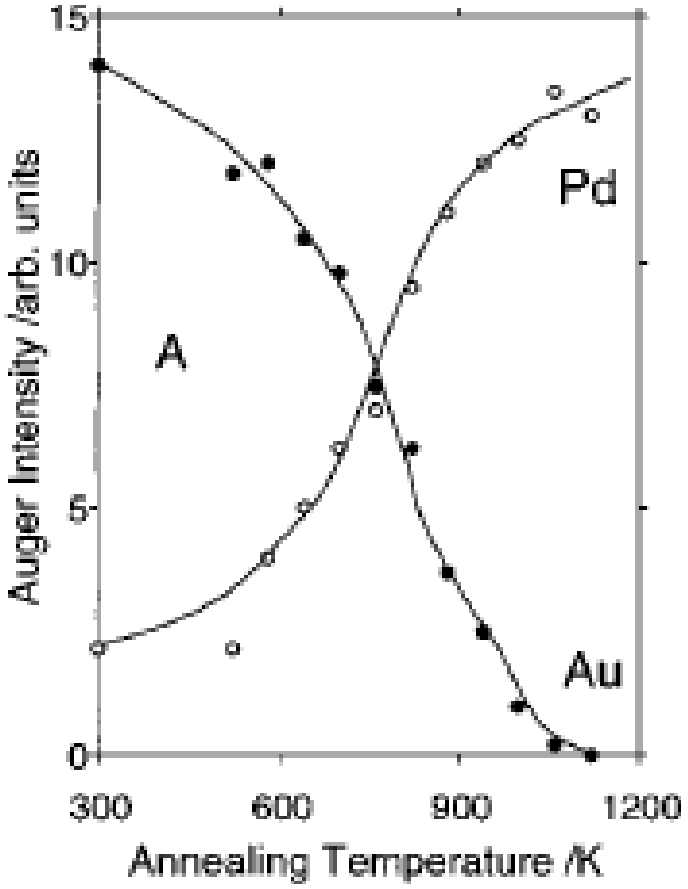

Figure 37: Plotted AES Au and Pd peak intensities for 4.5ML Au on Pd(111). [162]

estimation of the Pd-Au mixing when only 4ML of Au is deposited on Pd. Figure 37 shows the intermixing of the alloy, which begins at ~600K, has equivalent peak intensities at ~750K, and by annealing to ~1000K the Au completely disappears. CO chemisorption is used in order to determine the relative coverage for the sites at varying temperatures. Figure 38 shows TPD spectra of 4.5ML Au deposited on Pd(111) at increasing annealing temperatures. The prominent peak after preannealing to 300-750K is at 300K. A previous study correlated this to a single Pd surrounded by Au. As the preannealing temperature increases the surface becomes more Pd rich and the 300K peak disappears with a new peak at 350K appearing after a preanneal to 600K, which is assigned to 2 fold sites. After increasing the anneal temperature the peak at 445K takes over, associated with the 3 fold Pd site, dominates. [193]

HREELS is used in conjunction with TPD to discern the surface concentration and type of adsorption sites. Using 6ML Au on Pd(111) HREEL spectra of 30L adsorbed CO were obtained for preannealing temperature from 300-1090K. Unlike the inverse situation of Pd deposited on Au(111) the surface continuously changes as the preannealing temperatures are increased. The surface changes from a Au rich surface to a Pd rich surface. The HREELS spectra (Figure 39), at lower preannealing temperatures, reveals a feature at 2100cm^{-1}, which corresponding to the TPD peak at 300K, a single Pd atom surrounded by Au. The next feature seen is at ~1950 cm^{-1} and corresponds to the TPD peak at 445K, the three fold Pd adsorption site.

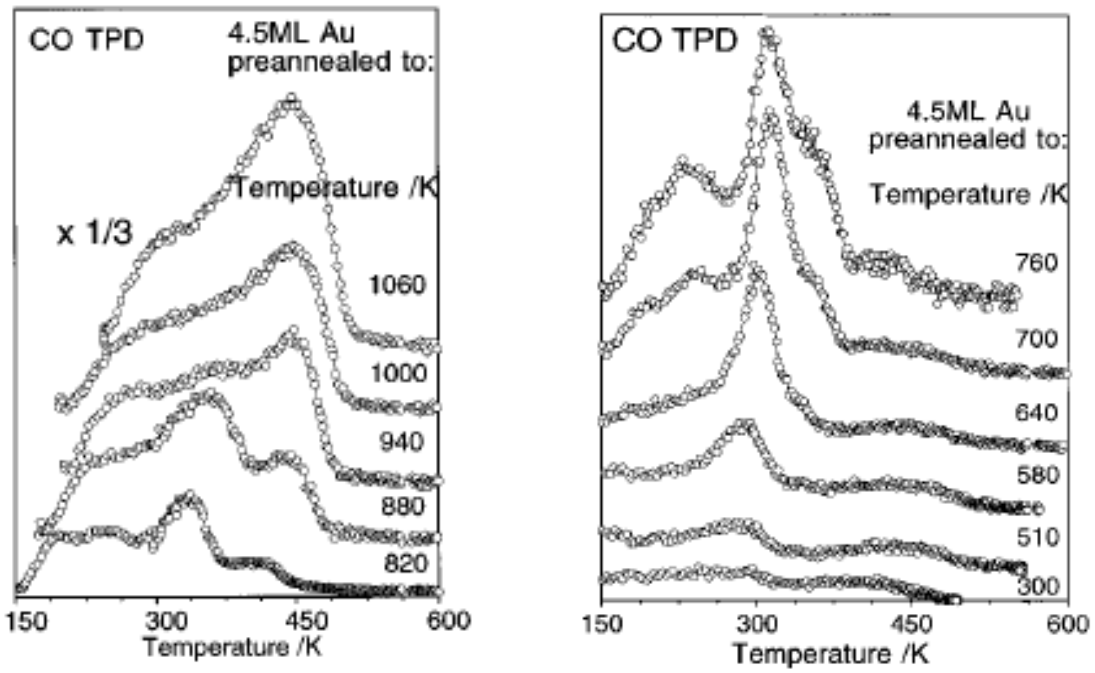

Figure 38: TPD spectra for 30L CO dosed at ~120K as a function of preannealing temperature for 4.5ML Au on Pd(111). [162]

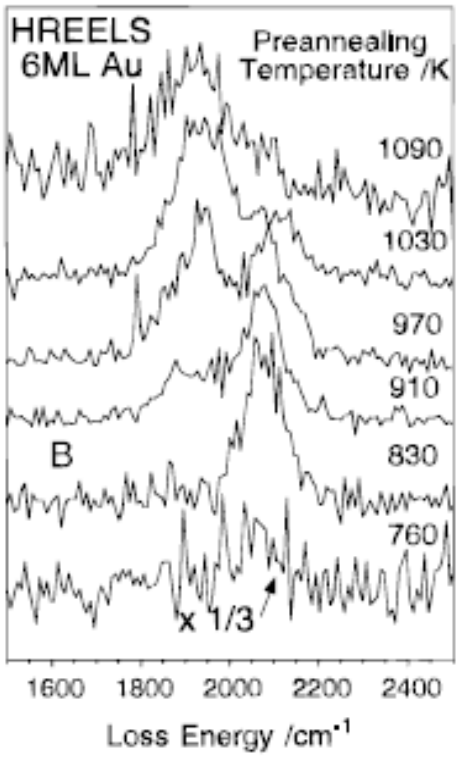

Figure 39: HREELS spectra of CO adsorbed at 150K on 6ML Au on Pd(111) as a function of preannealing temperatures. [162]

Once the type of sites on the surface and an estimation of the concentration have been ascertained the surface can be accurately defined and the surface composition can be related to the acetylene cyclotrimerization reaction. Temperature programmed reaction (TPR) was used by Baddeley at al. to determine the highest activity as a function of preannealing temperature. [164] The peaks in figure 40 [162] illustrates the desorption of benzene after deposition of 30L of acetylene on 4.5ML Au/Pd(111). The peak with the largest area occurs at a preannealing temperature of 860K. This is followed by a decrease in the amount of benzene produced at higher preannealing temperatures, which correlates to an increase in the amount of Pd on the surface. Figure 41 shows plots of the benzene yield as a function of the preannealing temperature. Baddeley et al. used the LEED data to provide a surface composition and concluded that the optimal benzene production, normalized to amount of Pd, occurs at ~80% Pd. While LEED, TPD, AES, and HREELS complement each other for determining surface sites, composition of the top layers, and lattice parameter of the alloys they do not provide an unambiguous surface composition. Thus, when comparing the surface of an alloy with the bulk a more direct method, such as LEISS, should be used in further conjunction with the methods already employed. Reconsidering the results, the HREELS feature at 2100cm^{-1} and TPD CO desorption peak correlating to the

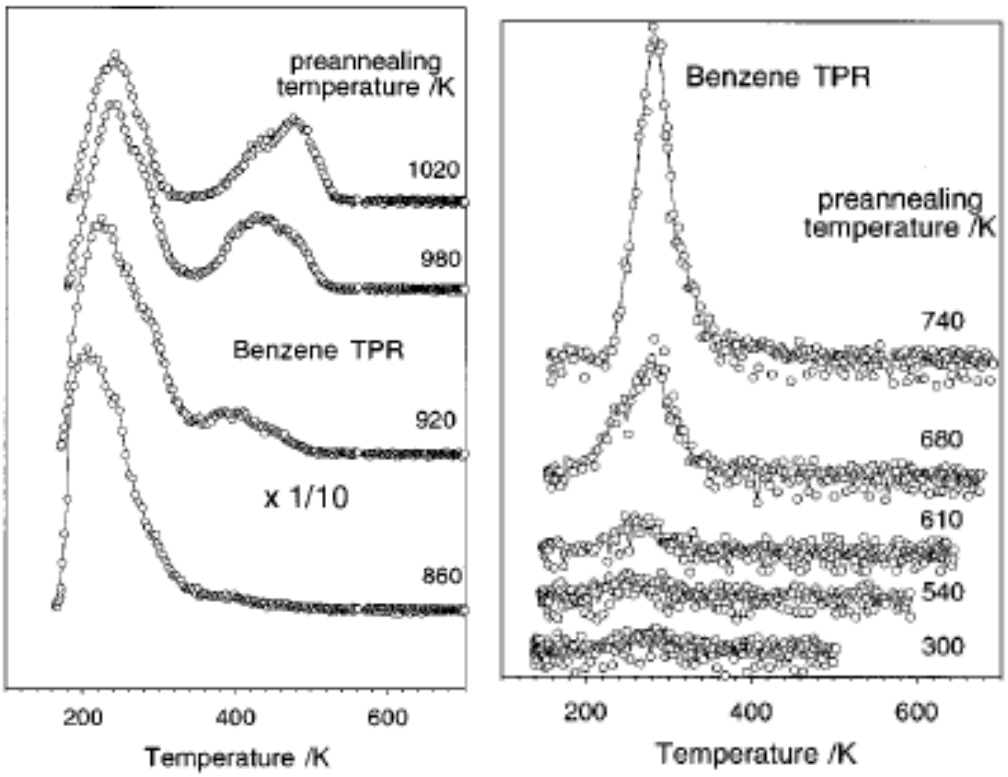

Figure 40: Benzene TPR spectra from 30L of C_2H_2 dosed at ~120K (function of preannealing temperature) for 4.5ML Au on Pd(111). [162]

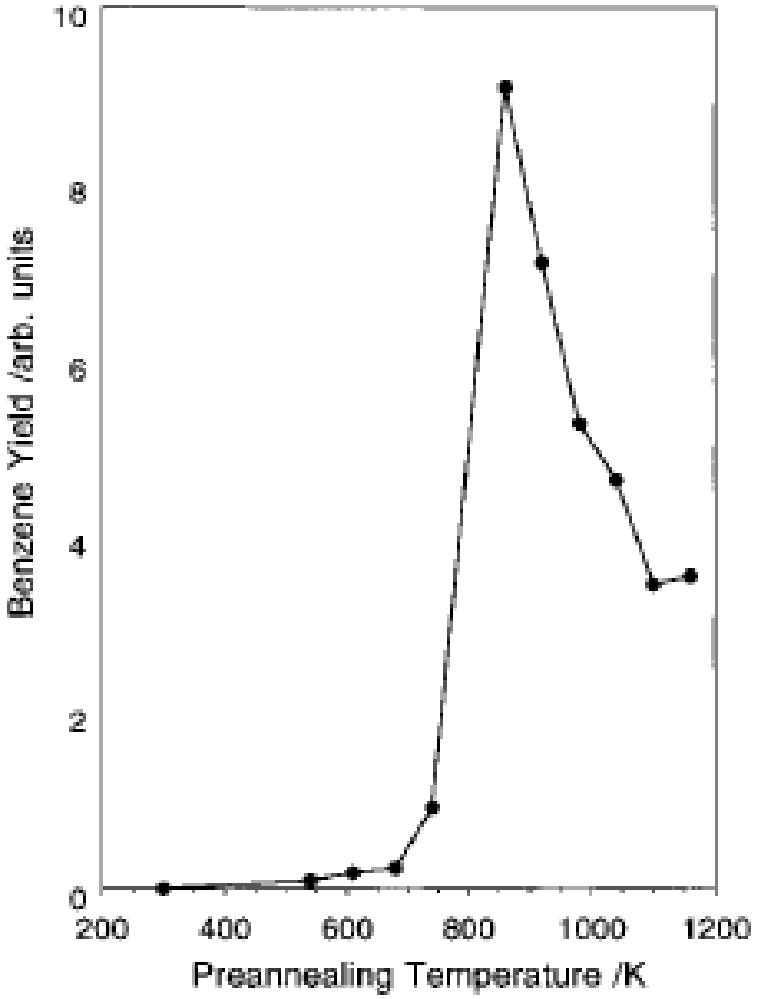

Figure 41: Total benzene yield as a function of sample preannealing temperature for 4.5ML Au deposited on Pd(111). [162]

single Pd surrounded by Au is the only feature at a preannealing temperature of 830K analogous to the highest benzene yield found when the surface was preannealed to 860K. [158]

Recent High Pressure Studies

Acetylene cyclotrimerization to benzene was studied at 300K on Pd/ Mo(110), Au/Mo(110), and Pd-Au/Mo(110) in a high pressure reactor. The composition was resolved by using XPS to determine the amount of Au or Pd deposited. Each metal is vapor deposited onto a Mo(110) single crystal and calibrated individually to identify a single monolayer using XPS peak area ratio of Au or Pd to Mo. This is then used to calibrate the metal loading based on the Mo(110) and used to determine multiple layer deposition. Each reaction surface was developed from 10ML of deposited Au, Pd, or a mix of both metals. The sample was then heated to 800K, a temperature proven to provide a reproducible surface composition as in figure 36. The surface composition was established by knowing the amount of each metal deposited on the Mo(110), maintaining a constant total deposition for both metals of 10ML, and comparing the XPS area ratio of the Au/Pd/Mo(110) system to LEISS data acquired on a separate chamber.[183]

The Pd-Au alloy surface was deposited on a cleaned Mo(110) surface by vapor deposition and annealed to 800K for 10 minutes. The sample was then transferred into the analysis chamber and an XPS spectrum taken at room

temperature.[167] Next, the sample is moved into position and the gate valve sealed the UHV chamber from the high pressure reactor. The kinetics for the cyclotrimerization of acetylene to benzene were analyzed utilizing the aforementioned high pressure reactor assembly and GC connected to the chamber. Each reaction was performed on a newly formed Au-Pd surface at a pressure of 10 torr for 3 hours at room temperature. The reactant gases were then collected in a loop submerged in liquid nitrogen and released through a six-way valve into the column for separation. A FID detector was used for reactant detection of the hydrocarbons. A post-reaction XPS spectrum was taken with the most noticeable change being the addition of a carbon 1s peak. The Pd and Au peaks remained the same as pre-reaction with a minor attenuation in the peak intensities. In figures 42 and 43 there is little perturbation in the binding energy indicating the electronic structure of Pd is unaltered by the addition of Au, even as the Au dominates the surface.

Figure 44 shows the data plotted with the turn-over-frequency per second per Pd atom as a function of Pd in the surface. The reaction on Mo(110) and pure Au was insignificant compared to the smallest amount of benzene produced with the Pd-Au alloy. The trend in figure 44 illustrates, as the amount of Pd on the surface decreases the TOF of benzene increases linearly with three distinct regions. The formation of benzene per Pd surface atom slowly rises as

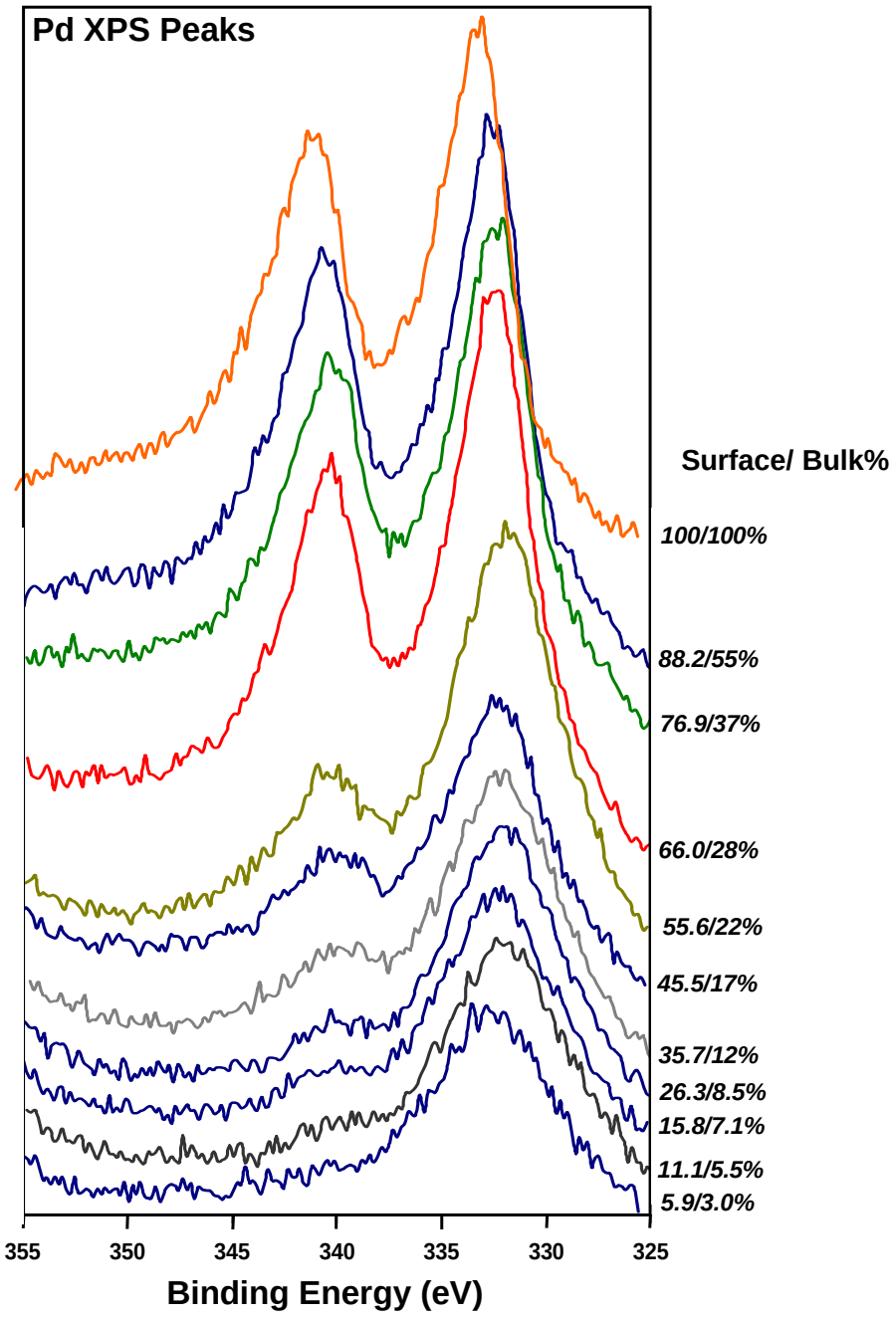

Figure 42: Pd peaks showing the composition of the bulk (XPS) and the surface (derived from ISS) for the acetylene cyclotrimerization reactions run.

the fraction of Pd decreases from a Pd surface coverage of 100-40%. As a result of the reduction of Pd on the surface the average seven atom ensemble, beginning as pure Pd, reduces to an average of three Pd and four Au per ensemble. Reducing the amount of surface Pd to ~40-30% the rate of benzene formation begins to intensify with the average seven atom ensemble possessing two surface Pd atoms. The benzene formation rate continues to increase linearly until the surface Pd fraction falls below 10% where the formation rate begins to accelerate. Below a surface Pd coverage of 8% the seven atom surface ensemble, on average, possesses less than one Pd atom. This further solidifies the proposal of an isolated Pd surrounded by Au atoms as the ensemble as having the highest benzene formation rate at room temperature.

A single Pd atom is the most prevalent surface ensemble (figure 34). Thus it can be easily assumed that, as the amount of surface Au increases, more ensembles with one Pd surface atom configuration are available as an active site for acetylene cyclotrimerization. [173] If this specialized configuration of a Pd surface atom surrounded by six surface Au atoms was optimal then the maximum TOF per surface Pd would be closer to 14% surface Pd. However, in figure 44 the maximum TOF is at a much lower loading of Pd surface atoms. This can be accounted for by analyzing the type of surface produced. At a lower loading fewer double and triple Pd surface atom grouping exist raising the probability of single Pd surface atoms, the ensemble associated with elevated benzene formation rate.

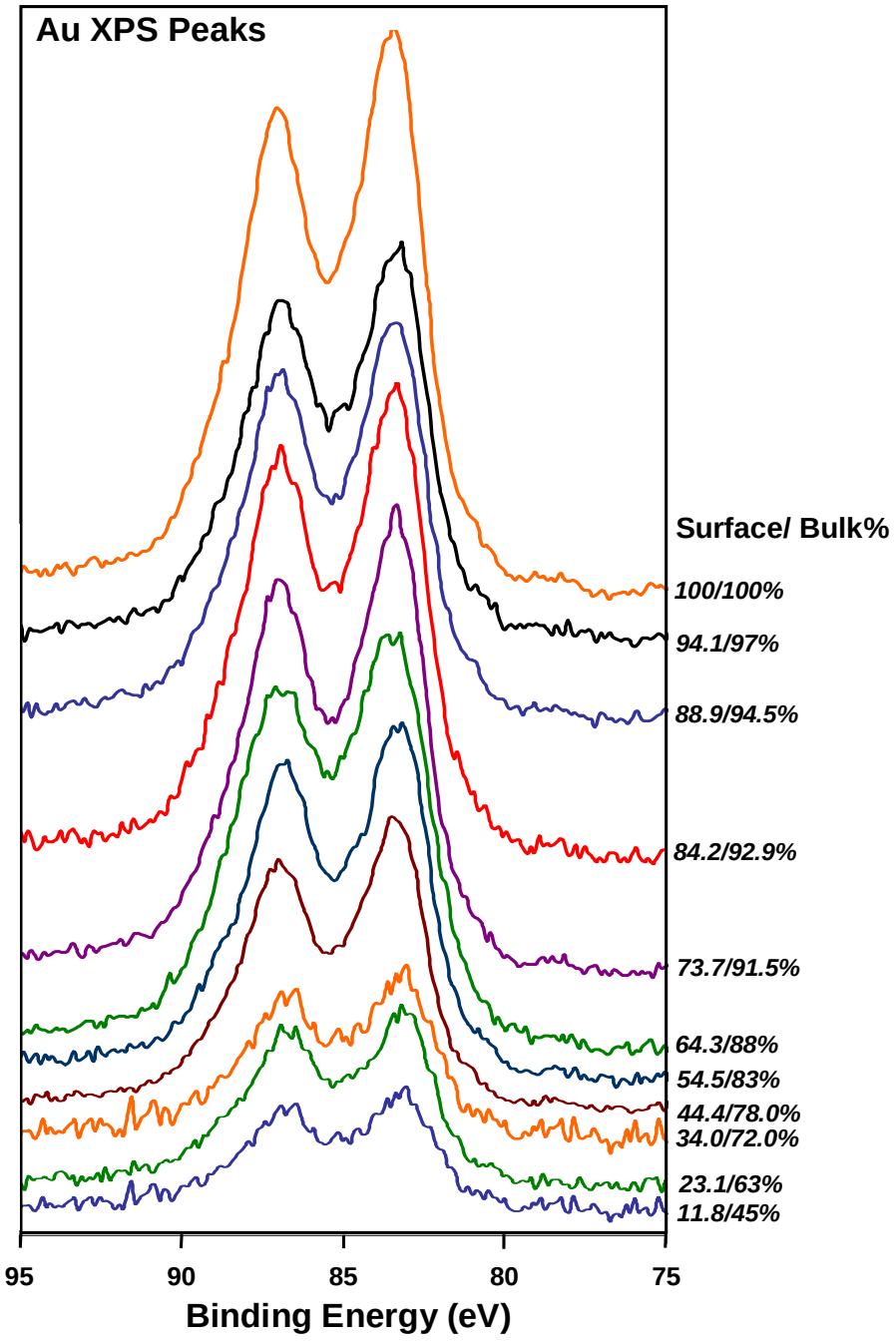

Figure 43: Au peaks showing the composition of the bulk (XPS) and the surface (derived from ISS) for the acetylene cyclotrimerization reactions run.

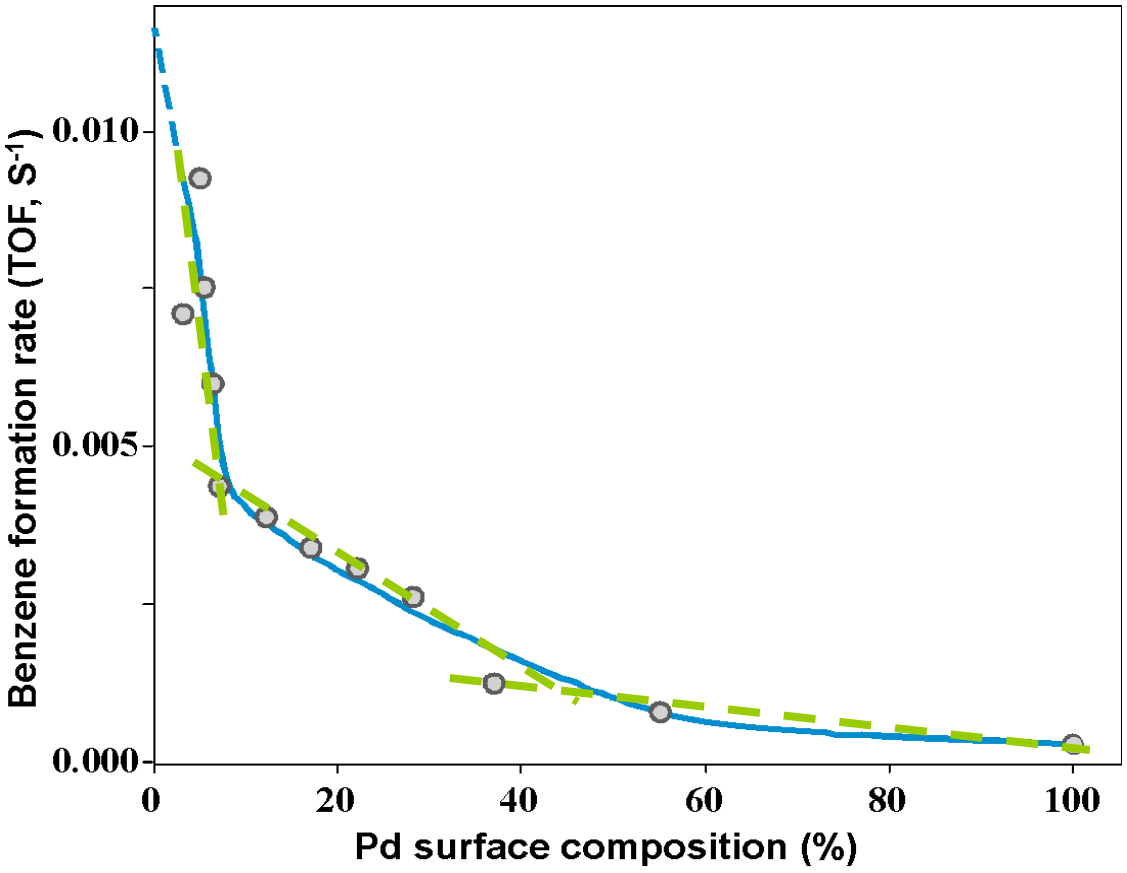

Figure 44: Benzene formation rate (TOF,s^{-1}) at 300K, on the bimetallic Au-Pd surface with varying composition, 0-100% Pd. The trend clearly predicts, that as the amount of Pd decreases on the surface the TOF increases per surface Pd. This entails, in terms of the seven atom ensemble, that the $PdAu_6$ has the highest reactivity at 300K.

CHAPTER VII

SUMMARY

CO Oxidation on Pt-group Metals

XPS was used to determine the surface composition of Rh(111), Pt(100), and Pd(100) during low and high pressure reactions. Low pressure *in situ* reactions at various temperatures on Rh(111) and Pt(100) revealed the highest CO_2 formation rate occurred where very little to no CO is detected on the surface. XPS and high pressure reactions performed in the high pressure cell on Pd(100) and transferred *in vacuo* showed a chemisorbed surface oxygen to be more prevalent species during the accelerated CO_2 formation than the thin or bulk oxides. Post reaction the oxygen was seen to migrate into the bulk, without sufficient reduction from CO.

Recent high pressure STM studies done on Pt(110) and Pd(100) used surface roughness as a bench mark for determining the surface composition during a CO oxidation reaction where the CO to O_2 gas mixture ratio was altered. However, using XPS and breaking down the experiments to pure oxygen showed that Pt(100) did not form a bulk oxide in pure oxygen at the same conditions. Similarly, CO oxidation at $CO:O_2$ ratios <1:5 on Pd(100) at high pressures showed a chemisorbed oxygen surface during the highest CO_2 formation rate.

Thus, on Pt-group metals, CO oxidation occurs at a higher rate where there is chemisorbed oxygen on the surface and CO is uninhibited from

adsorbing to the surface. The thicker oxide layers inhibit CO_2 formation by reducing the areas of CO adsorption.

Acetylene Cyclotrimerization to Benzene on Au-Pd/ Mo(110)

The cyclotrimerization of acetylene to benzene is well known at both UHV and at atmospheric conditions on single crystals and is typically carried out over dispersed Pd catalyst. The site for acetylene adsorption is the 3-fold hollow sites on the honeycomb structure of the Pd(111) utilizing the center Pd as a focal for the three acetylene molecules. The critical ensemble for benzene formation is seven palladium atoms. Desorption of the benzene is the rate limiting process for the pure Pd.

The addition of Au to the Pd enhances the activity. For these bimetallic systems the reactivity of the metal surface is a critical function of the composition and structure, which allow for industrial heterogeneous catalysts to be designed for a specific function.

The primary objective of this study was to determine the active site of the cyclotrimerization of acetylene over the bimetallic Au-Pd surface. Below a surface Pd coverage of 8% the seven atom surface ensemble, on average, possesses less than one Pd atom. This further solidifies the proposal of an isolated Pd surrounded by Au atoms as the ensemble as having the highest benzene formation rate.

REFERENCES

[1] G.A. Somorjai, Introduction to Surface Chemistry and Catalysis, Wiley, New York 1994

[2] J. Rogal, K. Reuter, M. Scheffler, Phys. Rev. Lett. 98 (2007) 046101

[3] G. B. Fisher, S. H. Oh, J. E. Carpenter, C. L. DiMaggio, S. J. Schmieg, D. W. Goodman, T. W. Root, S. B. Schwartz and L. D. Schmidt, (Eds.) A. Crucq , A. Frennet, Mechanisms of the Carbon Monoxide Oxidation and Nitric Oxide Reduction Reactions over Single Crystal and Supported Rhodium Catalysts: High Pressure Rates Explained Using Ultrahigh Vacuum Surface Science, in Catalysis and Automotive Pollution Control Vol. 30 Studies in Surface Science and Catalysis, Amsterdam, Elsevier, 1987

[4] X. Xu, J. Szanyi, Q. Xu, D.W. Goodman, Catalysis Today 21 (1994) 57

[5] L.M. Hendriksen, S.C. Bobaru, J.W.M. Frenken, Surf. Sci. 552 (2004) 22

[6] P. J. Berlowitz, C.H.F. Peden, D.W. Goodman., J. Phys. Chem.. 92 (1988) 5213

[7] C.H.F. Penden, D.W. Goodman, Surf. Sci. 90 (1985) 185

[8] N.V. Alov, J. of Anal. Chem. 60 (2005) 297-300

[9] http://www.ifw-dresden.de/, Leibniz Institute for Solid State and Materials Research Dresden Accessed on 25 September 2008

[10] C.D. Wagner, Handbook of X-ray Photoelectron Spectroscopy, New York, Perkin Elmer Corporation, 1979

[11] M.S. Chen, Y. Cai, Z. Yan, K. K. Gath, D. W. Goodman. Surf. Sci. 601 (2007) 5663

[12] D.A. Skoog, D.M. West, F.J. Holler, S.R. Crouch, (Eds.) D.A. Skoog, Analytical Chemistry: An Introduction, New York, Hardcourt Inc., 1999

[13] http://www.epa.gov/air/oaq_caa.html, 25 September 2008

[14] M.S. Chen, Y. Cai, Z. Yan, K. K. Gath, D. W. Goodman. Surf. Sci. 601 (2007) 5663

[15] E.M. Stuve, R J. Madix, C. R. Brundle, Surf. Sci. 146 (1984) 155-178

[16] J. Szanyi, Goodman, D.W., J. Phys. Chem. 98 (1994) 2972

[17] S. M. Vesecky, D. R. Rainer, D. W. Goodman J. Vac. Sci. Technol. A 14 (1996) 1457

[18] D.W. Goodman, C.H.F. Peden, J. Phys Chem 92 (1986) 4893

[19] G Paolucci, K. C. Prince, Phys. Rev. B 41,(1990) 3851

[20] H. Niehus, W. Heiland, E. Taglauer, Surf. Sci.Rep. 17 (1993) 213

[21] C.H.F. Peden, D.W. Goodman, D.S. Blair, G.B. Fisher, S.H. Oh, J. Phys Chem 92 (1988) 1563

[22] D.W. Goodman, C. H. F Peden, M. S. Chen., Surf. Sci. 601 (2007) L124

[23] D.W. Goodman, C.H.F. Peden, J. Phys Chem 92 (1986) 4893

[24] J. Liu, Liu, J; Xu, M; Zaera, F., Catal. Lett. 37 (1996)

[25] http://auto.howstuffworks.com/catalytic-converter.htm, How Stuff Works, Accessed on 25 September 2008

[26] http://www.nacatsoc.org/history.asp?HistoryID=5,
The North American Catalysis Society, Accessed on 25 September 2008

[27] G. Zheng, Altman, E.I., Surf. Sci. 504 (2002) 253-270

[28] S.L. Chang, Thiel, P.A., J. Chem. Phys. 88 (1988) 2071

[29] J. Rogal, K. Reuter, M. Scheffler, Phys. Rev. Lett. 98 (2007) 046101

[30] G. Zheng, Altman, E.I., J. Chem. Phys. 106 (2002) 1048

[31] E.M. Stuve, R J. Madix, C. R. Brundle, Surf. Sci. 146 (1984) 155-178

[32] J. Szanyi, Goodman, D.W., J. Phys. Chem. 98 (1994) 2972

[33] L.W. H. Leung, D.W. Goodman. Catal. Lett. 5 (1990) 353

[34] M. S. Chen, D. W. Goodman, Catal. Today, submitted for publication

[35] T. Engel, Ertl G., Adv. Catal. 28 (1979) 1-78

[36] S. M. Vesecky, X. Xu, P. J. Chen, D. W. Goodman, J. Vac. Sci. Technol. A 13(1995) 1539

[37] J.A. Rodriguez, D.W. Goodman, Surf. Sci. Rpt. 14 (1991) 1

[38] D.J. Liu, J.W. Evans, J. Chem. Phys. 125 (2006) 054709

[39] B.L.M. Hendriksen, Surf. Sci. 552 (2004) 229

[40] P. J. Berlowitz, C. H. F. Peden, D. W. Goodman, J. Phys. Chem.. 92 (1988) 5213

[41] F.P. Leisenberger, S. Surnev, G. Koller, M.G. Ramsey, F.P. Netzer, Surf Sci. 444 (2000) 211-220

[42] D.W. Goodman, C.H.F. Penden, J. Phys Chem 92 (1986) 4893

[43] E. Lundgren, A. Mikkelsen, J.N. Andersen, G. Kresse, M. Schmid and Peter Varga., J. Phys Condens Matter 18 (2006) R481

[44] C. H. F. Peden, D. W. Goodman, D. S. Blair, P. J. Berlowitz, G. B. Fisher, S. H. Oh Surf. Sci. 90 (1985)

[45] E. Lundgren, Phys. Rev. Lett. 92 (2004) 046101-1

[46] T.W. Orent, Bader, S.D., Surf. Sci. 115 (1982) 323

[47] S.L. Chang, P.A. Theil, J.W. Evans Surf. Sci. 205 (1988) 117-142

[48] W. K. Kuhn, J Szanyi, DW Goodman, Surf. Sci. Lett. 274 (1992) L611

[49] G. Ketteler, D.F. Ogletree, H. Bluhm, H. Liu, E. L. D. Hebensteit, M. Salmeron, J. Chem. Phys. 127 (2005) 18269-18273

[50] H. Gabasch, W. Unterberger, K. Hayek , B. Klotzer, E. Kleimenov, D. Teschner, S. Zafeiratos, M. Havecker, A. Knop-Gericke, R. Schlogl, J. Han, F. Ribeiro, B.A. Kiss, T. Curtin, D. Zemlyanov, Surf. Sci. 600 (2006) 2980-2989

[51] D. Zemlyanov, B.A. Kiss, E. Kleimenov, D. Teschner, S. Zafeiratos, M. Havecker, A. Knop-Gericke, R. Schlogl, H. Gabasch, W. Unterberger, K. Hayek, B. Klotzer, Surf. Sci 600 (2006) 983-994

[52] M. Todorova, E. Lundgren, V. Blum, A. Mikkelsen, S. Gray, J. Gustafson, M. Borg, J. Rogal, K. Reuter, J.N. Andersen, M. Scheffler, Surf. Sci. 541 (2003) 101-112

[53] F.P. Leisenberger, G. Koller, M. Sock, S. Surnev, M.G. Ramsey, F.P. Netzer, B. Klotzer, K. Hayek, Surf. Sci. 445 (2000) 380

[54] J. Han, D. Y. Zemlyanov, F. H. Rineiro, Surf. Sci. 600 (2006) 2752-2761

[55] J. Han, D. Y. Zemlyanov, F. H. Rineiro, Surf. Sci. 600 (2006)) 2730-2744

[56] M. Todorova, W. Xi, M.V. Gandugliap-Pirovano, C. Stampfl, K. Reuter, M. Scheffler, Phys. Rev. Lett. 89 (2002) 096103-1

[57] E. Lundgren, Phys. Rev. Lett. 88 (2002) 246103

[58] G. Zheng, Altman, E.I., Surf. Sci. 462 (2000) 151

[59] P. Salo, K. Honkala, M. Alatalo, and K. Laasone., Surf. Sci. 516 (2002) 247

[60] H. Gabasch, Knop-Gericke, A. R. Schlogl,vM. Borasio, C. Weilach, G. Rupprechter, S. Penner, B. Jenewein, K. Hayek, B. Klotzer Phys. PCCP 9 (2006) 533-540

[61] L.W. H. Leung, D.W. Goodman. Catal. Lett. 5 (1990) 353

[62] X. Xu, C.M. Friend, Surf. Sci. 113 (1991) 6779

[63] S. Schwegmann, H. Over, V. De Ronzi, G. Ertl, Surf. Sci. 375 (1997) 91

[64] K.C. Wong, W. Liu, K.A.R. Mitchell, Surf. Sci. 360 (1996) 137

[65] S. B. Schwartz, D.L. Schmidt, G.B. Fisher, J. Phys. Chem. 90 6194

[66] P.A. Thiel, J.T. Yates, W.H. Weinberg, Surf. Sci. 82 (1979) 22

[67] L. Kohler, G. Kresse, M. Schmid, E. Lundgren, J. Gustafson, A. Mikkelsen, M. Borg, J. Yuhara, J.N. Andersen, M. Marsman, P. Varga, Phys. Rev. Lett 93 (2004) 266103-1

[68] A. Baraldi, J. Cerda, J.A. Martm-Gago, G. Comelli, S. Lizzit, G. Paolucci, R. Rosei, Phys. Rev. Lett. 82 (1999) 4874

[69] K. D. Gibson, Mark. Viste, Errol .C. Sanchez, S.J. Sibener, J. Chem. Phys. 110 (1999) 2757

[70] H. Abbott, I. Harrison, J. Phys. Chem C. 111 (2007) 13137

[71] E. Lundgren, J. Gustafson, A. Resta, J. Weissenrieder, A. Mikkelsen, J.N. Andersen, L. Kohler, G. Kresse, J. Klikovits, A. Biederman, M. Schmid, P. Varga J. of Electron Spec. and Related Phenomena, 144-147 (2005) 367

[72] J. Wider, T. Greber, E. Wetli, T.J. Kreutz, P. Schwaller, J. Osterwalder, Surf. Sci. 417 (1998) 301-310

[73] F. Gao, Y. Cai, K.K. Gath, M.S. Chen, Q.L. Guo, D.W. Goodman, Surf. Sci., submitted

[74] E. Lundgren, A. Mikkelsen, J.N. Andersen, G. Kresse, M. Schmid, P. Varga, J. Phys. Condens. Matter 18 (2006) R481

[75] G. Krenn, I. Bako, R. Schennach, J. Chem. Phys. 124 (2006) 144703

[76] J. Gustafson, A. Mikkelsen, M. Borg, E. Lundgren, L. Kohler, M. Schmid, P. Varga, J. Yuhara, X. Torrelles, C. Quiros, J.N. Andersen, Phys. Rev. 92 (2004) 126102-1

[77] M.V. Ganduglia-Pirovano, M. Scheffler, A. Baraldi, S. Lizzit, G. Comelli, G. Paolucci, R. Rosei, Phys. Rev. B 63 (2001) 205415

[78] A. J. Jaworowski, A. Beutler, F. Strisland, R. Nyholm, B. Setlik, D. Heskett, J.N. Andersen, Surf. Sci. 431 (1999) 33

[79] J. Wider, T. Greber, E. Wetli, T.J. Kreutz, P. Schwaller, J. Osterwalder, Surf. Sci. 417 (1998) 301-310

[80] A.D. Logan, A.K. Datye, J.E. Houston, Surf. Sci. 245 (1991) 280

[81] C. W. Tucker, J. of Applied Physics 37 (1966) 3013

[82] A.H. Zhang, J. Zhu, W.D. Duan, J. Chem. Phys. 124 (2006) 234703

[83] R. Linke, D. Curulla, M.J.P. Hopstaken, J.W. Niemantsverdriet, J. Chem. Phys. 115 (2001) 8209

[84] I. Nakamura, Y. Kobayashi, H. Hamada, T. Fujitani, Surf. Sci. 600 (2006) 3235- 3242

[85] F.G. Requejo, E.L.D. Hebenstreit, D. F. Ogletree, M. Salmeron, J. Catal. 226 (2004) 83

[86] S. Ladas, R. Imbihil, G. Ertl, Surf. Sci. 219 (1989) 88

[87] B. Brandt, T. Schalow, M. Laurin, S. Schauermann, J. Libuda, H.-J. Freund, J. Phys. Chem. C. 111 (2007) 938

[88] B.C. Sales, J.E. Turner, M.B. Maple, Surf. Sci. 114 (1982) 381

[89] W. Liu, F. Zhu, J. S. Lian, Q Jiang, J. Phys. Chem. C 111 (2007) 1005

[90] L.H. Dubois, G.A. Somorjai, 91 (1980) 514-532

[91] H. Over, A. P. Seitsonen, Science 297 (2002) 2003

[92] P.A. Thiel, J.T. Yates, W.H. Weinberg, Surf. Sci. 82 (1979) 22

[93] J. Wider, T. Greber, E. Wetli, T.J. Kreutz, P. Schwaller, J. Osterwalder, Surf. Sci 417 (1998) 301

[94] P.R. Norton in: D.A. King, D.P. Woodruff (Eds.), The Chemical Physics of Solid Surfaces and Heterogeneous Catalysis, Vol. 4, Amsterdam, Elsevier,1982.

[95] N.A. Saliba, Y.-L. Tsai, C. Panja, B. E. Koel Surf. Sci. 419 (1999) 79-88

[96] R. Imbihl, M.P. Cox G. Ertl, H. Muller, W. Brenig, J. Chem. Phys. 83 (1985) 1578

[97] K. Griffiths, T. E. Jackman, J.A. Davies, P.R. Norton, Surf. Sci. 138 (1984) 113-124

[98] Q. Ge, P. Hu, D. A. King, M. H. Lee, J. A. White, M. C. Payne, J. Chem. Phys 106 (1997) 1210

[99] R. B. Shumbera, H. H. Kan, J. F. Weaver, Surf. Sci. 600 (2006) 2928

[100] M. A. Barteau, E. I. Ko, R. J. Madix, Surf. Sci 104 (1981) 161

[101] M. D. Ackermann, T. M. Pedersen, B. L. M. Hendriksen, O. Robach, S. C. Bobaru, I. Popa, C. Quiros, H. Kim, B. Hammer, S. Ferrer, J. W. M. Frenken Phys. Rev. Lett. 95 (2005) 255505

[102] P. R. Norton, P.E. Binder, and K. Griffiths J. Vac. Sci. Techol. 3 (1984) 1028

[103] G. Ertl, P. R. Norton, J. Rustig, Phys. Rev. Lett 49 (1982) 177-180

[104] C. Ellinger, A. Stierle, I. K. Robinson, A. Nefedov, H. Dosch, J. Phys.: Condens. Matter 20 (2008) 184013

[105] R. Imbihl, M.P. Cox G. Ertl, J. Chem. Phys. 84 (1986) 3519-3534

[106] P.A. Thiel, J.T. Yates, W.H. Weinberg, Surf. Sci. 82 (1979) 22

[107] C. W. Tucker, J. of Applied Physics 37 (1966) 3013

[108] B. L. M. Hendriksen, J. W. M. Frenken, Phys Rev. Lett., 98 (2002) 046101

[109] L.H. Dubois, G.A. Somorjai, Surf. Sci., 91 (1980) 514-532

[110] J. Gustafson, A. Mikkelsen, M. Borg, E. Lundgren, L. Kohler, M. Schmid, P. Varga, J. Yuhara, X. Torrelles, C. Quiros, J.N. Andersen, Phys. Rev. 92 (2004) 126102-1

[111] F. Gao, Y. Cai, K. K. Gath, M. S. Chen, Q. L. Guo, D. W. Goodman, J. Phys. Chem. C, in press

[112] R.B. Hoyle, A.T. Anghel, M. Proctor, D.A. King, Phys. Rev. Lett 98 (2007) 226102

[113] R.B. Shumbera, H.A. Kan, J. F. Weaver, J. Phys. Chem. 112 (2008) 4232-4241

[114] D. J. Burnett, A.T. Capitano, A.M. Gabelnick, A. L. Marsh, A. A. Fischer, J. L. Gland, Surf. Sci. 564 (2004) 29

[115] X. Su, P.S. Cremer, Y. R. Shen, G.A. Somorjai, J. Am. Chem. Soc. 119 (1997) 3994

[116] M. P. Harold, M.E. Garske, J. of Catal. 127 (1991) 553-575

[117] H.Tang, A. Van der Ven, B. L. Trout, Phys. Rev. B 70 (2004) 045420

[118] M. Mundschau, R. Vanselow, Surf. Sci. 160 (1985) 23-36

[119] R.B. Shumbera, H.A. Kan, J. F. Weaver, Surf. Sci. 601 (207) 235-246

[120] K. L. Kostov, P. Jakob, D. Menzel, Surf. Sci. 377-379 (1997) 802-807

[121] H. Conrad, G. Ertl, J. Kuppers, Surf Sci. 76 (1978) 323-342

[122] F.P. Leisenberger, G. Koller, M. Sock, S. Surnev, M.G. Ramsey, F.P. Netzer, B. Klotzer, K. Hayek, Surf. Sci. 445 (2000) 380

[123] J. Han, G. Zhu, D. Zemlyanov, F.H. Ribeiro, J. of Catal. 225 (2004) 7-15

[124] P. Kostelnik, N. Seriani, G. Kresse, A. Mikkelsen, E. Lundgren, V. Blum, T. Sikola, P. Varga, M. Schmid, Surf. Sci. 601 (2007) 1574-1581

[125] S.L. Chang, P. A. Thiel, Phys. Rev. Lett. 59 (1987) 296-299

[126] V. A. Bondzie, P. Kleban, D. J. Dwyer, Surf. Sci. 347 (1996) 319-328

[127] E.H. Voogt, A.J.M. Mens, O.L.J. Gijzeman, J.W. Geus, Catal. Today (1999) 321-323

[128] E.H. Voogt, A.J.M. Mens, O.L.J. Gijzeman, J.W. Geus, Surf. Sci. (1996) 21-31

[129] B.L.M. Hendriksen, Surf. Sci. 552 (2004) 229

[130] Y. Zhang, V. Blum, K. Reuter, Phys. Rev. B 75 (2007) 235406

[131] Y. Yun, J. Wang, E.I. Altman, J. of Catal. 253 (2008) 295-302

[132] S. H. Kim, J. Mendez, J. Wintterlin, G. Ertl, Phys Rev. B 72 (2005) 155414

[133] M. Grunze, H. Ruppender, O. Elshazly, J. Vac Sci. Technol. A 6 (1988) 1266

[134] G. Ketteler, uido Ketteler,* D. Frank Ogletree, Hendrik Bluhm Hongjian Liu, Eleonore L. D. Hebenstreit, and Miquel Salmeron J. AM. Chem. Soc. 127 (2005) 18269-18273

[135] D. J. Liu, J. W. Evans, J. Chem. Phys. 124 (2006) 154705

[136] H. Abbott, I. Harrison, J. Phys. Chem C. 111 (2007) 13137

[137] B.L. Hendriksen, S.C. Bobaru, J.W.M. Frenken, Surf. Sci. 552 (2004) 229

[138] J. Rogal, K. Reuter, M. Scheffler, Phys. Rev. B 75 (2007) 205433

[139] B.L.B. Hendriksen, S.C. Bobaru, J.W.M. Frenken, Catal. 105 (2005) 234-243

[140] P.E.M. Berthelot , C.R. Hebd, Seances Acad. Sci. 62 (1866) 905

[141] P.E.M. Berthelot, J. Liebigs, Ann. Chem. 139 (1866) 272

[142] J. C. Santos, V. Polo, J. Andrés. 406 (2005) 393

[143] H.E. Zimmerman, Ac. Chem. Res. 4 (1971) 272

[144] R. Havenith R. Havenith, P. Fowler, L. Jenneskens and E. Steiner J. Phys. Chem. A 107 (2003) 1867

[145] K. Houk, N. Houk, R. W. Gandour, R. W. Strozier, N. G. Rondan, L. A. Paquette J. Am. Chem. Soc. 101 (1979) 6797

[146] R.D. Bach, G.J. Wolber, H.B. Schlegel, J. Am. Chem. Soc. 107 (1984) 2837

[147] I. Morao, F.P. Cossio, J. Org. Chem. 64 (1999) 1868

[148] H. Jiao, P. von Ragué Schleye, J. Phys. Org. Chem. 11(1998) 655

[149] J. Cioslowski, G.H. Liu, D. Moncrieff, Chem. Phys. Lett 316 (2000) 536

[150] C.J. Baddeley, R.M. OrmerodA.W. Stephenson, R. M. Lambert, J. Phys. Chem 99 (1995) 5146

[151] R. M. Ormerod, R. M. Lambert, H. Hoffmann, F. Zaera, J. M. Yao, D. K. Saldin, L. P. Wang, D. W. Bennett and W. T. Tysoe, Surf. Sci.,295 (1993) 277

[152] K. Judai, A. S. Wörz, S. Abbet, J.M. Antonietti, U. Heiz, A. Del Vitto, L. Giordano. G. PacchioniI Phys. Chem. Chem. Phys., 7 (2005) 955

[153] C. Baddeley, M. Tikhov, C. Hardacare, J. Lomas, R.M. Lambert, J. Phys. Chem. 100 (1996) 2189

[154] R. M. Ormerod, R. M. Lambert, H. Hoffmann, F. Zaera, L. P. Wang, D. W. Bennett and W. T. Tysoe, J. Phys. Chem., 98 (1994) 2134.

[155] A.F. Lee, C.J. Baddeley, C. Hardacare, R.M. Ormerod, R. M. Lambert, H. West, G. Schmid J. Phys Chem 99 (1995) 6096

[156] K. Luo, K. Luo, T. Wei, C.-W. Yi, and D. W. Goodman., J. Phys. Chem. B 109 (2005) 23517

[157] H. Hoffmann, F. Zaera, R.M. Ormerod, R.M. Lambert, J.M. Yao, D.K. Saldin, L.P. Wang, D.W. Bennett, W.T. Tyso, Surf. Sci (1992) 268

[158] H. Sellers, J. Phys. Chem. 94 (1990) 8329

[159] T. Gentle, E.L. Muetterties, J. Phys Chem. 87 (1983) 2469

[160] T. Rucker, M.A. Logan, T.M. Gentle, E.L. Muetterties, G.A. Somorjai., J. Phys. Chem. 90 (1986) 2703

[161] S. Abbet, Abbet, U. Heiz, H. Häkkinen, U. Landman., J. Am. Chem. Soc. 122 (2000) 3453

[162] C.J. Baddeley, CJ Baddeley, RM Ormerod, AW Stephenson, RM Lambert., J. Phys Chem. 99(1995)5146

[163] J. H. Sinfelt, Acc. Chem. Res. 10 (1977) 15

[164] R.M. Lambert, R.M. Ormerod, Mater. Chem. Phys. 29 (1991) 105

[165] J. C. Santos, V. Polo, J. Andrés, Chem. Phys. Lett., 406 (2005) 393

[166] C.T. Campbell, Ann. Rev. Phys. Chem. 41 (1990) 775

[167] J.A. Rodriguez, D.W. Goodman, J. Phys. Chem. 95 (1991) 4196

[168] J.A. Rodriguez, C.T. Campbell, D.W. Goodman, J. Phys. Chem. 95 (1991) 5716

[169] J.A. Rodriguez, C.T. Campbell, D.W. Goodman, J. Vac. Sci. Technol. A 9 (1991) 1698

[170] J.A. Rodriguez, C.T. Campbell, D.W. Goodman, J. Vac. Sci. Technol. A 9 (1991) 2540

[171] J.A. Rodriguez, D.W. Goodman, Science 257 (1992) 897

[172] J.A. Rodriguez, C.T. Campbell, D.W. Goodman, Surf. Sci. 309 (1994) 377

[173] F. Maroun, F Ozanam, O.M. Magnussen, R.J. Behm., Science 293 (2001) 1811

[174] D.L. Trimm, Z.I. Onsan, Catal. Rev. 43 (1964) 2364

[175] M. Bonarowska, A. Malinowski, W. Juszczyk, Z. Karpiński, Appl. Catal. B. 30 (2001) 187

[176] E. G. Allison, G. Bond, Catal. Rev. 7 (1972) 233

[177] C.J. Baddeley, R.M. OrmerodA.W. Stephenson, R. M. Lambert, J. Phys. Chem 99 (1995) 5146

[178] D.D Eley. P. Luetic, Trans. Faraday Soc. 53 (1957) 1483

[179] G. Reinacker, S. Engels, Anorg. Allg. Chem. 336 (1965)259

[180] W.M.H. Sachtler, P. van der Plank, Surf. Sci. 18 (1969) 62

[181] M. Mavrikakis, B. Hammer, and J. K. Nørskov, Phys. Rev. Lett. 81 (1998) 2819

[182] A. Jablonski, S.H. Overbury and G.A. Somorjai l., Surf. Sci. 65 (1977) 578

[183] C.W. Yi, K. Luo, T. Wei, D. W. Goodman., J. Phys. Chem. B 109 (2005) 18535

[184] K. Luo, T. Wei, C.-W. Yi, D. W. Goodman., J. Phys. Chem. B 109 (2005) 23517

[185] P. Varga, G. Hetzendorf, Surf. Sci. 162 (1985) 544

[186] S. Abbet, U. Heiz, H. Häkkinen, U. Landman., J. Am. Chem. Soc. 122 (2000) 3453

[187] S. Schomann, E. Taglaue., Surf. Rev. Lett 3 (1996) 1823

188] L. Houssiau, P. Bertrand, Nucl. Instrum. Methods B. 125 (1997) 328

[189] M. Aschoff, G. Piaszenski, S. Speller, W. Heiland., Surf. Sci. 402-404 (1998) 770

[190] M. Aschoff, M. Aschoff, S. Speller, J. Kuntze, W. Heiland, E. Platzgummer, M. Schmid, P. Varga and B. Baretzky., Surf. Sci. 415 (1998) L1051

[191] B. E. Koel, A. Sellidj, M.T. Paffett, Phys. Rev. B 46 (1992) 7846

[192] H. Niehus, Phys. Status Solidi B 192 (1995) 357

[193] A. Noordermeer, G. Kok, B. Nieuwenhuys, Surf. Sci. 165 (1986) 375

[194] A.F. Lee, C.J. Baddeley, C. Hardacre, R.M. Ormerod, J. Phys Chem 99 (1995) 6096

[195] L. Hilaire, P. Legare, Y. Holl, G. Malre,, Surf. Sci. 103 (1981) 125

[196] J.C. Dunphy, Phys. Rev. B 57, (1998) R12705

VITA

Kerrie K. Gath grew up in San Antonio, TX and graduated from Texas A&M University in May of 2002 with a Bachelor of Science degree in chemical engineering as a member of Omega Chi Epsilon. She began her graduate studies in August 2003 under the direction of Dr. D. Wayne Goodman and received her Ph.D in physical chemistry in December 2008. She can be reached at: Care of Dr. Goodman, Department of Chemistry TAMU, College Station, TX 77843 - 3255.